

CHARACTERIZATION OF *A. thaliana* G-PROTEIN GAMMA SUBUNIT (AGG2)
and INVESTIGATION OF DTT EFFECT ON ITS OLIGOMERIC STATE

by

ANIL AKTÜRK

Submitted to the Graduate School of Engineering and Natural Sciences

in partial fulfillment of

the requirements for the degree of

Master of Science

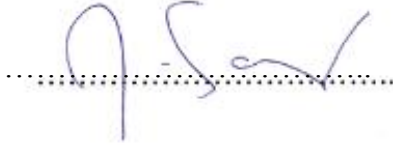
Sabancı University

July, 2012

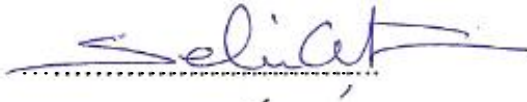
CHARACTERIZATION OF *A. thaliana* G-PROTEIN GAMMA SUBUNIT (AGG2)
and INVESTIGATION OF DTT EFFECT ON ITS OLIGOMERIC STATE

APPROVED BY:

Prof. Zehra Sayers
(Dissertation Supervisor)



Prof. Selim Çetiner



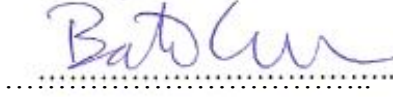
Prof. Yuda Yürüm



Assoc. Prof. Uğur Sezerman



Assoc. Prof. Batu Erman



DATE OF APPROVAL:

10.07.2012

©Anıl Aktürk, 2012

All Rights Reserved

CHARACTERIZATION OF *A. thaliana* G-PROTEIN GAMMA SUBUNIT (AGG2) and
INVESTIGATION OF DTT EFFECT ON ITS OLIGOMERIC STATE

Anil Akturk

Biological Sciences and Bioengineering, MSc Program, 2012

Thesis Supervisor: Prof. Zehra Sayers

Keywords: G-Protein, AGG2, DTT, Tetramer, Dimer

ABSTRACT

Heterotrimeric G-Proteins are vital effectors in signal transduction pathways in both animal and plants by transmitting the signal received by membrane bound receptors to downstream factors (Simon M. I., 1991). The protein complex consists of three subunits: α , β and γ . The alpha subunit has GTP hydrolysis activity and acts as a molecular switch for signal continuity or inhibition. Beta and gamma subunits act as a dimer for downstream signal transduction (Oldham, 2006). Odor, taste and phototransduction pathways are closely integrated to G-Protein transduction mechanism in mammalian organisms (Arshavsky V. Y., 2002). Plant cells utilize G-Protein signaling in germination, cell division, stress responses and morphological changes (Perfus-Barbeoch L., 2004).

This study is the first report in the literature for biophysical characterization of the *A. thaliana* G-Protein γ subunit, AGG2, independent of beta subunit. The gene was expressed in *E. coli* TOP10 cells using pETM-41 and pMCSG-7 vectors. Expression profiles of the proteins and growth curves of TOP10 cells with or without protein overexpression were optimized. The proteins were purified with affinity, ion exchange and size exclusion chromatography and were characterized with Dynamic Light Scattering (DLS), Circular Dichroism (CD) and Small Angle X-Ray Scattering (SAXS) methods. Furthermore alignment of AGG2 to mammalian G-Protein, transducin, gamma subunit was carried out and this was utilized for homology modeling. The monomer model was self-docked and the structural features of the dimer were further investigated.

Protein expression levels were such that the pETM-41 clone yielded insufficient protein for purification but pMCSG-7 clone (AGG2) and a previously prepared pQE80-L clone (AGG2*) could be utilized in biophysical characterization studies. Proteins AGG2 and AGG2* were obtained from the SEC column at different elution volumes indicating different properties for the same protein under the different conditions of SEC. This effect was traced back to presence/absence of DTT in elution buffers. Presence of DTT in the buffer resulted in a change in the size of the protein. DLS, SAXS, CD measurements as a function of DTT concentration (from 0 to 5 mM) showed that the protein changed its oligomeric state from tetramer to dimer as DTT concentration is increased and it has been possible to reduce this form to monomeric state. This effect was found to be independent of protein concentration. Homology modeling resulted in structures that were in agreement with those found from *ab initio* modeling based on SAXS data as well as that obtained from crystal structure of mammalian beta-gamma dimer. Theoretical SAXS curves obtained from the homology model of the dimer overlap well with the experimental SAXS curves. Significance of the dimer for function of the gamma subunit is discussed within the perspective of available literature on the plant G-protein heterotrimer. Modeling and biophysical characterization studies led to the conclusion that the dimeric form results from interaction of Cys108 of two monomers which are located in an intertwined ball like structure formed by C-termini loops of two monomers.

A.thaliana G-PROTEİN'İ GAMA ALTBİRİMİ (AGG2)'NİN KARAKTERİZASYONU VE
DTT'NİN OLİGOMERİK DURUMU ÜSTÜNE ETKİSİNİN İNCELENMESİ

Anıl Aktürk

Biyoloji Bilimleri ve Biyomühendislik, MSc Programı, 2012

Tez Danışmanı: Prof. Zehra Sayers

Anahtar Kelimeler: G-Protein, DTT, Tetramer, Dimer

ÖZET

Hetertrimerik G Proteinleri bitki ve hayvan hücrelerinde sinyal devamlılık yolları üstünde önemli yere sahiptirler. Hücre içine sinyali membrana bağlı bulunan reseptörlerden alıp aşağı yönde bulunan diğer faktörlere iletirler (Simon M. I., 1991). Protein kompleksi α β ve γ şeklinde üç altbirimden oluşmaktadır. Alfa altbirimi GTP hidroliz aktivitesini üstlenmekle beraber sinyal devamlılığı ya da durdurulmasını kontrol eden moleküler bir anahtar görevi görmektedir. Beta ve gama altbirimleri ise aşağı sinyal iletimini dimer olarak beraber yapmaktadırlar (Oldham, 2006). Memeli organizmalarında G-Proteinkeri koku, tat ve ışık algılama yollarına güçlü bir şekilde entegre olmuşlardır. Bitki hücreleri ise G-Proteinlerini filizlenme, hücre bölünmesi, stres tepkileri ve morfolojik değişim anlarında kullanmaktadır (Perfus-Barbeoch L., 2004).

Bu çalışma *A. Thaliana* G-proteini gama altbirimi olan AGG2'nin biyofiziksel karakterizasyonu üstüne literatürde bulunan ilk çalışmadır. Gen, *E.coli* TOP10 hücrelerinde pETM-41 ve PMCSG-7 plazmidlerinin yardımları ile sentezlenmiştir. Sentezlenen proteinin ekspresyon profili ve protein sentezleyen ve sentezlemeyen TOP10 hücrelerinin büyüme eğrileri optimize edilmiştir. Proteinler afinite, ion değişim ve boyut çıkarım (size exclusion) kromatografileri ile saflaştırılmış ve "Dynamic Light Scattering", "Circular Dichroism" ve "Small Angle X-Ray Scattering" metodları ile karakterize edilmiştir. AGG2 protein sekansının memeli G-protein'lerinden olan "transducin" proteininin gama altbirimi ile

hizalanma sonucunun programa girilmesi ile homoloji modelleme yapılmış, modelleme sonucu kendi üstüne yerleştirilerek bir dimer elde edilmiş ve yapısı incelenmiştir.

Protein ekspresyon seviyelerinin karşılaştırılması sonucu görüldü ki pETM-41 klonlaması ile elde edilen plazmid proteininin saflaştırmasında yeterli protein miktarına ulaşamamıştır, fakat pMCSG-7 (AGG2) ile daha önceden elde edilmiş pQE80-L (AGG2*) plazmidlerinde AGG2 sentezi biyofiziksel çalışmalar için yeterli miktarda elde edilmiştir. AGG2 ve AGG2* SEC kolonu sonucunda farklı boyutlarda ayrıştırılmış ve farklı boyutlarda iki protein görülmüştür. Bu farklılık proteinlerin saflaştırıldığı tampon solüsyonda bulunan/bulunmayan DTT indirgeme kimyasalına dayandırılmıştır. Tampon içinde bulunan DTT'nin protein boyutlarını küçülttüğü gözlemlenmiştir. Artan DTT konsantrasyonları ile yapılan (0 mM'den 5 mM'e kadar) DLS, CD ve SAXS deneylerinde artan DTT miktarı ile protein oligomer durumunun tetramerden dimere geçtiği görülmüştür. Oligomer durum değişiminin protein konsantrasyonuna bağlı olmadığı da kanıtlanmıştır. Homoloji modelleme sonuçları SAXS deneylerinden elde edilen verilerle yapılan *ab initio* modellerle ve memeli hücresinde bulunan homologları ile uyumluluk göstermektedir. Modelleme sonuçlarından elde edilen yapılardan elde edilen teorik SAXS eğrileri ile deneysel eğriler karşılaştırılmış ve uyumluluk gösterilmiştir. Dimer oluşumunun gama altbiriminin fonksiyonunu etkilemesi hali hazırda bulunan literatür bilgisi ile tartışılmıştır. Modelleme ve biyofiziksel karakterizasyon çalışmaları dimer formunun oluşumunun, homoloji modellemelerinde de gözlenen iki monomerin iç içe geçen C-terminus uçlarındaki loop' yapılarının oluşturduğu yapının içinde gizlenen Cys108 amino asidi olduğu sonucuna varılmıştır.

TABLE OF CONTENTS

1. INTRODUCTION

1.1. What are Heterotrimeric G Proteins?

1.2. G-Protein Signaling

1.3. Mammalian vs Plant G-Protein

1.3.1. Genome Based

1.3.2. Structure Based

1.4. Functions of G-Proteins in Mammals and in Plants

1.4.1. In Mammalian Cells

1.4.2. In Plant Cells

1.5. Regulation of G-Protein Signaling

1.6. Gamma Subunits of G-Proteins in Plants

1.7. Biophysical Methods used for Structural Investigation of AGG2

1.7.1. Circular Dichroism Spectropolarimetry

1.7.1.1. Determination of Secondary Structure with CD

1.7.2. Dynamic Light Scattering

1.7.3. Small Angle X-Ray Scattering

1.7.3.1. SAXS Data Processing

1.7.3.2. Model Generation from SAXS Data

1.7.3.3. DAMMIN

1.7.3.4. GASBOR

1.7.3.5. DAMAVER

1.7.3.6. CRY SOL

1.7.4. X33 Beamline, EMBL Hamburg

1.8. Objective of the Study

2. MATERIALS AND METHODS

2.1. Materials

- 2.1.1. Chemicals**
- 2.1.2. Primers**
- 2.1.3. Enzymes**
- 2.1.4. Vectors**
- 2.1.5. Cell Lines**
- 2.1.6. Buffers and Solutions**
- 2.1.7. Commercial Kits**
- 2.1.8. Culture Media**
- 2.1.9. Equipment**

2.2. Methods

2.2.1. Cloning AGG2 gene into Vectors

2.2.1.1. pETM-41 Vector Cloning

- 2.2.1.1.1. PCR**
- 2.2.1.1.2. Restriction Digestion with *NcoI* and *BamHI***
- 2.2.1.1.3. Ligation of AGG2 into pETM-41 Vector**
- 2.2.1.1.4. Transformation of Bacteria**
- 2.2.1.1.5. Colony Selection**
- 2.2.1.1.6. Plasmid Isolation**
- 2.2.1.1.7. Restriction Digestion and Replication (PCR) Screening of Samples**
- 2.2.1.1.8. Sequence Verification**

2.2.1.2. pMCSG-7 Vector (Ligand Independent Cloning Method)

- 2.2.1.2.1. PCR**
- 2.2.1.2.2. *SspI* Digestion of Plasmids**
- 2.2.1.2.3. T4 DNA Polymerase Reaction**
- 2.2.1.2.4. Annealing of Insert & Vector**
- 2.2.1.2.5. Transformation of Samples**
- 2.2.1.2.6. Plasmid Isolation**
- 2.2.1.2.7. Restriction Digestion and PCR Screening of Samples**
- 2.2.1.2.8. Sequence Verification of the Constructs**

2.2.2. Gene Expression

- 2.2.2.1. Monitoring the Expression of AGG2 Protein**
- 2.2.2.2. Culture Growth for Protein Purification**

2.2.3. Protein Purification

- 2.2.3.1. Affinity Chromatography by HisTrap Column**
- 2.2.3.2. Anion Exchange Chromatography by QTrap Column**
- 2.2.3.3. Size Exclusion Chromatography**

2.2.4. Analyses of Purified Protein

- 2.2.4.1. Absorbance Spectroscopy**
- 2.2.4.2. Circular Dichroism (CD) Spectropolarimetry**
- 2.2.4.3. Dynamic Light Scattering**
- 2.2.4.4. SDS and Native Polyacrylamide Gel Electrophoresis (PAGE) & Coomassie Staining and Western Blotting**

2.2.5. The Effect of DTT and Protein Concentration on the Oligomeric State of the Protein

- 2.2.5.1. Preparation of the samples for DTT Treatment**
- 2.2.5.2. Biophysical Analysis on both DTT and Protein Concentration Series**
- 2.2.5.3. SAXS and *Ab Initio* Low Resolution Molecular Envelope Modelling**

2.2.6. Homology Modeling of AGG2 Protein

- 2.2.6.1. Alignment of AGG2 Sequence with 1TBG**
- 2.2.6.2. Modeling of AGG2**
- 2.2.6.3. Docking of Monomers**
- 2.2.6.4. Comparison of Dimer Models with CRY SOL**

3. RESULTS

3.1. pETM-41 Cloning

- 3.1.1. AGG2 gene Amplification**
- 3.1.2. Production of the pETM-41 + AGG2 Construct**
- 3.1.3. Transformation of Bacteria**
- 3.1.4. Verification of Cloning**

3.2. pMCSG-7 Cloning

- 3.2.1. Gene Amplification for pMCSG-7 Cloning**
- 3.2.2. Blunt end Digestion of pMCSG-7 vector for ligation of AGG2 gene**
- 3.2.3. Digestion of LIC sites for Ligation with T4 DNA Polymerase**
- 3.2.4. Transformation of Bacteria**
- 3.2.5. Verification of Ligation of AGG2 gene**

- 3.3. Gene Expression & Growth Curve**
- 3.4. AGG2 Protein Purification**
 - 3.4.1. Nickel Affinity Chromatography of AGG2**
 - 3.4.2. Ion Exchange Chromatography**
 - 3.4.3. Size Exclusion Chromatography**
 - 3.4.4. Comparative Analysis of AGG2 and AGG2***
- 3.5. DTT Effect on the Oligomeric State of the Protein**
 - 3.5.1. SAXS Measurements**
 - 3.5.2. CD Measurements**
 - 3.5.3. DLS Measurements**
 - 3.5.4. PAGE Analysis of DTT Treated AGG2**
- 3.6. Effect of Protein Concentration of AGG2**
 - 3.6.1. SAXS Measurements**
 - 3.6.2. CD Measurements**
 - 3.6.3. DLS Measurements**
 - 3.6.4. Native – PAGE results**
- 3.7. Homology Modeling of AGG2**
- 3.8. Crystallization of AGG2**
- 4. DISCUSSION**
 - 4.1. AGG2 Cloning**
 - 4.2. AGG2 Protein Purification**
 - 4.2.1. Nickel Affinity Chromatography**
 - 4.2.2. Ion Exchange Chromatography**
 - 4.2.3. Size Exclusion Chromatography**
 - 4.2.4. Analyses of Purified Protein**
 - 4.3. DTT Effect on the Oligomeric State of the Protein**
 - 4.3.1. SAXS Measurements**
 - 4.3.2. CD Measurements**
 - 4.3.3. DLS Measurements**
 - 4.3.4. PAGE Analysis**
 - 4.4. Effect of Protein Concentration**
 - 4.5. Homology Modeling of AGG2**
- 5. CONCLUSION and Future Works**

APPENDIX A

APPENDIX B

APPENDIX C

APPENDIX D

APPENDIX E

To my grandfather...

I can still hear you calling "Tosunum" to me...

ACKNOWLEDGEMENTS

When I was lost, hopeless and with no clue to do for my future, Zehra “Hocam” held from my hand and opened a window that changed the way I look and I think. Without her aid and her leading personality, I would have no clue about deterministic work or going after one’s dreams. Although, sometimes I pushed her to the limits, she did not give up on me and always showed her kindness. The sleepless SAXS measurements in Hamburg are all among the best moments of my life. She all showed every one of us what “stamina” is. Hocam, the things that I want to list here are limitless, but the most sincere thing that I can say is for the rest of my life, you will be my dearest and #1 “hoca” in my academic career...

Remember Mert, when we all planned to attend grad studies in Sabanci and go abroad for PhD? We shared the same unlucky situation of rejection, but again shared the same great moments in Sabanci. You had been, and will be a “best buddy”. Then Erhan, you joined our little “crazy” team and brought a whole new color. The tiring nights in lab and the tiring running phases in Hamburg were completely full of fun and full of unforgettable moments. The things that you had done for my “kına” and wedding ceremony are also invaluable. Simply put, thanks guys for being there with me...

My teachers, Selim Cetiner, Yuda Yurum, Batu Erman and Ugur Sezerman... Thanks for being kind in my thesis presentation. Also, sorry for the burdens that I had been causing (especially talking with my friends) in your courses. Selim Hocam, I still hold the promise to ride your car when I buy a fine suit and take you to Kalamis to eat Doner with you...

All my friends; Ani, Nazli, Melda, Elif, Kaan, Emre, Canan, Beyza, Ayca, Ali, Tugsan, Tugce & Tugce (sorry for the ones that I did not name)... Thanks for being there when I needed someone to talk and for all the fun that we had together...Each and every one of you is very precious to me...

My “ex-patrons”, Burcu and Filiz, thanks for all the things that you had taught me. Your helps and the experiences that you shared were all wondrous for me...

Nurten, I do not want to acknowledge you here, for until my last breath is given, I will be by your side and continue to be your biggest problem in the world :)

Biraz da aileme teşekkür etmek isterim. Annem, babam: sizin ne olursa olsun bana koşulsuz desteğiniz olmasa idi bu günlere gelmeyi hayal bile edemezdim...Size minnetim her zaman artarak büyüyecek. Teyzem, halam, annanem, dedem, babannem, amcam ve kuzenlerim...Sevginizin ve desteginizin her yerde ve her zaman yanımda olacağını biliyorum.

LIST of FIGURES

Figure 1.1 Heterotrimeric G Protein interacting with a GPCR

Figure 1.2 The G-Protein complex interacting with a GPCR

Figure 1.3 Comparison of bovine G-protein complex (PDB:1TBG) with plant homolog

Figure 1.4 The initiation of olfactory pathway in humans. The GPCR (OR) is activated by odorant molecules

Figure 1.5 Activation of tastant pathway by G-Protein

Figure 1.6 The localization shift of rhodopsin due to light reception

Figure 1.7 A general scheme for the function of G-protein regarding the tissue and the interval of a plant's life span

Figure 1.8 Probable functions of AtRGS1

Figure 1.9 The alignment of human gamma subunits with AGG1 and AGG2

Figure 1.10 The effect of silencing of AGG2 genes in seed development of *A. thaliana*

Figure 1.11 A brief summary of functional difference of AGG1 & AGG2

Figure 1.12: CD spectra of α -helix (dots), β -sheet (short dashes) and random coil (solid line) shown and used as references

Figure 1.13 The scheme of laser hitting a particle in a solution and the detection done by the detector in DLS machine

Figure 1.14 An intensity vs size graph of a typical DLS measurement

Figure 1.15 Monodisperse and Polydisperse particles in a solution

Figure 1.16 The overall summary of Dynamic Light Scattering

Figure 1.17: Distance distribution function from examples for simple structures

Figure 1.18: EMBL Hamburg X33 beamline sketch

Figure 3.1 Amplified *AGG2* gene for cloning with pETM-41

Figure 3.2 Verification of double digestion of pETM-41 & amplified *AGG2*

Figure 3.3 Comparison of thickness of bands to determine the concentration of digested & purified samples

Figure 3.4 Results of digestion and PCR screening of constructs

Figure 3.5 Verification of amplification of *AGG2* with LIC Site

Figure 3.6 *SspI* Digestion of pMCSG-7 Plasmid

Figure 3.7 Concentration Determination before Annealing of *AGG2* into pMCSG-7 vector

Figure 3.8 Digestion and PCR Screening of Construct (left, construct, right pQE80-L for both digestion and PCR reaction results)

Figure 3.9 Growth Curve of native and transformed TOP 10 cells with pMCSG-7 Construct

Figure 3.10 SDS-PAGE of Samples from 250 minute of induced and non-induced cells

Figure 3.11 The scheme for protein purification

Figure 3.12 Nickel affinity column fractionation of recombinant *AGG2* proteins

Figure 3.13 Results of SDS-PAGE analysis of HisTrap *AGG2* Pools

Figure 3.14 Ion Exchange Chromatography Elution Profiles of *AGG2*

Figure 3.15 SDS-PAGE Results of Ion Exchange purified *AGG2* Pools

Figure 3.16 Elution profile of Size Exclusion Chromatography

Figure 3.17 SDS-PAGE analysis results of Size Exclusion Chromatography peaks

Figure 3.18 Results of DLS and CD measurements on *AGG2** (top) and *AGG2* (bottom)

Figure 3.19 Dependence of the X-ray scattering from 1.2 mg/ml *AGG2* on the DTT concentration in the buffers

Figure 3.20. Averaged *ab initio* models of *AGG2*

Figure 3.21 CD Spectra of DTT Concentration Series of *AGG2*

Figure 3.22 DLS measurements of change in size of AGG as a function of DTT concentration

Figure 3.23 Coomassie Stained Native – PAGE for DTT Concentration Series of AGG2

Figure 3.24 Western Blot Results of DTT Concentration Series of AGG2

Figure 3.25 Dependence of radius of gyration (R_g) on the AGG2 concentration

Figure 3.26 CD Spectra of DTT Concentration Series of AGG2

Figure 3.27 DLS Intensity Graph for Protein concentration series of AGG2

Figure 3.28 Coomassie stained Native –PAGE Results of Protein Concentration Series

Figure 3.29 Alignment of AGG2 amino acid sequence with that of gamma subunit of transducin

Figure 3.30 Homology Modelling of AGG2 by MODELLER program

Figure 3.31 Protein Docking Server Results for the dimerization of AGG2

Figure 3.32 Overlap of GramX docking result with *ab initio* modeling of SAXS measurement

Figure 3.33 Overlapping the result obtained from the CRY SOL software and the data obtained from SAXS Measurement

Figure 3.34 Picture taken by the robotic system at EMBL Hamburg PETRA crystallization facility

LIST of TABLES

Table 2.1: Primers used to insert AGG2 gene into pMCSG-7 and pETM-41 vectors

Table 2.2 PCR Reaction Chemicals

Table 2.3 PCR conditions used for addition of cloning sites to AGG2 gene

Table 2.3 The Restriction Digestion reaction of AGG2 gene and pETM-41 plasmid

Table 2.4 Ligation reaction of AGG2 into pETM-41 vector

Table 2.5 PCR Reaction Chemicals

Table 2.6 PCR conditions used for addition of cloning sites to AGG2 gene

Table 2.7 *SspI* reaction Content

Table 2.8: The Reaction Content of T4 DNA Polymerase

Table 2.9: Digestion Screening of Construct

Table 3.1 AGG2 Structural Characterization after Size Exclusion Chromatography

Table 3.2 Oligomeric state transition shown as tetramer – dimer percentages

Table 3.3 Effect of DTT on the oligomeric state of AGG2

ABBREVIATIONS

AGB1	Beta Subunit of <i>A. thaliana</i> G-Protein
AGG2	2. Gamma Subunit of <i>A. thaliana</i> G-Protein
bp	Base pair
BSA	Bovine serum albumin
CD	Circular dichroism
Cys	Cysteine
C-terminus	Carboxyl terminus
Da	Dalton
DNA	Deoxyribonucleic acid
DLS	Dynamic light scattering
d_{\max}	Maximum distance
dNTP	Deoxyribonucleotide triphosphate
DR	Dummy residues
DTT	Dithiothreitol
EDTA	Ethylenediaminetetraacetic acid
EFPI:	EDTA-Free protease inhibitor cocktail
FT:	Flow Through
GPA1:	Alpha Subunit of <i>A. thaliana</i> G-Protein
GPCR:	G-Protein Coupled Receptor
GTPase:	Enzyme hydrolyzing GTP to GDP
HCl	Hydrochloric acid
HEPES	4-(-2-hydroxyethyl)-1-piperazineethanesulfonic acid
IPTG	Isopropyl- β -D-thiogalactoside

I(0)	Forward scattering
kDa	Kilodalton
mg	Milligram
MgCl ₂	Magnesium chloride
ml	Milliliter
μl	Microliter
NaCl	Sodium chloride
Ni	Nickel
nm	Nanometer
N-terminus:	Amino Terminus
PAGE	Polyacrylamide gel electrophoresis
PBS	Phosphate buffered saline
PCR	Polymerase chain reaction
PMSF	Phenylmethanesulphonylfluoride
P(r)	Pair distance distribution function
R _g	Radius of gyration
R _h	Radius of hydration
SDS	Sodium dodecyl sulfate
SAXS	Small angle X-Ray scattering
α	Alpha
β	Beta
Δε	Molar ellipticity
θ	Ellipticity

1. INTRODUCTION

1.1. What are Heterotrimeric G Proteins?

Heterotrimeric guanine-nucleotide binding (G) Proteins are vital effector proteins in the signal transduction pathways of both animals and plants by transmitting the signal received by membrane bound receptors to the downstream factors (Simon M.I., 1991). G-Proteins consist of three different subunits: α , β and γ . Proteins upstream of G-Protein are all classified under a common name: G-Protein Coupled Receptors (GPCR). Signals received by GPCRs forces a conformational change in heterotrimeric complex and the protein dissociates into two components: α subunit and $\beta\gamma$ dimer.

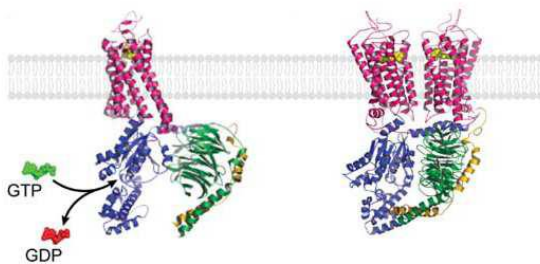


Figure 1.1 Heterotrimeric G Protein interacting with a GPCR (Oldham, 2006).

1.2. G-Protein Signaling

α subunit of G – Proteins contains a Ras-like domain which has a GDP/GTP binding domain and a GTP hydrolysis activity. When interacting with $\beta\gamma$ dimer, the binding site of α subunit contains a single GDP. The interaction of activated GPCR by an external signal causes a conformational change in the structure of α subunit and causes the release of the GDP and binding of a single GTP to the empty cleft (Morris A.J., 1999). When the activity of alpha subunit is diminished, the GTP bound is hydrolyzed to GDP and the heterotrimer forms in its basal form. The initial studies assumed that only α subunit is responsible of the protein

activity, but more and more work showed that the $\beta\gamma$ dimer also involves in signal transduction activity (M. E. Ma H., 1990).

The signaling of the G-Protein is tightly connected to the state of the guanine in the cleft of alpha subunit. Thus regulation of the state of guanine becomes the main switch of the signal transduction related to G-Proteins. The activity upon guanine is initiated by the GPCR interacted. The conformational change of GPCR causes the GDP to be exchanged by a GTP, so the GPCR in this situation acts as a guanine exchange factor (GEF). Additional to the initiation of the signal, there are Regulator of G-Protein Signaling (RGS) proteins that specifically accelerate the GTPase activity of α subunit (Blundell TL., 2000). The RGS proteins bind the alpha subunit from the site that effector proteins bind, so they inhibit the GEF activity of other proteins additional to their GTPase – accelerating protein (GAP) activities (Siderovski D.P., 1996). The signaling of G-Proteins is summarized in the figure 1.2 below:

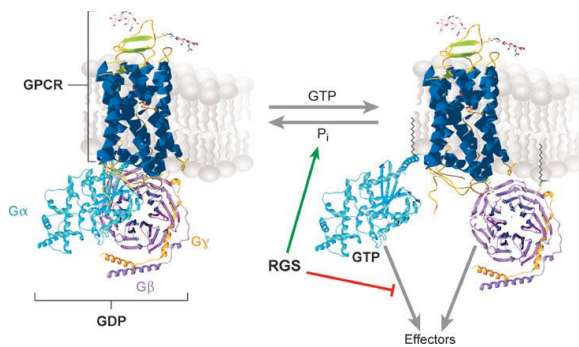


Figure 1.2 The G-Protein complex interacting with a GPCR. The interaction of GPCR forces the bound GDP inside the cleft of alpha subunit to exchange with a GTP, thus activating the heterotrimeric complex. The RGS proteins enhances the GTPase activity of alpha subunit, thus inhibits the signal transduction downstream of G-Protein (Temple B., 2007)

1.3. Mammalian vs Plant G-Protein

1.3.1. Genome Based

There are 16 α subunit genes in human genome which encode 23 different alpha subunits that are divided in four distinct groups both according to the expressing cell and function (Simon M. I., 1991). 5 different β subunits are expressed in human cells (Fletcher J.

E., 1998) and 12 different human γ subunits are reported that are crucial for the localization & formation of the heterotrimer and direct function of the $\beta\gamma$ dimer itself (Clapham D. E., 1997).

In comparison to the mammalian homologs, only one α subunit is reported for plant model organisms *Arabidopsis thaliana* and rice observed in every cell (the expressed protein is named as GPA1) (Fujisawa Y., 2001). Likewise, plants are observed to contain only one β subunit homolog (protein expressed named as AGB1) (Weiss CA., 1994). Until recently, it was thought that the plants happened to have 2 γ subunits in their genomes (Kato C., 2004) but a very recent study showed that a third gamma subunit is located in the *A. thaliana* genome. The function of the third homolog is unclear but new studies are imminent for its function (Thung L., 2012) (the names of the gamma subunits are denoted as AGG# where the hash tag is either 1, 2 or 3).

1.3.2. Structure Based

The α subunit of G – Proteins consist of an N-terminus helical tail that has a helical groove to bind $\beta\gamma$ dimer, a Ras-like GTPase domain and a large α -helical domain. The guanine bound to the subunit acts as a coordination point between the last two domains; changing the conformation of the protein in active and inactive form (Perfus-Barbeoch L., 2004). Amino acid sequence of the plant variant of α subunit is highly similar to the mammalian homolog; especially regarding the residues important for the functioning.

Beta subunit acts as a scaffold protein and interacts with other proteins, γ and α subunits; thus being the most crucial subunit in the signal transduction process. The subunit was first found to be a major signaling element in yeast (Chen JG., 2004). The seven WD-40 repeats, a tryptophan – aspartic acid sequence that repeats every 40 amino acids, is also involved in beta subunit sequence which helps to form a beta-propeller structure by seven antiparallel beta-sheets, that is also seen in mammalian homologs (Neer E. J., 1994).

Gamma subunits in plants were initially discovered by genomic studies. The expression level was confirmed by yeast-two hybrid studies that used β subunit as bait (Mason MG., 2001). The mammalian homologs have a mass of 8 to 10 kDa; the subunits tend to be small in all mammalian organisms (Ray K., 1995). The *A. thaliana* subunits AGG1 and AGG2 have a mass of around 11 kDa (Mason MG., 2000).. The C-terminus of the subunit has a CAAX box for isoprenyl modification and an N-terminal α helical coiled-coil domain for

beta subunit interactions. Also, the N terminus of gamma subunits of almost all organisms tend to be very similar up to first 20 amino acids (Cook L., 2001).

Heterotrimeric complex of G-protein has been well established in literature through many studies. The first and well-known structure of G-Protein was modeled from bovine tissue and nomenclatured as '1TBG' in Protein Data Bank (PDB) (Sondek J., 1996). The structural difference of the bovine heterotrimer with the plant homolog is detailed in figure 1.3 below:

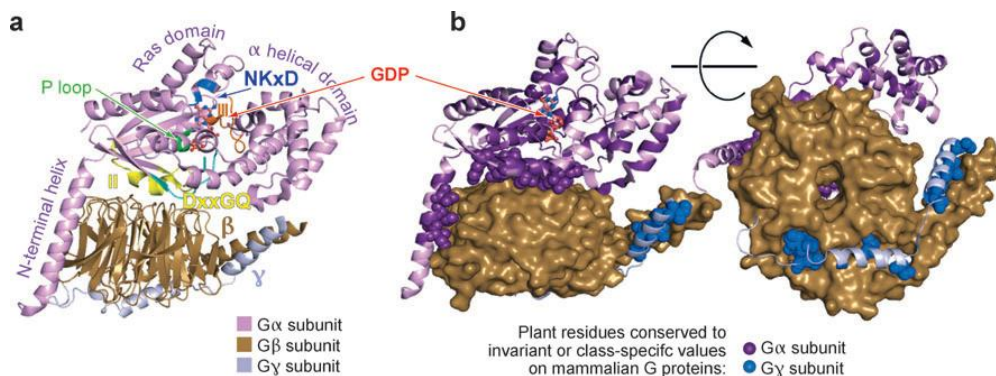


Figure 1.3 Comparison of bovine G-protein complex (PDB:1TBG) with plant homolog (a. the bovine G-protein complex, b. The resemblance of the plant homolog) (Temple B., 2007)

The bovine homologs of the subunits were used for the modeling of the plant heterotrimer complex. The comparison showed that the protein interaction sites are conserved in the plant homolog. α subunit residues show conservation that are class-specific; the four alpha classes in mammals. This was found to be a clue that the G-Protein in the plants diverted from the mammalian homologs by the earliest ancestors of the protein. The latter is the same for both gamma and beta subunits. These subunits show approximately 80% resemblance to their mammalian homologs. The conserved residues of the gamma subunits lie at the N and C termini of the protein, except the interaction sites with β . Interesting part is that the beta subunit interaction sites are conserved among plant species. The rest of the residues that don't show resemblance to the mammalian homologs of gamma subunit are species specific (Temple B., 2007). In the figure 1.3.b, the blurry regions show the conserved regions of the protein in plant homologs.

1.4. Functions of G-Proteins in Mammals and in Plants

1.4.1. In Mammalian Cells

Besides the structure of the protein, the functions of heterotrimeric G-proteins have been a hot topic. Especially, the ever increasing numbers of studies about the G-Protein Coupled Receptors (GPCR) incremented the importance on the G-Proteins back again. It is stated that there are at least 800 GPCRs in mammalian cells that share 25% or more sequence identity in a particular subfamily but show a slight or simply no similarity among families (Pierce KL., 2002).

α subunit and $\beta\gamma$ dimer both contribute to certain signal transduction pathways. The very first alpha subunit function in mammalian cells found was interaction with adenylyl cyclase (AC). α_i was found to inhibit the action of AC and the α_s was found to stimulate the functionality of AC; two homologs in mammalian cells. Studies around the globe showed that the expression pattern of AC is tissue-specific and responds positively or negatively to different sets of alpha subunits (Sunahara R. K., 2002). Regulation of cyclic GMP-gated $\text{Na}^+/\text{Ca}^{2+}$ in sensory pathways is also achieved by alpha subunit (Arshavsky V. Y., 2002). Phosphoinositide-specific phospholipases like 'PI-PLC' are also influenced by direct intervention of G-Proteins (Rhee G., 2001). The most crucial pathway that G-Proteins involve can be accounted as the sensory transduction through GPCRs.; the odorant, tastant and phototransduction pathways. The cDNA library of the olfactory pathway included a special G-Protein, G_{olf} , which activated the adenylyl cyclase to initiate the odour reception (Ronnelt G., 2002):

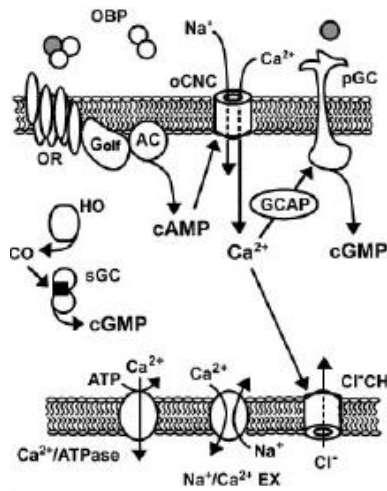


Figure 1.4 The initiation of olfactory pathway in humans. The GPCR (OR) is activated by odorant molecules. The conformational change activates the G_{olf} , then AC is activated, so on and so forth (Ronnett G., 2002)

The taste stimulus is dependent to the G-protein presence. GPCRs specific to the tastant pathway (TRs) activate a special G-protein, G_{gust} , and the complex further activates $PLC\beta 2$:

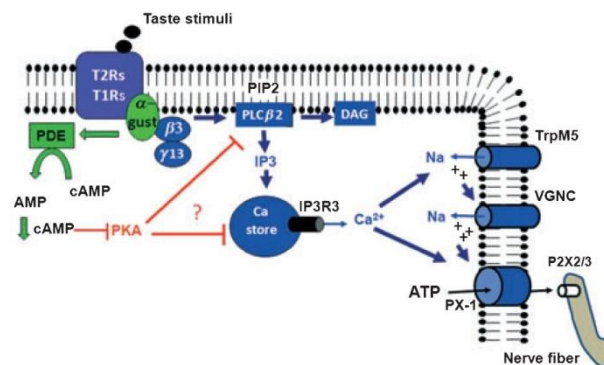


Figure 1.5 Activation of tastant pathway by G-Protein. The activated GPCR (T2R of T1R) activates G_{gust} and the complex further activates $PLC\beta 2$ (Kinnamon S., 2012)

Phototransduction is, with no surprise, governed by G-proteins. Again, a special G-protein, transducin, is responsible for the initiation of molecular basis of sight. Rhodopsin is the GPCR that is activated by light and initiates the phototransduction process. The protein is embedded in a lipid bilayer surrounded by phospholipids within the disk membranes of rod cells in the eyeball (Avediano MI., 1995). By the reception of light, the localization of rhodopsin gets in close proximity to transducin and initiates the phototransduction pathway:

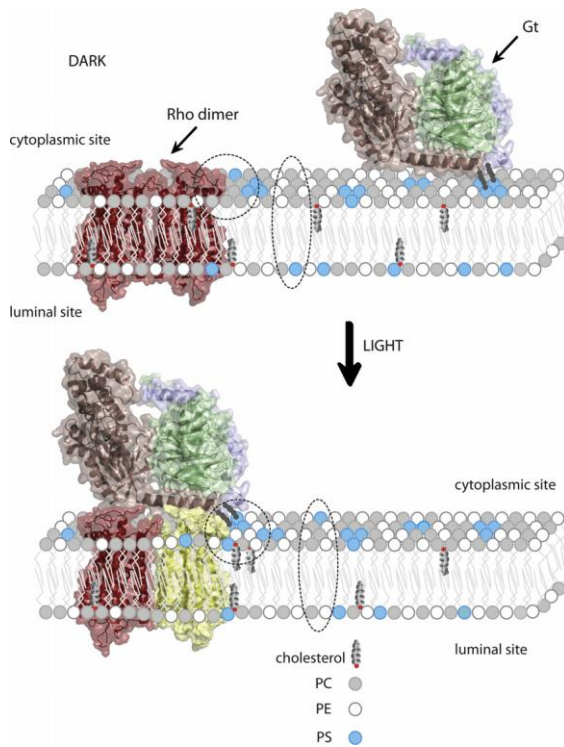


Figure 1.6 The localization shift of rhodopsin due to light reception (Jastrzebska B., 2011).

1.4.2. In Plant Cells

The functionality of the G-Protein in plants is not well established, just like the structure compared to mammalian homologs. The studies all depend on the overexpression or deletion of G-protein subunit genes and recording the changes occurring further. A simple but general scheme for the function of G-protein subunits in plant cells (here, *A. thaliana* as the model organism) is shown in figure 1.7:

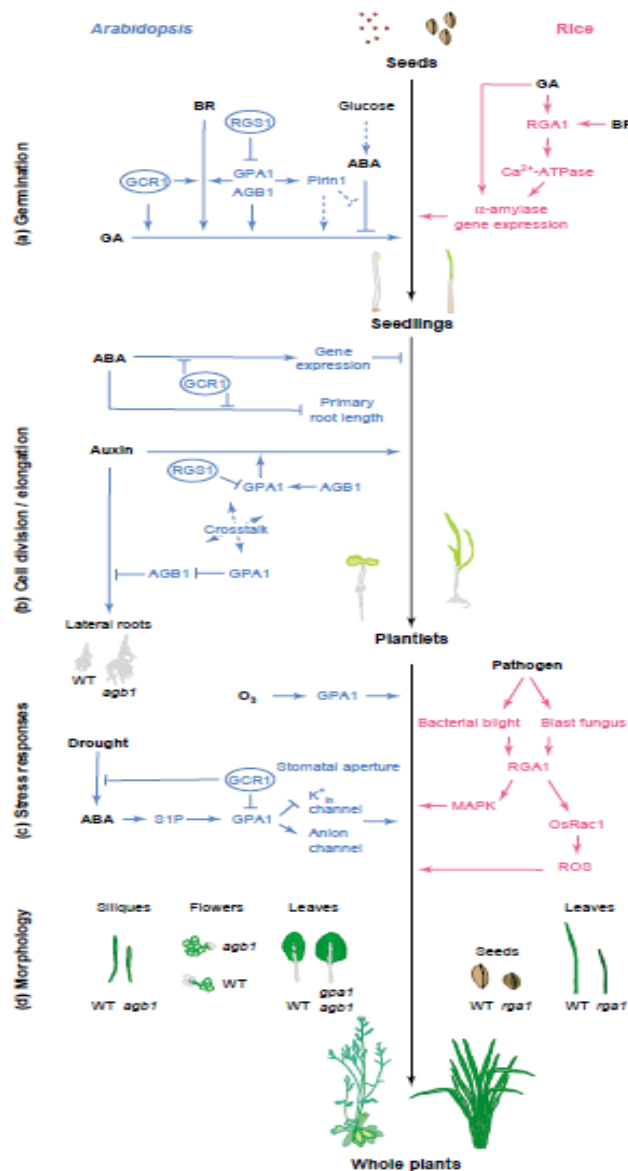


Figure 1.7 A general scheme for the function of G-protein regarding the tissue and the interval of a plant's life span (Perfus-Barbeoch L., 2004)

Direct involvement of G-protein in different lapses and tissues of the *A. thaliana* have been reported by many researchers. When the GPA1 gene is silenced, the seeds turn into a more dormant state. Abscisic acid (ABA) is known to inhibit the seed germination, and the addition of ABA to the mutated *A. thaliana*, the germination inhibition is more stable (Lapik YR., 2003). The silencing of AGB1 shows a very similar effect as GPA1. The overexpression of GPA1 and AGB1 also show an approximately million fold increase in sensitivity of germination signals like gibberellins (GA) (Ma H., 2001).

Primary root growth in *A. thaliana* is hindered when GPA1 gene is silenced and cell proliferation is imminent when the protein is overexpressed (Chen J.G., 2003). Like the situation in seeds, silencing of AGB1 gene slows the cell proliferation process. Interestingly, the case for lateral roots is different, the silencing of AGB1 gene inhibits the lateral root growth and the silencing of GPA1 gene greatly enhances the lateral root growth. This contradiction simply shows that the GPA1 subunit of *A. thaliana* G-protein enhances the root growth and AGB1 subunit enhances it; a fine example of different roles for two functioning units of G-proteins (Ullah H., 2003).

Stress induction to *A. thaliana* causes certain mechanisms to overwhelm the mortal effects to the plant. Without surprise, G – Protein is involved in such responses. The O₃ exposure to the plant reduces stomatal apertures (Mansfield T.A., 1998). The response is also revoked by abscisic acid. The silencing of GPA1 exhibits reduced response to O₃ in plant at whole leaf level. Within the single guard-cell level, GPA1 silenced plants shows implications of ABA insensitivity. The K⁺ channel and phosphatidylinositol-phospholipase C (PLC) mechanism is found to be hindered for the lack of response in absence of GPA1. This is a direct evidence to the relation of stomatal opening to G-proteins (Ng C.K., 2001) (Jacob T., 1999).

The molecular basis of all the functions detailed show high levels of similarity to well-defined mammalian G-Protein complexes. The Ca²⁺ channels are directly linked to the G-Protein in neuroendocrine and cardiac tissues. The opening of the channel is initiated by G-protein signaling (Catterall W.A., 2000). Pathogen sensitivity response invoked by Ca²⁺ channels is greatly enhanced by overexpression of alpha subunit of plant cells and silencing causes the diminish of the response; a direct correlation of the function similarity between plant and mammalian G-proteins (Gelli A., 1997). In mammalian cells, a direct interaction between K⁺ channels and G-proteins has been detected via an important class of heterotetrameric ion channel called “G-protein-activated inwardly rectifying potassium” (GIRK) (Mark M.D., 2000). Cardiac GIRK was found to be interacting with a phospholipid metabolite named sphingosine-1-phosphate (S1P) which interacts with a distinct set of GPCRs (Himmel H.M., 2000). Stomatal opening inhibition mediated by ABA happens through the activity of K⁺ channels. The silencing of GPA1 gene creates insensitivity to the ABA effect by inward K⁺ current. Thus, the leaves of these plants lose water through these stomatal openings (Wang X-Q., 2001).

1.5. Regulation of G-Protein Signalling

Earlier studies claimed that the only regulation in G-protein signaling was achieved via the intrinsic hydrolysis rate of GTP in the cleft of α subunit and acceleration of the rate by certain alpha subunit effectors such as PLC proteins (Berstein G., 1992). A study in 1996 showed that there is a class of proteins that function as GTPase accelerating factors (GAPs) that are later named as “regulators of G-protein signaling” (RGS) proteins (Druey K.M., 1996). The proteins contain a 120 amino acid long RGS domain, which contains a nine alpha-helix bundle which interacts with the switch region of alpha subunit that stabilizes the transition state for GTP hydrolysis (Tesmer J.J., 1997). Initially the protein was thought only to negatively regulate the function of alpha subunit, but more and more studies showed new homologs of RGS proteins and varying regulatory function that are cell-specific (Doupnik C.A., 1997).

For a long time, no homologs of RGS proteins were to be found in plant cells. In 2003, a hybrid protein that contained an RGS box and a 7 transmembrane (7TM) was discovered and named as AtRGS1 (Chen J.G., 2003). The protein possess both GEF (from 7TM) and GAP (from RGS-box) properties. The GAP activity of the protein is confirmed by biochemical studies, but GEF function is yet to be discovered. The figure 1.8 shows certain scenarios for the probable functions of the AtRGS1 protein:

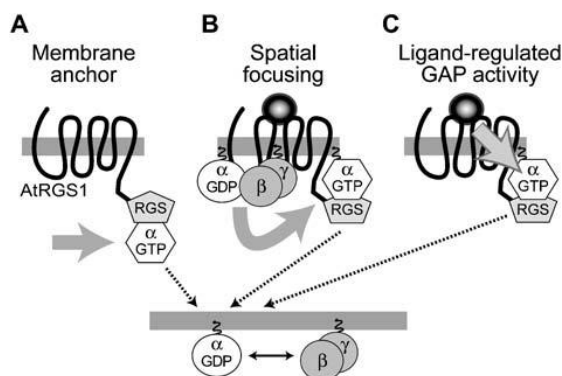


Figure 1.8 Probable functions of AtRGS1. A – Protein may recruit activated GPA1 proteins to specific membrane microdomains. B – AtRGS1 may be a ligand activated GPCR that can regulate the catalysis of both guanine nucleotide exchange in heterotrimeric G-

Protein complex and GTP hydrolysis by the activated alpha subunit. C – AtRGS1 may act directly as a GAP protein that deactivates the GPA1 protein (McCudden C.R., 2005).

1.6. Gamma Subunits of G-Proteins in Plants

The main focus of this study is based on the AGG2, one of the three γ subunit homologs in *A. thaliana*. The protein was first cloned, expressed and interacted with AGB1 by yeast two hybrid in a study in 2001, confirming the protein to be a subunit of plant G-protein complex (Mason MG., 2001). The specific regions that are well-defined in mammalian homologs of γ subunits are also found in AGG2: A CAAX box on its C terminus for prenyl binding and a coiled coil alpha helical structure for β subunit interaction (Bohm A., 1997).

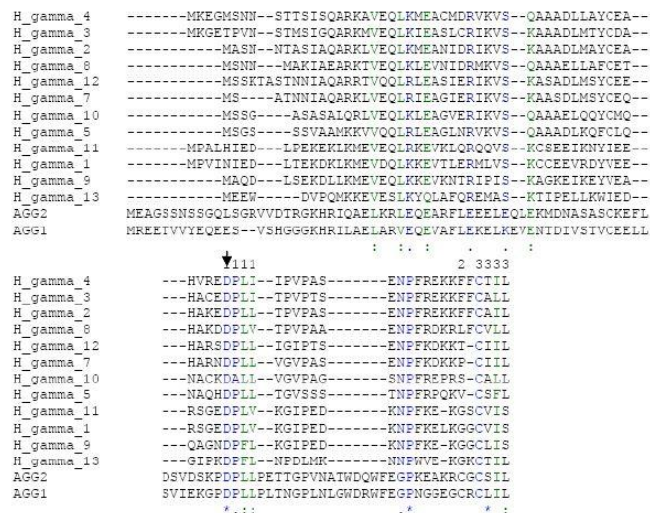


Figure 1.9 The alignment of human gamma subunits with AGG1 and AGG2. Denoted ‘1’ in the figure shows the β – γ interactions sites. ‘2’ and ‘3’ denotes the CAAX box for prenylation (Kaplan, 2009).

Functional studies for AGG1 & AGG2 proteins involve either silenced version of the plants or the overexpression of protein in certain tissues. D-Glc and osmotic sensing during germination has been shown to be dependent on AGG expression (Trusov Y., 2007b). The seedling development of *A. thaliana* is hindered when the AGG homologs are absent:

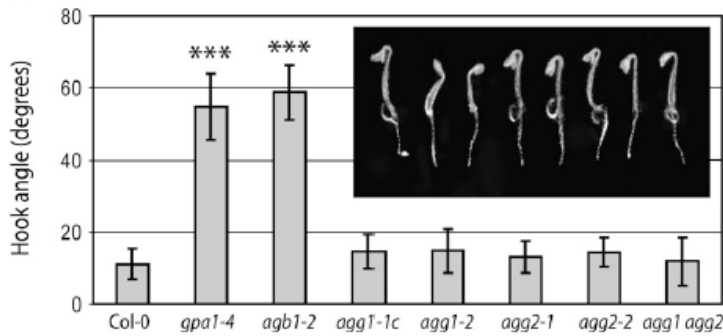


Figure 1.10 The effect of silencing of AGG2 genes in seed development of *A. thaliana*. The names in the X-axis denote the silenced genes in the plant (Trusov Y., 2008).

Different expression patterns were observed for AGG1 and AGG2 in a tissue-specific manner. The patterns generally show that where there is AGG2, AGG1 expression is hindered and vice versa (Trusov Y., 2007a). The changes in the localization bring in change in the functionality of the proteins. The examples are varying:

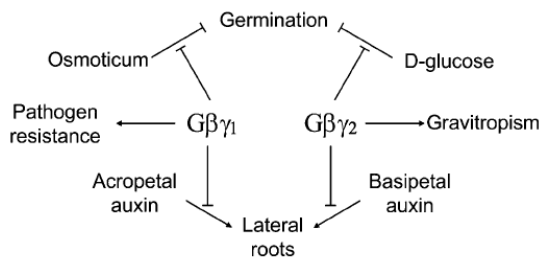


Figure 1.11 A brief summary of functional difference of AGG1 & AGG2 (Trusov Y., 2007a)

1.7. Biophysical Methods used for Structural investigation of AGG2

1.7.1. Circular Dichroism Spectropolarimetry

Circular dichroism (CD), arising from differential absorption of left and right handed circularly polarized light by proteins and nucleic acids in a solution, is a commonly used technique for spectroscopic characterization of proteins due to the techniques unique to get a grasp of secondary structures of proteins because the secondary structure of proteins show a very specific spectra pattern. CD differentially absorbs circularly polarized light by proteins and nucleic acids in solution: both right and left handed. Even though CD provides only low

resolution structural information, its extreme sensitivity to *changes* in oligomerization state of a protein makes it a powerful tool for phenomena such as dimer-tetramer oligomeric state changes of proteins. Additionally, CD measurements can be done with small sample volumes in a wide range of buffer systems.

The reasons to apply CD for protein characterization can be summarized as;

- 1) Protein secondary structure estimation by using additional softwares,
- 2) Detection of conformational changes of proteins and nucleic acids caused by changes in pH, salt concentration, solvents
- 3) Unfolding conditions and states for proteins and nucleic acids,
- 4) Ligand interactions of proteins and/or nucleic acids,
- 5) Kinetics of macromolecule interactions. (Martin & Schilstra, 2008)

Figure 1.12 shows CD spectra of secondary structure elements such as α -helix, β -sheet and random coils in the near UV-range (180 to 260 nm) (Brahms & Brahms, 1980).

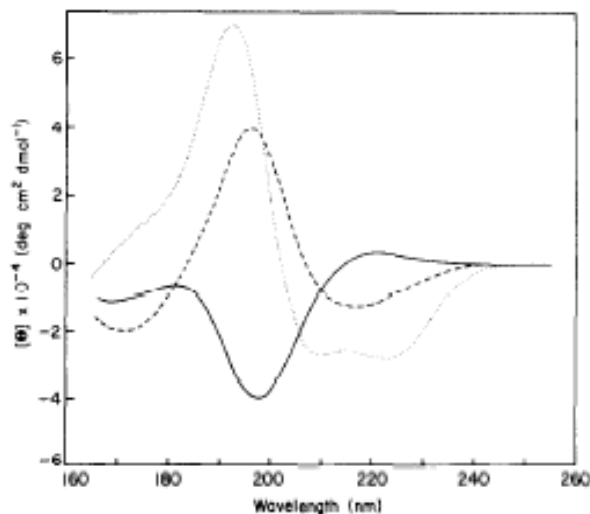


Figure 1.12: CD spectra of α -helix (dots), β -sheet (short dashes) and random coil (solid line) shown and used as references. (Brahms & Brahms, 1980)

1.7.1.1. Determination of Secondary Structure with CD

Deduction of secondary structure information from CD spectra starts by converting ellipticity values to molar ellipticity ($\Delta\epsilon$), eliminating the changes arising from concentration differences among the used samples. Following formula is used for the operation described:

$$(1.1) \quad \Delta\epsilon = \frac{100*\theta}{C*l*kDa}$$

Where θ is ellipticity in milidegrees, C is concentration in molar, l is pathlength in centimeters and $\Delta\epsilon$ is molar ellipticity in $\text{deg cm}^2 \text{ dmol}^{-1}$ and kDa referring the weight of a protein calculated by its amino acid sequence.

Spectra of secondary structures of proteins are unique and very easily observed during the measurements. Specific natures of secondary structures help to maintain such stability and specificity. The consequence of this property helped scientists to develop methods and algorithms to deconvolute CD spectra into secondary structure information present in a single protein molecule in a solution; providing invaluable information about the overall secondary structure of a protein (Whitmore L., 2007). Libraries obtained from the spectral measurements of various proteins with varying secondary structures help build the main frame of CD deconvolution. Early methods of deconvolution included simple linear and non-linear least squares analyses based on representative reference spectra of secondary structures previously exemplified (Chang C., 1978). The problem of having exact solutions was further compensated by requiring calculated fractions of all the secondary structure components to be non-negative and by normalizing the solution obtained to a total amount of one so that the sum of the values obtained would not require having a precise knowledge of protein concentration, Also this way, the addition of components would not cancel each other for the components of the secondary structure of a protein can't hinder each other. Additional to all the information provided, it is also important to state that the alpha helices in a protein are easier to detect because a) the alpha helices are well defined and generally more regular and b) the CD signals of alpha helices are very intense and highly specific. Beta sheets in return are more variable having both parallel and antiparallel natures and different twists and turns (Whitmore L., 2007)

DichroWeb is a valuable tool that is used by many users that are trying to evaluate their CD spectra regarding the secondary structures of proteins (Whitmore L., 2011). After

creating an account, the data that has been altered using the molar ellipticity formula explained above is loaded to the system. The wavelength range and the step range of the file input is given as an input to the system. As the next and final step, algorithm for the data set is chosen according to the needs of the user. Many algorithms are listed for users to choose especially regarding the difference of the quality and the data range of the measurements.

1.7.2. Dynamic Light Scattering

Dynamic light scattering (DLS), also known as Photon Correlation Spectroscopy, is one of the most popular methods to define the size of the particles in a solution. The method simply measures the light that is scattered from dissolved macromolecules or suspended particles. The method depends on the time dependent fluctuations in the scattering intensity arising from the Brownian motion of the particles in the solution. The hit of the laser causes a Doppler Shift and changes the wavelength of the moving particle (Arzensek D., 2010).

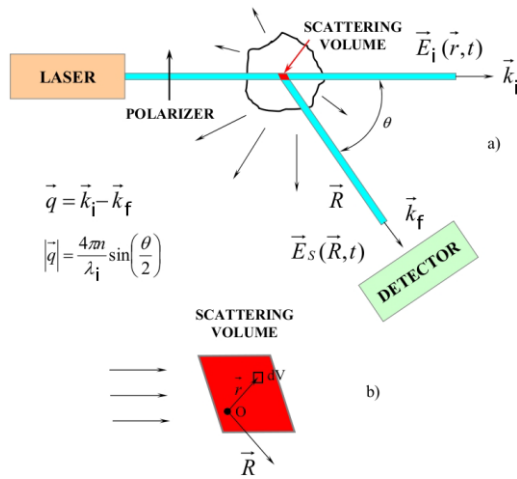


Figure 1.13 The scheme of laser hitting a particle in a solution and the detection done by the detector in DLS machine (Arzensek D., 2010)

The fluctuations of the particles are collected by the detector. If the data collected is identical, then there would be no cancellation and the intensity of the beam increases. All these data are stored in an intensity function and further converted by a correlation function (this is also applicable to the volume and the number of particles in the solution):

$$G(\tau) = \lim_{T \rightarrow \infty} \left| \frac{1}{T} \int_0^T I(t) I(t + \tau) dt \right|$$

With the help of the formula given above, the diffusion coefficient, D_T , can be calculated (Lomakin A., 2005). The diffusion coefficient further helps to find the hydrodynamic radius of the particles in the solution. Stokes – Einstein equation leads to the finding of hydrodynamic radius:

$$R_h = \frac{k_b T}{6\pi\eta D_T}$$

where R_h is the hydrodynamic radius, k_b is the Boltzmann constant, T is temperature in Kelvin and η is the viscosity of the solvent. The Laplace transformation of the size distribution gives the last intensity graph of the molecules in the solution (Wen J. H., 2010):

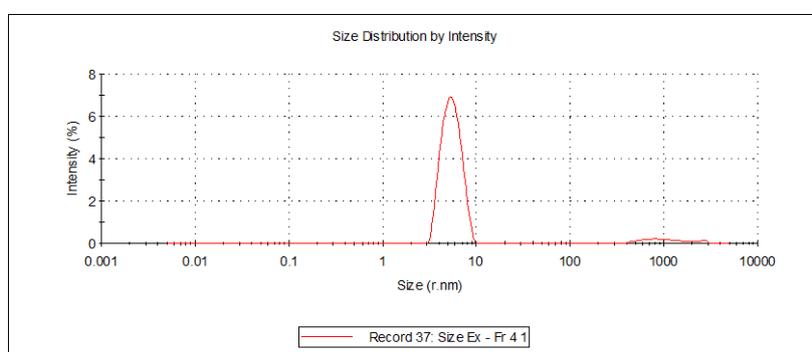


Figure 1.14 An intensity vs size graph of a typical DLS measurement.

Proteins do not always found in a solution in a single conformation or in a singular oligomeric state. The polydispersity of the proteins can also be measured in a DLS measurement with the help of the intensity graph obtained:

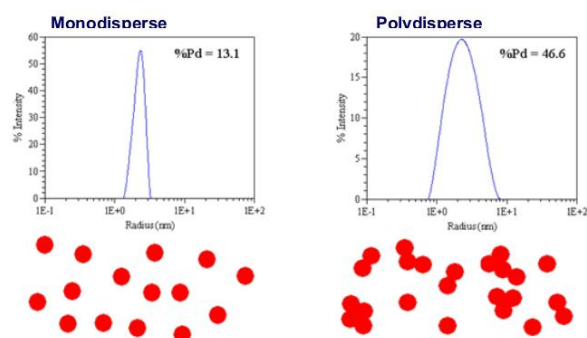


Figure 1.15 Monodisperse and Polydisperse particles in a solution (Instruments, 2009)

The width of the graph gives a strong clue about the disparity level of the protein solution and the percentage of polydispersity can be found by Gaussian distribution:

$$\text{Polydispersity perc.} = \frac{\sigma^2}{Z_D^2}$$

where σ is the standard deviation and Z_D is the average size of the particles (Arzensek D., 2010). A general outline of the DLS system and the measurement evaluation is given in the figure below:

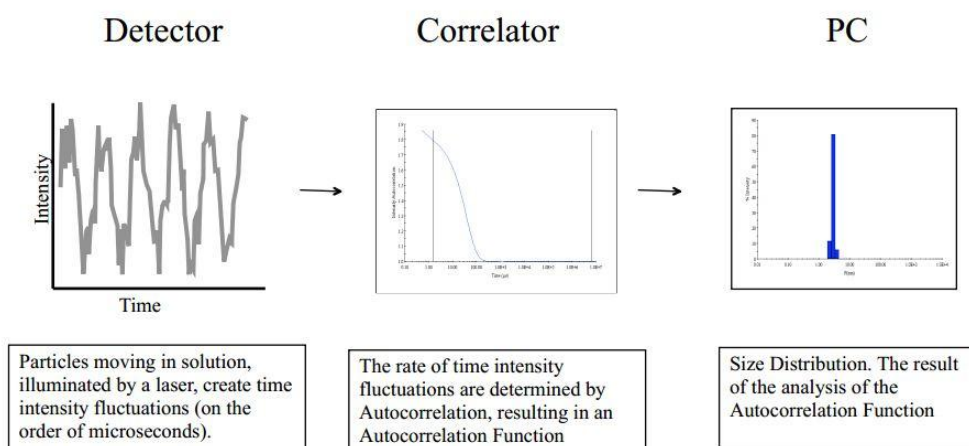


Figure 1.16 The overall summary of Dynamic Light Scattering (Yao B., 2004)

1.7.3. Small angle X-Ray scattering

Small angle X-Ray scattering (SAXS) is used for low concentration homogeneous particles in solution to determine their structures. Easy sample preparation brings data obtained to be in low quality (D. I. Svergun & Koch, 2003) and extraction of three-dimensional structure information from one dimensional causes many problems and difficulties. Reliable SAXS data can only be collected using synchrotron radiation because of the short half life of measured molecules and their weak scattering patterns (Michel H. J. Koch, Vachette, & Svergun, 2003)

1.7.3.1. SAXS Data Processing

$I(s)$, SAXS curve, is obtained after subtracting the different scattering pattern of buffer from of the sample. The obtained data and the curve are radially symmetrical from all possible orientations of the particle. The scattering is caused by the electron distribution in the particle. The pair distribution function, $P(r)$, shows the probability distribution of all distances between pairs of atoms in the particle. Calculation of the pair function can be done through a

Fourier transform of the scattering curve. $P(r)$ gives clues about the overall molecular shape of the protein and its maximum dimension, d_{\max} . Direct information about the outer shape of the protein can be deduced by the shape of the $P(r)$: Bell-shaped symmetric $P(r)$ is a clue for spherical shape and asymmetric $P(r)$ for elongated rod-like particles.

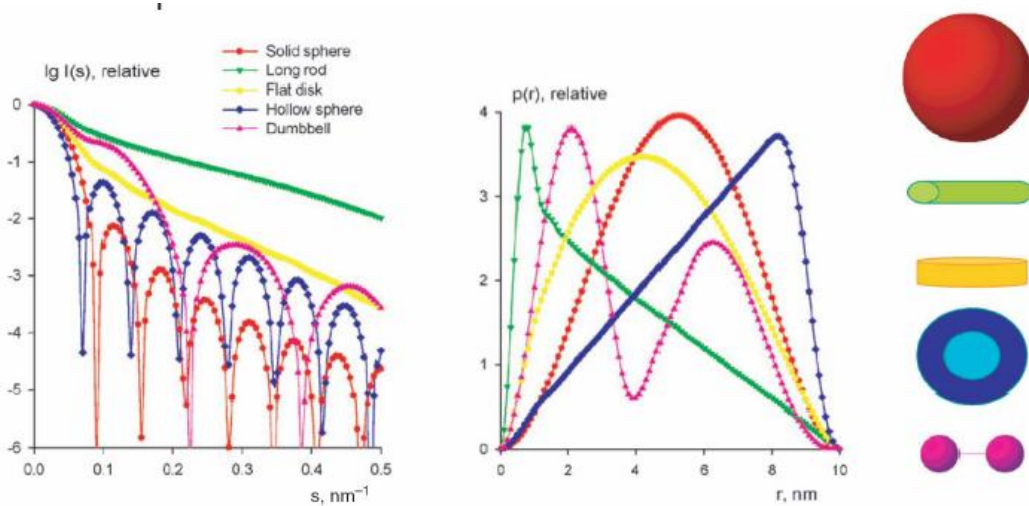


Figure 1.17: Distance distribution function from examples for simple structures (Dmitri & Michel, 2003).

Scattering intensity $I(s)$ can be calculated from the formula below:

$$(1.2) \quad I(s) = \frac{e^{\mu t}}{cD(s)} \left[\frac{I_x(s)}{I_0} - \frac{I_B(s)}{I_0} \right]$$

Where $e^{\mu t}$ represents the absorbance of a solution of thickness t , $I_x(s)$ and $I_B(s)$ scattering intensities of sample and buffer respectively, c concentration and $D(s)$ detector response.

Also taking inverse Fourier transform of $I(s)$ as shown in the formula can give out the $P(r)$:

$$(1.3) \quad I(s) = 4\pi \int_0^\infty r^2 p(r) \frac{\sin(2\pi sr)}{2\pi sr} dr$$

Lowest resolution portion of a SAXS curve (Guinier region) is directly related to the radius of gyration (R_g) of the particle, which is the square root of the average squared distance of each scattered point from the particle center (Putnam, Hammel, Hura, & Tainer, 2007). Intensity measured at zero angle, $I(0)$, is directly proportional to the molecular mass of the scattering protein. Determination of $I(0)$ is available only by extrapolation because

experimental set-up declares this point as the spot where beam hits the detector. A plot of $\log(I(s))$ against q^2 in the region $0.6 < R_g < 1.3$ (Guinier plot) should be a straight line and can be used to extract R_g and $I(0)$. Any nonlinearity indicates polydispersity or inhomogeneities in the sample (Guinier, 1955). R_g is independent of protein concentration for the fact that any deviation in the measurement should suggest a specific state of oligomerization or aggregation of the sample.

1.7.3.2. Model Generation from SAXS Data

Reconstruction of three-dimensional model from one-dimensional scattering data is a very fundamental problem for SAXS experiments: many three dimensional structures can be deduced from one dimensional data (Dmitri & Michel, 2003). The first attempts were based on modeling in a trial and error fashion, until the innovative envelope function for *ab initio* modeling; allowing generation of unique models by the help of spherical harmonics (Stuhrmann, 1970a, 1970b) . Inevitably, use of envelope function was limited to simple shapes, especially for the molecules that do not have structures that contain hole structures within.

1.7.3.2.1. DAMMIN

Modeling based on fitting rigid beads – that have very small r_0 radius – in the pre-defined shape envelope densely created the first basis for SAXS data modelling. According to this, the bead predicted can either belong to the sample or the solvent, and the DAMMIN algorithm distributes random beads in the defined data's volume, calculated according to R_g , and then refines the interior features of the volume in a Monte Carlo-like search (D. I. Svergun, 1999).

1.7.3.2.2. GASBOR

The hindered algorithm of DAMMIN forced for better defined algorithm to predict more complex structures. With the GASBOR algorithm(D. I. Svergun, Petoukhov, & Koch, 2001), the protein is represented as a complete block of dummy residues (DR), where residues correspond to the building blocks of the biological molecule; here, amino acids of a protein. Modeling is done by fitting the scattering from DRs to the experimental data. The algorithm starts by placing all available DRs into a spherical volume determined by d_{max} obtained from the experimental data. The algorithm proceeds with simulated annealing method and replaces

DRs constrained by d_{\max} . Avoiding residue clashes and/or discontinued DRs, being ≈ 0.38 nm apart from each other, constitutes the second error excluding factor of GASBOR. With this constraint, every DR is forced to have two neighbors at about 0.38 nm.

1.7.3.2.3. DAMAVER

Multiple models generated with DAMMIN and GASBOR arise because of initiating the modeling from presumptions and a single linear plot. All the individual models that are obtained by the algorithms can be superimposed and analyzed for stability by the DAMAVER algorithm (Volkov & Svergun, 2003). Among every individual model aligned, the most stable model – the most probable one – is taken as a reference. All others – excluding the extreme outliers – are aligned to the reference model and a density map of beads or residues are calculated, each of them being in the envelope.

1.7.3.2.4. CRY SOL

Experimental results of SAXS yield *ab initio* models of proteins. The models obtained should be cross-checked with known crystal structures if available. The CRY SOL software evaluates the solution scattering of macromolecules with known atomic structures and fits them to experimental scattering curves from SAXS data. The input file can be a PDB with an X-Ray or NMR structure of a protein. The program uses multipole expansion of the scattering amplitudes to calculate the spherically averaged scattering pattern of a given structure and takes the hydration shell into account. The fitting is done by minimizing the discrepancy. Three variables are considered for the fitting action: average displaced solvent volume per atomic group; contrast of the hydration shell and relative background arising from the buffer used (Svergun D.I., 1995).

1.7.4. X33 Beamline, EMBL Hamburg

Recently the X33 SAXS beamline at European Molecular Biology Labs (EMBL) Hamburg was upgraded (figure 1.18 (a) before and (b) after). Optics, electronics, detector, sample stage and data acquisition system was upgraded for shorter measurement times and increased turnover (Round, et al., 2008).

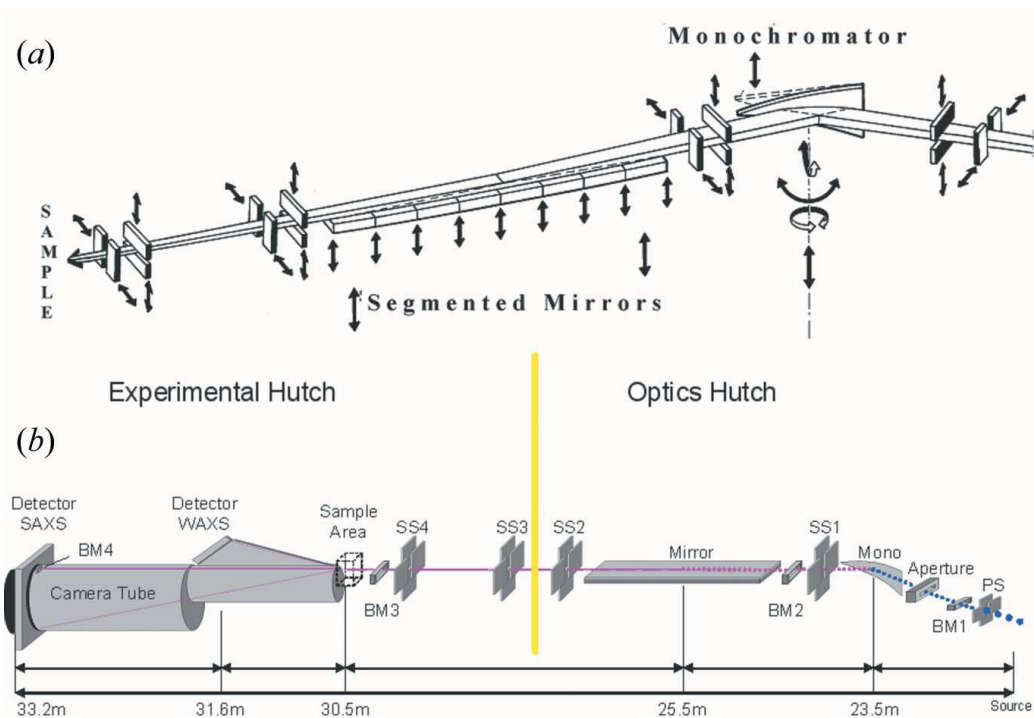


Figure 1.18: EMBL Hamburg X33 beamline sketch (Round, et al., 2008).

1.8. Objective of the Study

Aims of the work presented in this thesis are cloning and expression of the *A. thaliana* heterotrimeric protein gamma subunit gene, optimization of purification of the recombinant protein and investigation of its biophysical properties by several complementary techniques including DLS, CD, SAXS, SEC, SDS - and native - PAGE.

This work is part of a project where overall objective is obtaining the *A. thaliana* G-protein as a complete heterotrimer. The plant subunits have been expressed and purified by many researchers, but the formation of the heterotrimer hasn't been reported yet. The α subunit of the protein has been crystallized and the structure has been solved as a dimer, but the monomeric structures of β and γ subunits has not been managed yet. The protein of focus in this study is AGG2, gamma subunit of G-protein and up to now, no literature exists to show any biophysical study that has been done solely for AGG2. Thus, the scope of the project is claimed to understand the nature and biophysical character of AGG2.

2. MATERIALS AND METHODS

2.1. Materials

2.1.1. Chemicals

All chemicals were supplied by Stratagene, QIAGEN, Merck (Germany), Bioron, Fermentas, Riedel, Amresco, AppliChem, and SIGMA (USA).

2.1.2. Primers

Primers for the cloning of AGG2 for both pMCSG-7 and pETM-41 vectors were designed according to literature (Swarbreck, 2000).

		Sequence	Cloning Site
Primers for pETM-41 Cloning	Forward	5' – GCGCCATGGACGAAGCGGGTAGC – 3'	NcoI
	Reverse	5' – GCCGGATCCAAATCAAAGAATGGAGCAG – 3'	BamHI
Primers for pMCSG-7 Cloning	Forward	5' – TACTTCCAATCCAATGAAATGGAAGCGGGTA – 3'	LIC
	Reverse	5' – TTATCCACTTCCAATGAAATCAAAGAATGGAG – 3'	LIC

Table 2.1: Primers used to insert AGG2 gene into pMCSG-7 and pETM-41 vectors

The red nucleotides denote the cloning site used for the insertion of the gene into the region of interest on the plasmid; the yellow sequences denote the nucleotides added not to change the open reading frame; the green nucleotides shown in pMCSG-7 primers denote the stop signals for LIC (described below) and blue nucleotides denote the sequence of the gene either from the five or three primes.

2.1.3. Enzymes

Restriction enzymes *NcoI*, *BamHI* and *SspI*; ligation enzyme T4 DNA polymerase; LIC specific enzyme T4 DNA polymerase; and PCR reaction enzyme Taq polymerase enzymes were purchased from Fermentas.

2.1.4. Protein Purification Columns

HisTrap 5 ml Column (GE Healthcare) for affinity chromatography, QTrap 5 ml Column (GE Healthcare) for ion exchange chromatography and HiLoad 16/60 Superdex 75pg column (GE Healthcare) were used for size exclusion chromatography.

2.1.5. Vectors

Maps of pETM-41 (EMBL) and pMCSG-7 (Harvard) vectors can be found in Appendix C. pETM-41 vector contains maltose binding protein (MBP) as a fusion protein and 6 histidine (His) amino acids as a tag for chromatography (6-His is upstream of MBP). The amino acids “Glu-Asn-Leu-Tyr-Phe-Gln-Gly”, all of which constitute TEV Protease cleavage site, follow MBP. When needed, TEV protease protein can cleave the fused proteins from cloned protein.

pMCSG-7 vector contains only 6 His as a tag for affinity chromatography. Just like pETM-41 plamid, there is a TEV cleavage site downstream of 6 His and upstream of gene of interest.

2.1.6. Cell Lines

E. coli strains BL21 (DE3), DH5 α , BL21+* and TOP10 (provided by EMBL, Hamburg) were used.

2.1.7. Buffers and Solutions

Lysis buffer contains: 50 mM NaPO₄, pH7.4, 150 mM NaCl, 2 mM MgCl₂ 1X EDTA Free Protease Inhibitor, 5% glycerol and 2 mM PMSF.

Binding buffer for HisTrap Chromatography contains: 50 mM NaPO₄, pH7.4, 150 mM NaCl, 2 mM MgCl₂

Wash buffer for HisTrap Chromatography contains: 50 mM NaPO₄, pH7.4, 150 mM NaCl, 2 mM MgCl₂ and 10 mM Imidazole

Elution buffer for HisTrap chromatography contains: 50 mM NaPO₄, pH7.4, 150 mM NaCl, 2 mM MgCl₂ and 1 M Imidazole

Dialysis buffer before QTrap chromatography contains: 50 mM Tris –HCl pH: 8.0

Binding buffer for QTrap Chromatography contains: 50 mM Tris –HCl pH: 8.0

Elution buffer for QTrap Chromatography contains: 50 mM Tris –HCl pH: 8.0 + 700 mM NaCl

Dialysis and Running buffer for Size Exclusion Chromatography (Hepes Buffer) contains: 20 mM Hepes, 50 mM NaCl, 1 mM PMSF

All buffers and solutions, except those provided by commercial kits were prepared according to (Sambrook, 2000). Other buffers used in electrophoresis, etc. and their compositions are given in Appendix D. All protein buffers were degassed before applying to columns.

2.1.8. Commercial Kits

Qiaquick PCR Purification, Qiaquick Gel Extraction and Qiaprep Spin Miniprep Kits (QIAGEN) were used in recombinant DNA manipulations and molecular screenings.

2.1.9. Culture Media

LB (Luria-Bertani) Broth was prepared manually with following ingredients; 10 g Tryptone, 5 g Yeast extract, and 5 g NaCl for 1 liter.

LB Broth Agar was prepared by adding 15g agar-agar for 1 liter of LB Broth medium.

Terrific Broth (TB) contained 12 g Tryptone, 24 g yeast extract, 4 ml glycerol, 2.31 g KH₂PO₄ and 12.54 g K₂HPO₄ per 1 liter.

2.1.10. Equipment

The equipments used in this study is further listed in the Appendix E.

2.2.Methods

2.2.1. Cloning AGG2 Gene into Vectors

2.2.1.1. pETM – 41 Vector (Restriction Digestion Method)

2.2.1.1.1. PCR

The PCR reaction tube contained the chemicals listed in Table 2.2.

Chemical	Amount (µl)
Master Mix (5X)	5
Primers (20mM)	1 each
Template	1
Taq Poly	1
dH2O	16
Total	25

Table 2.2 PCR Reaction Chemicals

The template for the reaction is a construct of pQE80-L plasmid that contains AGG2 gene. The primers were designated in Table 2.1.

Reaction was carried out in a thermal cycler with the conditions detailed in Table 2.3:

95 °C, 5 minutes	
95 °C, 1 minute	Total of 35 cycles
62 °C, 45 sec	
72 °C, 45 sec	
72 °C, 5 minutes	
4 °C	Until further use

Table 2.3 PCR conditions used for addition of cloning sites to AGG2 gene

PCR products were analyzed by 1% agarose gel electrophoresis with TAE buffer. Samples were mixed with 6X loading buffer and gels were run at 100 mV for 30 minutes. Size of DNA fragments were estimated by using MassRuler DNA ladder mix (Fermentas) and visualized by ethidium bromide staining.

2.2.1.1.2. Restriction Digestion with *NcoI* and *BamHI*

The restriction digestion of both vector pETM-41 and AGG2 were managed by the methods suggested by Fermentas Company as in Table 2.3.

	AGG2	pETM-41
Tango Buffer (10X)	3 µl	3 µl
NcoI	2unit(u)	2u
BamHI	2u	2u
Template	1.5 µg	1.5 µg
dH2O	Needed Amount	
	30 µl	

Table 2.3 The Restriction Digestion reaction of AGG2 gene and pETM-41 plasmid

The digestion took place at 37°C and for 4 hours. The digested vector was loaded onto 1% agarose gel and further purified with Gel Purification Kit. A portion of the digested gene was loaded to 1% agarose gel for confirmation of digestion and then incubated on ice for ligation reaction.

2.2.1.1.3. Ligation of AGG2 into pETM-41 vector

The content of the ligation reaction was adjusted as suggested in the manual of the enzyme as described in Table 2.4

	Molar Ligation Ratio		
	1/3	1/6	1/10
Vector	160 ng	160 ng	160 ng
Insert	13 ng	26 ng	40 ng
T4 Ligase	2 unit (u)	2 (u)	2 (u)
Buffer	1,5 µl	1,5 µl	1,5 µl
dH2O	Needed Amount		
Total (ul)	15		

Table 2.4 Ligation reaction of AGG2 into pETM-41 vector

The concentrations of insert and vector to put into the reaction mix were determined by molar ligation ratio calculation:

$$\left(\frac{(ng \text{ vector}) * (kb \text{ size of insert})}{(kb \text{ size of vector})} \right) * (Molar \text{ ratio of insert/vector}) = (ng \text{ insert})$$

The reaction tube was incubated o/n at 16°C.

2.2.1.1.4. Transformation of Bacteria

TOP10 cells were transformed with the ligated samples. Previously prepared competent cells were taken from -80 fridge, thawed on ice and the 10 µl ligation results were added onto the competent cell tubes. After 30 min incubation on ice, the cells were heated to 42°C for 90 sec, placed on ice for 2 min. 800 µl LB were added to the tubes and the cells were incubated at 37°C for 1.5 hours. The grown cells were centrifuged at 9.800 rpm for 5 min, resuspended in 200 µl medium and spread on Kan⁺ LB agar plates.

2.2.1.1.5. Colony Selection

Observable and well-grown colonies were picked and incubated in liquid LB-Kanamycin (50 µg/ml) to prepare glycerol stocks and for plasmid isolation.

2.2.1.1.6. Plasmid Isolation

Colonies were grown in 10 ml of LB-Kanamycin (50 µg/ml) medium overnight at 37 °C at 270 rpm. Plasmid isolation was done with Qiaprep Spin Miniprep Kit (QIAGEN). The final concentration of plasmid DNA was calculated by measuring the absorbance at 260 nm in Nanodrop spectrophotometer (Thermo) and using $0.020 (\mu\text{g/ml})^{-1} \text{ cm}^{-1}$ for the extinction of DNA.

2.2.1.1.7. Restriction Digestion and Replication (PCR) Screening of Samples

The purified plasmids were tested for the validation of insertion of AGG2 gene. Digestion of the samples and the amplification of the gene from the plasmid were done accordingly as detailed in Table 2.2 and Table 2.3. The content of the reaction tubes were run on 1% agarose gel. The gels were then observed under UV light with the help of ethidium bromide dye.

2.2.1.1.8. Sequence Verification

Plasmids were purified with QIAGEN Plasmid Mini Kit (QIAGEN) and were sequenced by Refgen company (Ankara).

2.2.1.2. pMCSG – 7 Vector (Ligand Independent Cloning (LIC) Method)

2.2.1.2.1. PCR

The PCR reaction tube contained the chemicals listed in Table 2.5

Chemical	Amount (µl)
Master Mix (5X)	5
Primers (20mM)	1 each
Template	1
Taq Poly	1
dH2O	16
Total	25

Table 2.5 PCR Reaction Chemicals

The template for the reaction is a construct of pQE80-L plasmid that contains AGG2 gene. The primers were designated in Table 2.1.

Reaction was carried out in a thermal cycler with the conditions detailed in Table 2.6:

95 °C, 5 minutes	
95 °C, 1 minute	Total of 35 cycles
48 °C, 45 sec	
72 °C, 45 sec	
72 °C, 5 minutes	
4 °C	Until further use

Table 2.6 PCR conditions used for addition of cloning sites to AGG2 gene

PCR products were analyzed by 1% agarose gel electrophoresis with TAE buffer. Samples were mixed with 6X loading buffer and gels were run at 100 mV for 30 minutes. Size of DNA fragments were estimated by using MassRuler DNA ladder mix (Fermentas) and visualized by ethidium bromide staining.

Validated PCR product was further purified with isopropanol precipitation: the amplicons were pooled down to a single Eppendorf tube and 10 µl 3M NaOAc, pH 5.2 + 5 µl Linear Polyacrylamide (LPA) + 250 µl isopropanol (100%) are added to the tubes. The tubes were incubated at -80°C o/n, centrifuged for 15 min at max speed and resuspended in 250 µl

70% EtOH. The resuspended amplicons were again centrifuged for 5 min at max speed and dried in laminar flow. The samples then were resuspended in 25 μ l ddH₂O.

2.2.1.2.2. *SspI* Digestion of Plasmids

Cells containing pMCSG-7 plasmids were incubated in LB medium and were purified by Qiaspin Miniprep Kit. The purified samples were digested by *SspI* enzyme. This enzyme cuts the AATATT pallindromic sequence bluntly. This enables the enzyme to be exposed to the activity of T4 DNA Polymerase enzyme. The reaction is installed as in Table 2.7:

	pMCSG - 7
Ssp1	1 (5unit)
Template	10 μ g
dH20	Needed Amount
Buffer	3 μ l
Total	30 μ l

Table 2.7 *SspI* reaction Content

Digested plasmids were run on 1% agarose gel and then further purified with the help of Qiaquick Gel Extraction Kit.

2.2.1.2.3. T4 DNA Polymerase Reaction

T4 DNA Polymerase has two functions: formation of a phosphodiester bond from 5' to 3' and exonuclease activity from 3' to 5'; both cutting and pasting nucleotides. When the enzyme recognizes a nucleotide, the polymerase function gets activated, if not, the enzyme simply acts as an exonuclease. The strategy can be summarized like this: only one type of dNTP is added to the reaction tube so the enzyme simply creates single strand DNA's out of any blunt-ending oligonucleotide it encounters that does not possesses that specific dNTP. When T4 Polymerase reaches the nucleotide complementary to the dNTP, the enzyme both adds and cuts the same nucleotide over and over again so a flanking single strand DNA of interest can be obtained (Stols L, 2002). To manage this strategy, there are specifically designed sites in the plasmid: downstream of a number of A - T nucleotides, LIC site of vector carries a single G and the LIC site of insert (which the designed primers provide) contains single C nucleotides. The reaction conditions are stated in Table 2.8:

Insert Reaction	
ddH ₂ O	As needed
5X Buffer	14 µl
dCTP	35 nmol
Insert	*
T4 DNA Pol.	10 unit
V _f	70 µl

Vector Reaction	
ddH ₂ O	As needed
5X Buffer	14 µl
dGTP	35 nmol
Vector	**
T4 DNA Pol.	10 unit
V _f	70 µl

*All available sample from the isopropanol precipitation in 2.2.1.2.1

*All available sample retrieved after the gel extraction in 2.2.1.2.2

Table 2.8: The Reaction Content of T4 DNA Polymerase

Reaction takes place at 20 °C for 50 min and the activity of the enzyme is suspended by heat inactivation at 70°C for 30 min. The inactivated reaction complex then precipitated with ethanol same as the method described in the section 2.2.1.2.1.

The concentrations of the precipitated samples were determined by running them on a 1% agarose gel. Incrementing amounts (1µl and 2µl) of samples and DNA marker were loaded consecutively on a gel to compare the concentration of bands of samples with the corresponding bands of the marker; an additional NanoDrop concentration reading

2.2.1.2.4. Annealing of Insert & Vector

The concentrations determined in the previous step are used to calculate the insert to vector ratio for the annealing reaction. Both vector and insert possess single strand flanking regions that are complementary so when two are placed in a tube, the flanking regions will be complementarily ligate and form a complete plasmid without the aid of any other enzyme. Thus, the insert and vector were placed in a tube according to the molar ratio defined (1/3) and were incubated at room temperature o/n.

2.2.1.2.5. Transformation of Samples

The transformation of the constructs into TOP10 cells were performed the same way as described in the section 2.2.1.1.4. The only difference is the usage of Amp⁺ LB Agar plates instead of Kan⁺ because of the resistance gene on pMCSG-7.

2.2.1.2.6. Plasmid Isolation

Several colonies on the plate were chosen and grown in LB medium containing 50 μ M Ampicillin. Plasmids were isolated by Qiaquick Miniprep kit. The concentrations of the plasmids were calculated spectrophotometrically by NanoDrop machine.

2.2.1.2.7. Restriction Digestion and PCR Screening of Samples

The cloning site of pMCSG-7 contains restriction sites of *Bam*HI and *Kpn*I enzymes for screening purposes. PCR reaction for the screening was done according to the scheme detailed in the section 2.2.1.2.1 and the restriction digestion was done as detailed in Table 2.9:

	Construct	pQE80 + AGG2
Buffer BamHI (10X)	3 μ l	3 μ l
KpnI	4 unit (u)	4 u
BamHI	2 u	2 u
Template	1.5 μ g	1.5 μ g
dH2O	As needed	As needed
Total	30 μ l	30 μ l

Table 2.9: Digestion Screening of Construct

pQE80 + AGG2 construct was also digested as a positive control for the existence of the AGG2 gene in the new construct.

2.2.1.2.8. Sequence Verification of the Construct

Isolated plasmids were sent to Refgen Company (Ankara) for sequencing. The results were evaluated with the CLC Main Workbench program.

2.2.2. Gene Expression

All the experiments explained in this section are conducted in a highly specific manner for both of the pMCSG-7 and pETM-41 constructs. Additionally, the expression of the gene was also experimented with a previous construct: pQE80-L + AGG2 plasmid (Kaplan, 2009). The only difference among the expression of the constructs is the antibiotics selected (ampicillin for pQE80-L and pMCSG-7 constructs and kanamycin for pETM-41 construct).

2.2.2.1. Monitoring the Expression of the AGG2 Protein

The monitoring of protein expression and the growth of the cells were initiated by preparing the glycerol stock of cells for o/n growth (37°C and 270 rpm) in 10 ml LB medium + 50 µg/ml antibiotics. Next day, the 600 nm optical density (OD₆₀₀) of the samples were measured and the cells were placed on fresh 50 ml LB + 50 µg/ml antibiotics to have a final OD₆₀₀ of 0.15. The cells were incubated at 37°C and 270 rpm until the OD₆₀₀ reaches an interval of 0.8 – 1. When reached, the protein expression is induced by addition of 1 mM IPTG. During the overexpression of a particular gene, the high levels of protein can harm the growth of cells and the cells either start to die or quickly initiate the degradation of the protein. In order to tackle the problem, the metabolisms of the induced cells are slowed down. Eventually, the cells are incubated at 27°C and 250 rpm. Starting from the zero point (t=0), samples were collected every 40 min for 200 min total (4.5 hours). After measuring the OD₆₀₀ of the samples, the cells were pelleted by centrifugation at 10.000 rpm for 20 min with SLA-3000 rotor. Pellets were lysed with a buffer consisting of 25 mM Tris, 10 mM EDTA, 50 mM Glucose and 1 mg/ml lysozyme. The lysed samples were boiled at 95°C for 5 min and dyed with 6X SDS loading dye. Expression of the gene was monitored by 12% SDS polyacrylamide gels. Gels were first run at 100 V and voltage was increased to 120V once the samples reached separating gel. Samples were run until the dyes of the samples were at the lower border of the gel. Protein bands were visualized by coomassie blue staining. Protein molecular weight markers and protein ladders (Fermentas) were used to identify the molecular weights of expressed proteins.

2.2.2.2. Culture Growth for Protein Purification

Cells were cultivated in 2L media for large scale expression of AGG2 gene (the medium for pQE80 – L containing cells is LB and medium for pETM-41 and pMCSG-7 is Terrific Broth). Cell culture of 50 ml medium + 50 µg/ml antibiotics was grown o/n at 37 °C shaking at 270 rpm as a starter culture. Following day, OD₆₀₀ of o/n grown cultures were measured and transferred to 2L media (4*500 ml in 2L flasks) to have an OD₆₀₀ value of 0.15. When the cells reach OD₆₀₀ between 0.8 to 1, 1mM IPTG was added to the cultures to induce the expression of the gene. Because of the reasons explained in the section 2.2.2.1, cells were grown at 27 °C and 250 rpm for 4.5 hours and pelleted by centrifugation at 9500 rpm for 20

minutes using a Sorvall centrifuge with SLA 3000 rotor. Pelleted cells were stored at -80°C fridge for further usage.

2.2.3. Protein Purification

2.2.3.1. Affinity Chromatography by HisTrap Column

Pellets of cells were resuspended in lysis buffer detailed in the section 2.1.6. Cells were further lysed by 15 minutes of sonication at 4 °C (8 second of pulse and 9 second rest period). TritonX-100 was added to the cell mixture to have a final concentration of 1% and then the mixture was incubated in cold room for 45 min with a constant gentle shake. Treated cells were centrifuged at 14000 rpm, 4 °C for 1 hour with SS34 column. During this preparation procedure, the nickel affinity chromatography column HisTrap (GE Lifesciences) was prepared with AKTA Prime chromatography system: first the column was washed with water, then the column is cleansed with Elution buffer (section 2.1.6) and equilibrated with Binding buffer. The cell lysate (app. 50 ml) was applied to the AKTA system and injected to the column. The flow through (FT) from the column was collected and the column was further washed with 40 ml of wash buffer (section 2.1.6) and collected. Proteins were eluted with a gradient between wash buffer and elution buffer that last for 30 ml and finishes in 100% Elution buffer. The eluant was collected in 1ml fractions.

Lysate, FT, wash and fractions from the elution were all loaded to a 12% SDS-PAGE to see the quality, concentration and dispersity of the protein. The gel was incubated in coomassie stain, then the content of the loaded samples were observed. The fractions that contained the protein were dialysed against 20 mM Tris pH8.0 + 1 mM PMSF. Dialysis buffer was refreshed after 3-4 hours of incubation in the cold room.

2.2.3.2. Anion Exchange Chromatography by QTrap Column

The dialysed samples were centrifuged at 13.000 rpm for 25 min with a table-top centrifuge to precipitate the aggregated protein samples. The absorbance of the samples at 280nm (A280) were measured by NanoDrop and the concentration of the samples were determined by the extinction coefficient ($1.17 \text{ M}^{-1}\text{cm}^{-1}$ for AGG2). The ion exchange column QTrap (GE Lifesciences) was equilibrated in the same fashion of the HisTrap column: washed with water, cleansed with QTrap Elution buffer and equilibrated with QTrap Binding buffer. The centrifuged samples were then loaded to the AKTA system, flow through was collected, column was washed with QTrap Binding buffer and the protein was eluted with a gradient

between binding buffer and elution buffer lasting for 25 ml and ending at 100% Elution buffer.

Sample before dialysis, sample after dialysis, sample of flow through & wash and fractions of interest were all loaded to a 12% SDS-PAGE. The gel was dyed with coomassie stain and the samples were observed. The fractions that contained protein were dialysed against Hepes Dialysis buffer (section 2.1.6).

2.2.3.3. Size Exclusion Chromatography

The dialysed samples were centrifuged at 13,200 rpm for 25 min with a table-top centrifuge to get rid of the precipitated and aggregated protein samples. The concentration of the sample was calculated as told in section 2.2.3.2. The column HiLoad 16/60 Superdex 75pg (GE Healthcare) is used for size exclusion chromatography, which was calibrated previously (Aydin, 2011). The column was washed with 2 column volume of water and Hepes buffer (section 2.1.6). After calibration, the protein is loaded to the AKTA FPLC system (GE Lifesciences). The flow speed of the system is adjusted to 1ml/min and 1ml fractions were collected when protein peaks were observed. With the help of the calibration curve, the molecular weight of the protein is calculated.

2.2.4. Analyses of Purified Protein

2.2.4.1. Absorbance Spectroscopy

Nanodrop Spectrophotometer (Thermo) was used for all absorbance measurements. The machine is used according to the instructions in the manual. The program (Protein A280) was used for concentration determinations. The concentration of the protein was calculated by the normalization formula shown below:

$$(2.2) \quad \varepsilon * 10^{-4} (M^{-1}cm^{-1}) = \frac{A}{c * l} * 10^{-4}$$

Where A is absorbance, c is concentration in molar, l is pathlength in centimeters and ε is the extinction coefficient.

2.2.4.2. Circular Dichroism (CD) Spectropolarimetry

CD is observed by the differential absorption of left and right handed circularly polarized light by proteins, and has high sensitivity for nonchiral environments.

200 μ l protein samples were prepared for CD spectropolarimetry analyses by diluting them 1/5 because of the hindering effects of high salt concentration of HEPES buffer. A Jasco J-815 CD Spectropolarimeter connected to a computer with Spectra ManagerTMII installed was used for CD measurements.

1mm pathlength quartz cuvettes were used for measurement Spectra ManagerTMII software was used for data manipulation. The concentration values of the proteins were all varied, so the values were all normalized according to their concentration. The methodology is detailed in section 1.7.1.

2.2.4.3. Dynamic Light Scattering (DLS)

Zetasizer Nano ZS (Malvern Instruments) machine was used for DLS measurements. The machine determines the size of the particles in a solution by the measurement of Brownian motion of the particles via dynamic light scattering. Brownian motion of particles changes scattering pattern of the light. Correlation of this deviation with the diffusion speed yields the information to calculate the size.

Small particles move quicker than large particles. The relationship between the size of a particle and its speed with Brownian motion is defined by Stokes & Einstein equation. The velocity of Brownian motion is determined by translational diffusion coefficient. The fluctuation in the intensity of speckle pattern will change slowly for large particles compared to small ones.

The calculations described below yields a size distribution among the particles in the solution and the type of the distribution is intensity related. Then the software converts the data to have both volume and number related distributions. Rayleigh approximation states that the sixth power of a particles diameter is proportional to this particular intensity of scattering. So instead of evaluating the data regarding the volume and number distribution, the intensity distribution yields more reliable and consistent results.

2.2.4.4. SDS and Native Polyacrylamide Gel Electrophoresis (PAGE) & Coomassie Staining and Western Blotting

The recipe of the SDS-PAGE preparation is given in Appendix ... (Laemmli, 1970). 20 μ l protein samples were mixed with 4 μ l 6X SDS gel loading buffer (125mM Tris-HCl pH 6.8, 2% SDS, 20% glycerol, 0.2% bromophenol blue, 10% (v/v) β -mercaptoethanol) and

boiled at 95 °C for 4 minutes. 10 µl was loaded into 12 % SDS polyacrylamide gels having 5% of stacking gel. Gels were run in 1X SDS running buffer (25 mM Tris, 192 mM glycine, 0.1 % (w/v) SDS). For the stacking part, samples were run at constant 100V and for separating, voltage was increased to 120V.

The recipe for the native gels is also given in Appendix 10 µl protein samples were mixed with 2 µl 6X Native-PAGE sample buffer (200 mM Tris-HCl pH 7.5, 20 % glycerol, 10 %, 0.2 % bromophenol blue) and loaded into 10 % non-denaturing PAGEs. Gels were run in 1X Native running buffer (25 mM Tris, 192 mM glycine). For the stacking part, samples were run at constant 100V and for separating, voltage was increased to 120V.

For visualization, SDS- and Native- polyacrylamide gels were incubated in coomassie blue solution for staining and de-stained in 35% EtOH. The recipe of coomassie blue solution is given in Appendix D.

The initiation of western blotting is the running of SDS-PAGE gels the same way as told above except the markers were used PreStained instead of unstained. Then, the blotting continues by transferring the protein samples on PVDF membrane (Thermo). The transfer occurred in Transfer buffer (14.41 g. Tris base, 3.028 g. Glycine and 200 ml methanol in 1 L) for 75 min by 225 mA. The PVDF membrane then was blocked with Non-Fat Dried Bovine Milk (Sigma) in TBS solution (50mM Tris Base, 0.9% NaCl, pH 8.4). The blocked paper was later subjected to antibody (RGS-6His antibody (Invitrogen) for PQE-80L construct and 6His (Roche) for pMCSG-7 and pETM-41 constructs). After antibody binding, the samples were washed with TBS + Tween20 3 times for 10 min. The washed transfer paper is treated with Pierce ECL Western Blotting Substrates (Thermo) and the signals were blotted on Kodak Exposure Films (Kodak) in the dark room. The exposure of the transfer paper to the films varied and was noted.

2.2.5. The Effect of DTT and Protein Concentration on the Oligomeric State of the Protein

The effect of DTT and Protein concentration on the oligomeric state of the protein was always tested after dialyzing the proteins in Hepes Buffer (section 2.1.6). After the dialysis, the protein was either directly treated with DTT or the protein was loaded in Superdex 16/60 column for size exclusion chromatography and later on treated with DTT.

2.2.5.1.Preparation of the Samples for DTT Treatment

After retrieving the samples from the dialysis environment, the protein was centrifuged and its concentration was measured (as told in section 2.2.3.3). DTT concentration series always had the same fashion: 0 mM DTT, 0.1 mM, 0.3 mM, 0.5 mM, 1 mM and 5 mM DTT. 1 mM DTT concentration is the most frequent concentration used in protein purification so the series was intended to increment until reaching the universal concentration. The last 5mM DTT concentration had the intention of checking the effects of excess amount of DTT on the protein. The protein concentration in the DTT series was always adjusted to 1 mg / ml (app. 70 μ M) and the dilutions were done by Hepes buffer. The tubes containing the mixtures were gently shaken in cold room for at least 30 min.

Protein concentration series depended on the quality and the concentration level of the protein after dialysis against Hepes buffer. Eventually, the concentration series decreased in a $\frac{1}{2}$ dilution manner.

2.2.5.2.Biophysical Analysis on both DTT and Protein Concentration Series

After incubating the series samples in cold room, the experiments discussed in section 2.2.4 were all conducted on the samples. All these experiments were done from the same sample within the same interval of two days.

2.2.5.3.SAXS and *Ab Initio* Low Resolution Molecular Envelope Modelling

Small angle X-ray scattering (SAXS) measurements were conducted on the EMBL X-33 beamline (M. H. J. Koch & Bordas, 1983) at the DORIS storage ring, DESY, Hamburg. The beamline, which is specifically optimised for low background data collection from macromolecular solutions (Roessle, et al., 2007), is equipped with a photon counting Pilatus 1M pixel detector ($67 \times 420 \text{ mm}^2$) with a sample-detector distance of 2.7 m. The samples to be exposed are kept in a vacuum cell with polycarbonate windows at 18 °C and data collection is done in 3 consecutive one minute frames. The radiation damage to be observed during measurements is guessed from comparison of scattering patterns from different frames. The Data collected from DTT series were all observed in 1 mg/ml concentration, but the concentration series varied from a range of 0.5 to 3.8 mg/ml in 20 mM HEPES pH 8.0, 100 mM NaCl buffer.

Presentation of the data is obtained as logarithm of the scattered intensity ($I(s)$) against momentum transfer s ($s = 4\pi\sin\theta/\lambda$, where 2θ is the scattering angle and λ is the wavelength:

0.15 nm). All the preliminary data analysis involving correction for beam intensity, background correction, buffer subtraction and concentration normalization were carried out using the PRIMUS (Konarev, Volkov, Sokolova, Koch, & Svergun, 2003) software in the ATSAS suit of programs (Petoukhov, Konarev, Kikhney, & Svergun, 2007) at EMBL Hamburg. The data is thus reduced and the correction and manipulation of the data is continued to determine the forward scattering $I(0)$ and the radius of gyration R_g of the proteins. Additionally, Porod plot is drawn to obtain information about the structural flexibility of the macromolecule (Porod, 1982).

R_g and molecular mass of the protein in solution can be calculated by Guinier approximation (Guinier, 1955). Guinier approximation states that for a monodisperse solution the scattered intensity at small angles, $I(s)$ is a linear function of s^2 and the scattered intensity extrapolated to $s=0$, $I(0)$, is proportional to the molecular mass of the protein in solution. The slope of the linear regression yields the radius of gyration and for globular particles at s values where $sR_g < 1.3$;

$$I(s) \cong I(0) \exp\left(-\frac{1}{3} R_g^2 s^2\right)$$

For molecular mass (MM) determinations the scattering obtained from a reference protein (e.g. BSA) can be used and the unknown molecular mass calculated as:

$$MM_s = \frac{I(0)_s}{c_s} * \frac{c_{BSA} * MM_{BSA}}{I(0)_{BSA}}$$

where MM_s , $I(0)_s$, c_s , MM_{BSA} , $I(0)_{BSA}$, c_{BSA} stand for molecular mass of the sample, scattering intensity at zero degrees, concentration of the sample, molecular mass of BSA, scattering intensity at zero degrees for BSA and concentration of BSA, respectively. For the measurements, the reference protein is chosen to be BSA and was dissolved in 20 mM HEPES, pH 8.0, 150 mM NaCl and 1 mM DTT and a concentration of app. 5 mg/ml.

The pair distribution function is proportional to the probability of observing a given distance inside the particle and can be simply calculated using the indirect transform package GNOM (D. Svergun, 1992). The output of GNOM analysis is further usurped in molecular modeling calculations. *Ab initio* calculations were carried out using the algorithms DAMMIN (D. I. Svergun, 1999). The models are calculated using dummy residues or beads by a simulated annealing procedure and the difference between the scattering from the model and

the experimental scattering intensity are minimized. Twenty different models were calculated and convergence of the models formed a similar shape. The final average model was obtained using DAMAVER software.

2.2.6. Homology Modeling of AGG2 Protein

2.2.6.1. Alignment of AGG2 Sequence With 1TBG

The initiation of homology modeling requires an alignment with a protein which has been crystallized and modeled. For this purpose, the protein sequence of Gamma chain of bovine transducin (PDB ID: 1TBG) is aligned with the sequence of AGG2 with the help of the online software Biology WorkBench (SDSC). The sequences are aligned by Blossum 60 algorithm.

2.2.6.2. Modeling of AGG2

The alignment obtained and the single PDB file of the gamma chain of transducin were loaded to the Modeller program (Eswar, 2006). The program retrieves the secondary structure of the input PDB file and models the aligned sequence (AGG2) accordingly.

2.2.6.3. Docking of Monomers

The dimer of the protein is modeled by the protein-protein docking server GRAMM-X (Tovchigrecho A., 2006). Both receptor and ligand options were chosen for AGG2 model and sent to the server. 10 dimer structures were modeled.

2.2.6.4. Comparison of Dimer Models with CRY SOL

All of the dimer models were run on CRY SOL software (Svergun D.I., 1995). The program evaluates the scattering curves of macromolecules of known atomic structures and fits them to experimental scattering curves from obtained SAXS measurements. A single PDB file is enough for the evaluation of the program. Multipole expansion of the scattering amplitudes is used to calculate the spherically averaged scattering patterns and takes the hydration shell into account. CRY SOL software fits this theoretical scattering onto the experimental data. If the two curves are matching, the model can be said to be fitting the experimental data or vice versa.

3. RESULTS

3.1. pETM-41 Cloning

3.1.1. AGG2 gene amplification

The *agg2* gene to be cloned into the pETM-41 vector was amplified from pQE80-L + AGG2 construct (Kaplan, 2009) using primers containing *Bam*HI (5') and *Nco*I (3') restriction sites for ligation to pETM-41 vector (section 2.1.2.). It is expected that this amplification will yield a fragment which is about 330 bp long. Preliminary confirmation of the amplicon was achieved by determining the fragment length on 1% agarose gel as shown in figure 3.1.

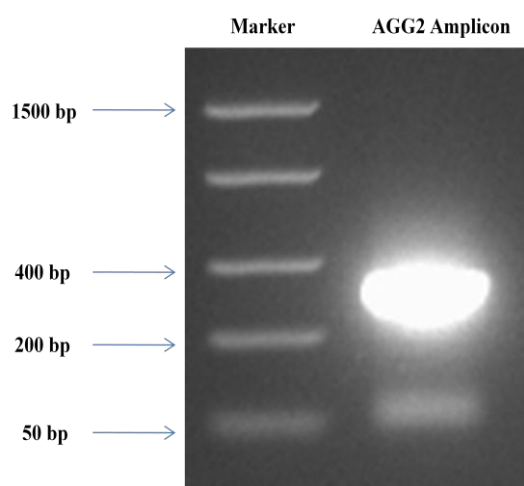


Figure 3.1 Amplified AGG2 gene for cloning with pETM-41. AGG2 fragment was analysed on a 1% agarose gel is visualized by EtBr staining.

3.1.2. Production of the pETM-41 + AGG2 Construct

During the amplification procedure, restriction sites *Bam*HI (5') and *Nco*I (3') were introduced to the AGG2 gene to facilitate ligation with the expression vector. Figure 3.2 shows electrophoretic analysis of both the pETM-41 plasmid and the gene digested with these enzymes prior to ligation.

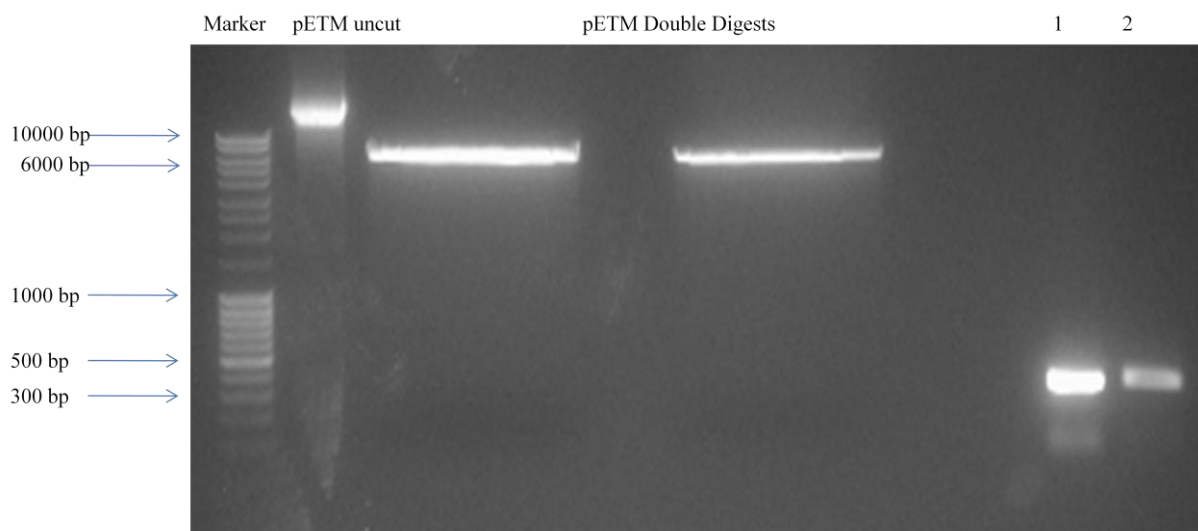


Figure 3.2 Verification of double digestion of pETM-41 & amplified AGG2 by electrophoresis on 1% agarose gel. Lane 1 – AGG2 amplicon, 2 – AGG2 double digested)

After digestion, the plasmid and the AGG2 gene were purified from the enzymes and digestion products using a gel extraction kit (Qiagen). Estimation of DNA concentration for ligation was conducted by comparing intensity of sample bands at different loadings (1 and 2µl) with those of the marker bands at known concentration as shown in Figure 3.3.

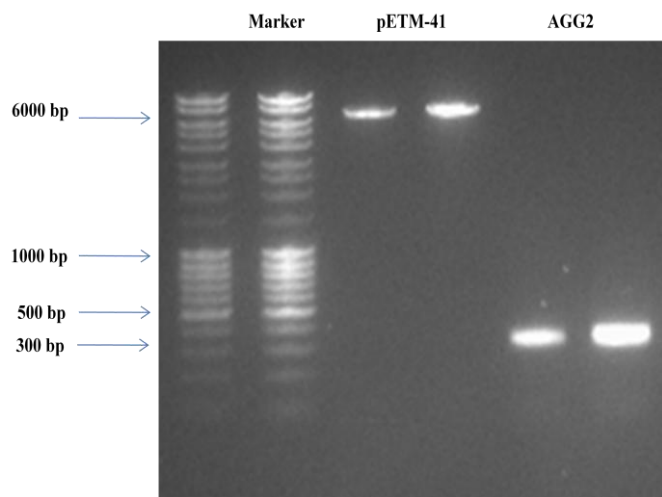


Figure 3.3 Comparison of thickness of pETM-41 and AGG2 with those from the marker for concentration determination of digested & purified samples

The linearized plasmid and the digested amplicon were following standard procedures.

3.1.3. Transformation of Bacteria

TOP10 Cells were transformed with the construct and were spread on LB-agarose + 50µg/ml kanamycin plates. Cells were grown o/n at 37 °C and on the surface of plates, transformed cells formed colonies were stored at +4°C for further use.

3.1.4. Verification of Cloning

Single large colonies selected from plates were grown in LB cultures for plasmid isolation in order to validate the insert. Results of screening were analyzed on 1% agarose gel as shown in figure 3.4.

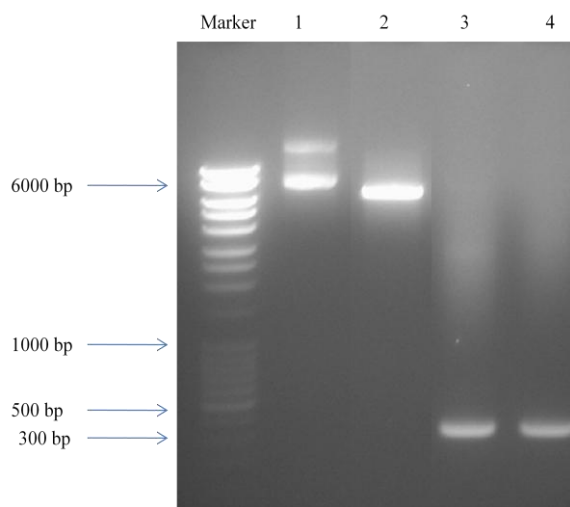


Figure 3.4 Results of digestion and PCR screening of constructs analyzed on 1% agarose gel. Lane 1 – Isolated construct 2 – Result of digestion of the construct by the enzymes NcoI and BamHI, 3 – PCR product obtained from the construct using AGG2 primers, 4 –PCR product obtained directly from AGG2 gene

Bands corresponding to 330 bps were observed and thus the presence of the inserted gene into the constructs was verified. The verified constructs were then sent to the Refgen Company (Ankara) for sequence verification. Results were analyzed by the CLC Main Workbench software. Alignment of the known sequence of AGG2 from literature and the data obtained by the sequencing gave high scores and verified that AGG2 gene was inserted into the plasmid without sequence modifications (Appendix XX).

3.2. pMCSG-7 Cloning

3.2.1. Gene amplification for pMCSG-7 Cloning

The gene to be cloned into the pMCSG-7 vector was amplified from the same vector used for pETM-41 cloning. The primers specifically designed for LIC with pMCSG-7 insertion were used in the PCR amplification process (the sequences of the primers are shown in section 2.1.1.) The size of the amplified fragment was verified by analysis on 1% agarose gel as shown in figure 3.5.

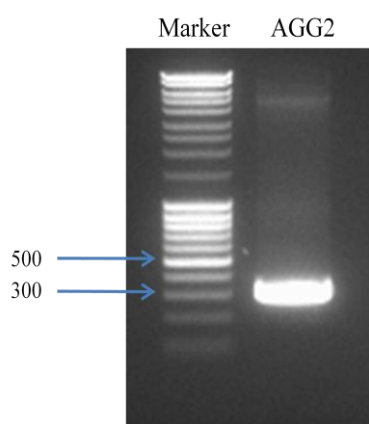


Figure 3.5 Verification of amplification of AGG2 with LIC Site

Amplification of the gene with the specific primers added the LIC sites to both 5' and 3' ends of the AGG2. The amplified gene was precipitated with isopropanol as detailed in the section 2.2.1.2.1 and visualized on an agarose gel. The length of the fragment observed was around 330 bps and this was used in the ligation independent cloning step.

3.2.2. Blunt end Digestion of pMCSG-7 vector for ligation of AGG2 gene

The plasmid pMCSG-7 was digested with SspI to get a blunt-end digested plasmid. The blunt ends of the plasmid reveal the LIC sites of the plasmid for T4 DNA Polymerase digestion. The digestion of the gene was verified by analysing on 1% agarose gel as shown in figure 3.6.

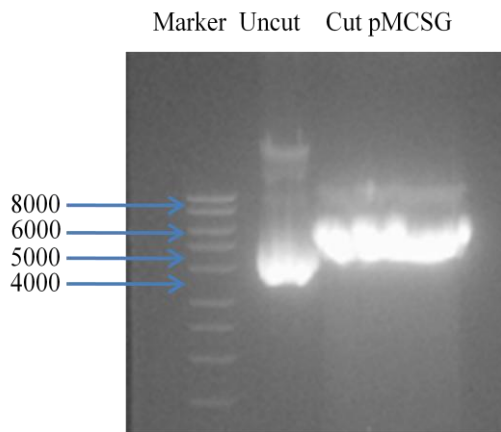


Figure 3.6 SspI Digestion of pMCSG-7 Plasmid

A clear shift was observed on the lane for the cut pMCSG-7 plasmid. The shift is due to the linearization of the plasmid by the SspI enzyme. This step was followed by the T4 reaction.

3.2.3. Digestion of LIC sites for ligation with T4 DNA Polymerase

The digested plasmid and the amplified & purified gene were digested by T4 DNA polymerase. The digested samples were precipitated with ethanol and resuspended in 10 μ l ddH₂O each to increase the level of concentration of samples. Concentrations of the samples were determined as explained in section 3.1.2 by analysis on 1% agarose gel and comparison of the band intensities with those of the marker as shown in figure 3.7.

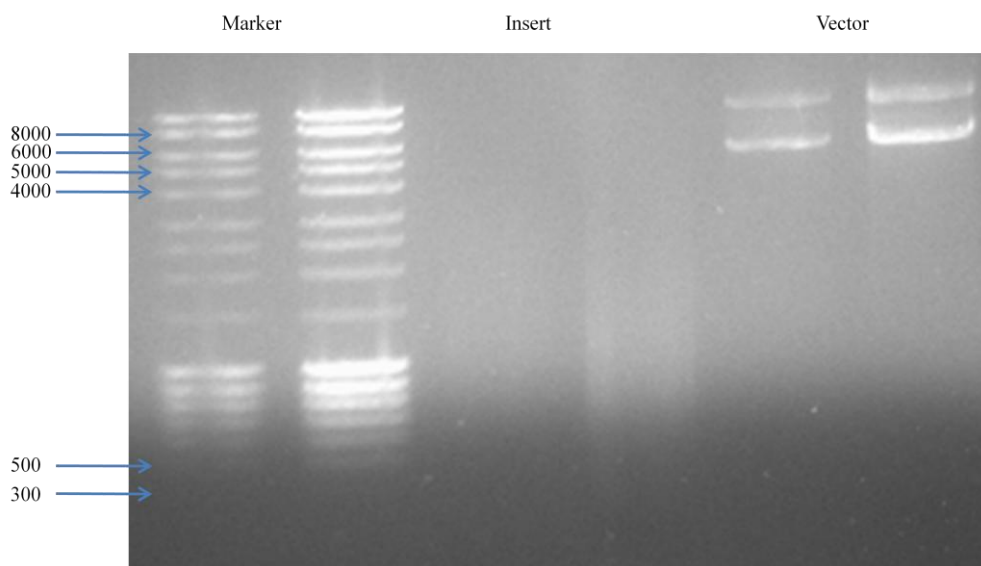


Figure 3.7 Concentration Determination before Annealing of AGG2 into pMCSG-7 vector

The width of the bands may be different, but the lengths of the bands are different. When the molarities of the oligomers are considered, the concentrations of digested plasmid and insert are approximately equal.

3.2.4. Transformation of Bacteria

Transformed TOP10 Cells were spread on LB plate + 50 µg/ml Ampicillin and grown o/n and were checked for growth the day after. Plates were stored at 4°C for further usage.

3.2.5. Verification of Ligation of AGG2 Gene

Colonies were screened for the presence of the AGG2 gene by plasmid isolation and carrying out restriction digestion and PCR reactions. BamHI and KpnI sites that are located in the LIC cloning region of the plasmid were used for restriction analysis and the PCR was conducted using the isolated plasmids as templates and the cloning primers. The pQE80-L + AGG2 construct was used as positive control for both restriction and PCR screening. The results of verification experiments are shown in figure 3.8.

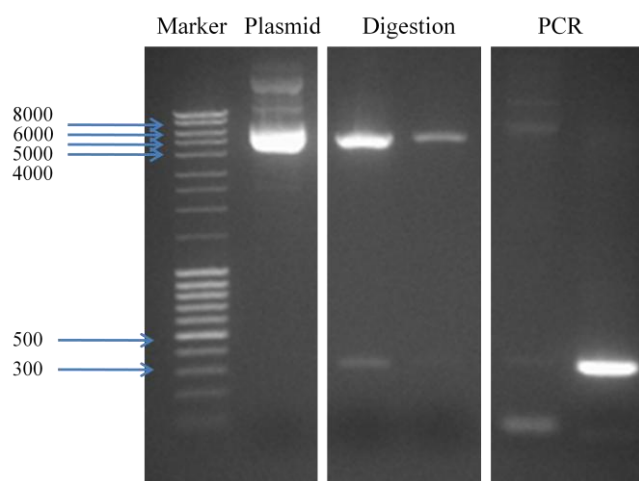


Figure 3.8 Digestion and PCR Screening of Construct (left, construct, right pQE80-L for both digestion and PCR reaction results)

Bands of about 300 bp length corresponding to the cloned gene were observed in the gels for both PCR and digestion reactions. The positive clones were sequenced and results were aligned with CLC software with the AGG2 gene sequence in literature. The score of alignment is high enough to verify that the gene has been inserted to the pMCSG-7 plasmid. Sequencing result is given in Appendix XX.

3.3. Gene Expression & Growth Curve

Gene expression and synthesis of AGG2 protein were investigated by obtaining growth curves and total protein extracts from both untransformed and transformed TOP10. Samples were taken every 40 min, starting by addition of 1 mM IPTG for induction at t=0, and the OD600 values were measured for induced and non-induced cells. A typical growth curve can be seen in figure 3.9.

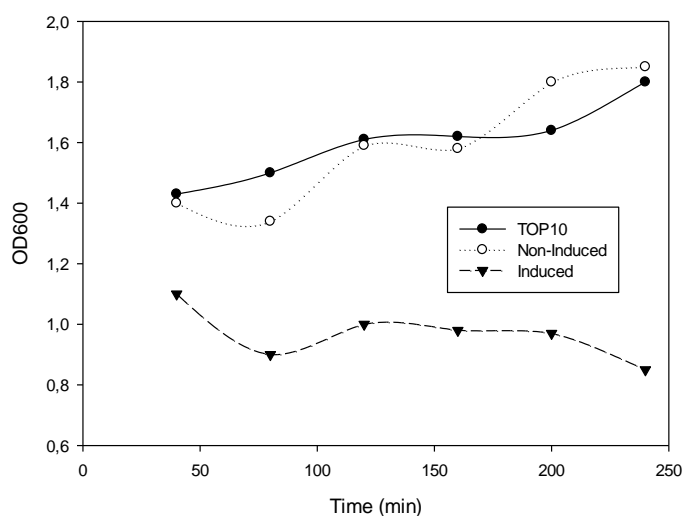


Figure 3.9 Growth Curve of native and transformed TOP 10 cells with PMCSG-7 Construct

The difference between the induced and non-induced samples can be readily seen and it is clear that expression of AGG2 hinders the growth of cells. Part of the cells taken for OD600 measurements were pelleted and analysed by SDS-PAGE on 12% polyacrylamide gels. The expression profiles of AGG2 can be seen in figure 3.10.

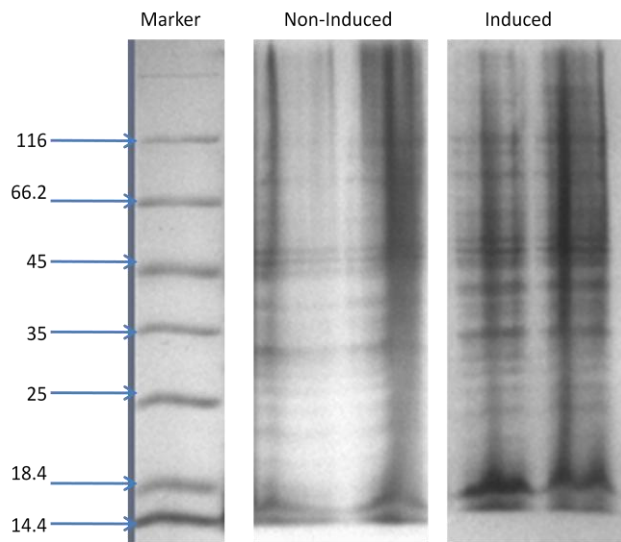


Figure 3.10 SDS-PAGE analysis of samples from 250 minute of AGG2 induction. A sample from non-induced cells is also shown as control.

A band slightly above the 18.4 kDa band of the ladder is visible for the induced samples, corresponding to recombinant AGG2. The band appears to be weak due to small amount of lysed cells and because no extra effort was made to purify the protein at this point.

3.4. AGG2 Protein Purification

A general scheme for purification of AGG2, detailed in figure 3.11, was applied for constructs of pQE80-L, pETM-41 and pMCSG-7.

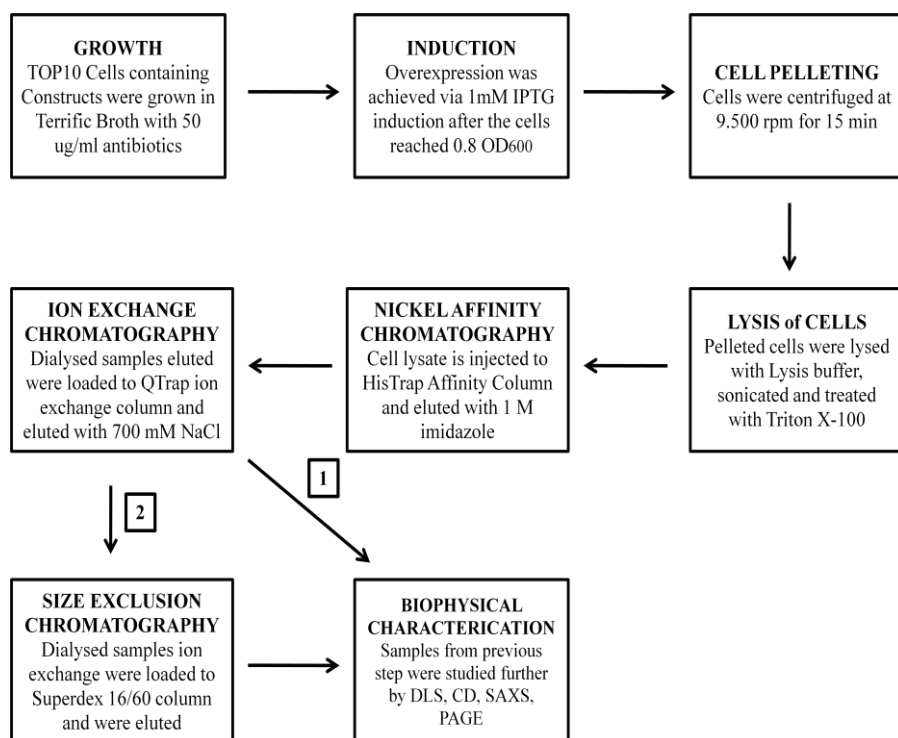


Figure 3.11 The scheme for AGG2 purification. Two alternative paths were followed: biophysical studies were conducted either after ion exchange chromatography or size exclusion chromatography.

Growth of cells used for overexpression of AGG2 was tried both in Terrific broth (TB) and Lucius Broth (LB). As expected, use of TB yields much higher biomass than LB, and it was used for cell growth for AGG2 purification.

Purification of the proteins was achieved as summarized in figure 3.11. We conducted biophysical characterization of the protein that was purified by both procedures. The results presented in this thesis are obtained using AGG2 purified following the second path.

3.4.1. Nickel Affinity Chromatography of AGG2

Initial crude purification of AGG2 was achieved by making use of the His-tag introduced to the protein by the cloning vectors. The lysate was directly applied to the 5 ml HisTrap affinity chromatography column (GE Lifesciences) and using the AKTA PRIME system (Amersham) 50 ml cleared lysate could be loaded on the column in one step with the help of 50 ml superloop. Elution profiles of the AGG2 proteins (from different constructs) from the column with imidazole gradients are shown in figure 3.12.

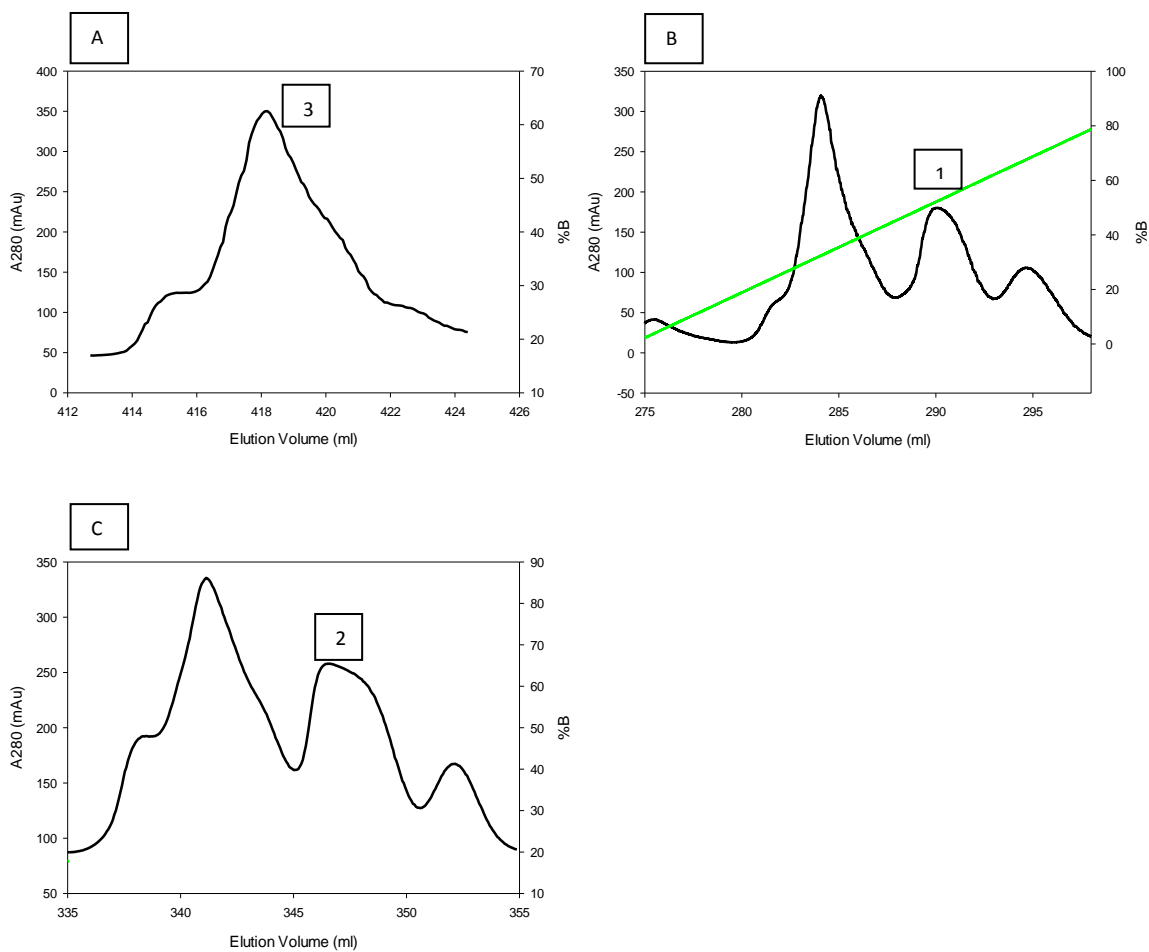


Figure 3.12 Nickel affinity column fractionation of recombinant AGG2 proteins. A) from pETM-41; B) from pQE80-L; C) from pMCSG-7 constructs. The numbers correspond to the pools that are loaded to the SDS-PAGE.

Before proceeding, fractions were pooled yielding on the average a total of about 7 ml of crude AGG2 preparation. Protein concentration could not be determined because of the imidazole in the elution buffer, which absorbs light at 280 nm and interferes with the protein

measurements. AGG2 concentrations were estimated by the thickness of bands seen by SDS-PAGE analyses as shown in figure 3.13.

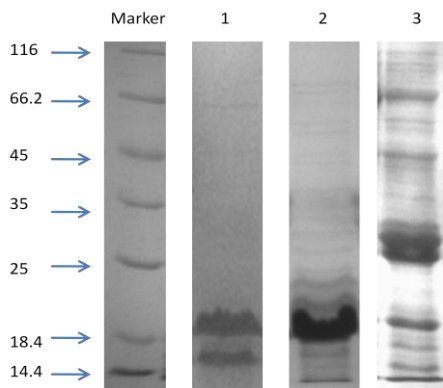


Figure 3.13 Results of SDS-PAGE analysis of HisTrap AGG2 Pools. The gels were Coomassie Stained. 1- from pQE-80 construct; 2- from pMCSG -7 construct; 3- from pETM-41 construct

The purification procedure was identical for all three constructs but as can be seen from the chromatogram and the SDS-PAGE results, AGG2 from the pETM-41 appears to be more contaminated. The only peak comes at a level of gradient that does not correspond to AGG2 elution position in the other chromatograms. As can be seen from figure 3.13, there are more contaminating bands on the gel compared to protein obtained from the other two constructs. There appears to be a band which can correspond to AGG2, but if we consider that the samples loaded in lanes 1 and 2 are 1/5 times diluted, the low level of protein synthesis with pETM-41 construct becomes more obvious. Based on these results it was decided not use AGG2 expressed from the pETM-41 construct for further analyses.

From now on, the recombinant protein expressed with the pMCSG-7 vector will be denoted as **AGG2** and the protein expressed with pQE80-L plasmid will be denoted as **AGG2***.

3.4.2. Ion Exchange Chromatography of AGG2

Imidazole was eliminated from the AGG2 pools by dialysis and concentration of protein solutions were calculated for loading on ion exchange chromatography columns. It was found that the optimum load was about 20 mg total for both proteins. A 5 ml QTrap Ion exchange chromatography column (GE Lifesciences) was used and proteins were eluted with

a NaCl gradient as described in the section 2.2.3.2. The elution profiles for both recombinant proteins are shown in the figure 3.14.

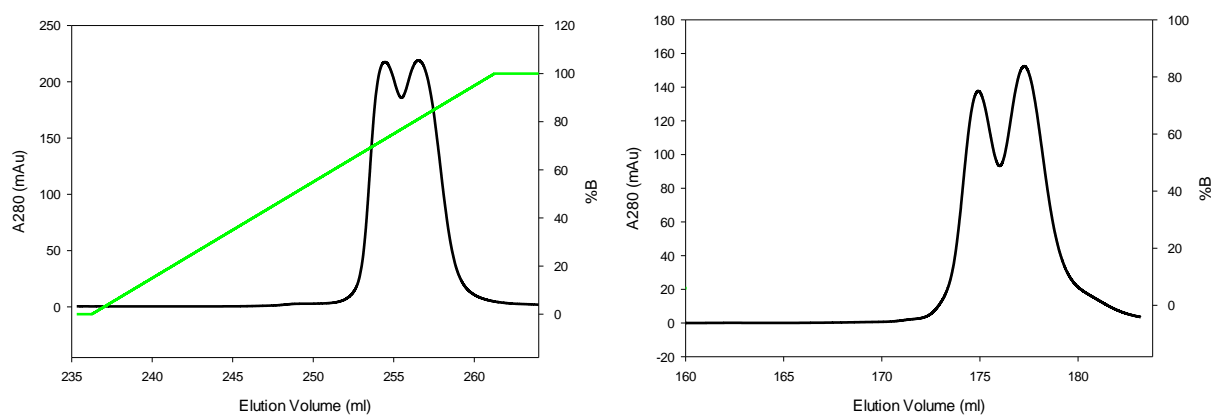


Figure 3.14 Ion Exchange Chromatography Elution Profiles of AGG2. Left – AGG2, right – AGG2*.

Initially the two peaks observed in each of the ion exchange chromatograms were pooled individually, however, observations on numerous purifications showed that the fractions in these peaks display very similar biophysical properties (data not shown). It was subsequently decided to pool all fractions together to obtain a total of about 7 ml protein.

The pooled samples were analyzed by SDS-PAGE and the quality and dispersity levels of the proteins are checked in figure 3.14.

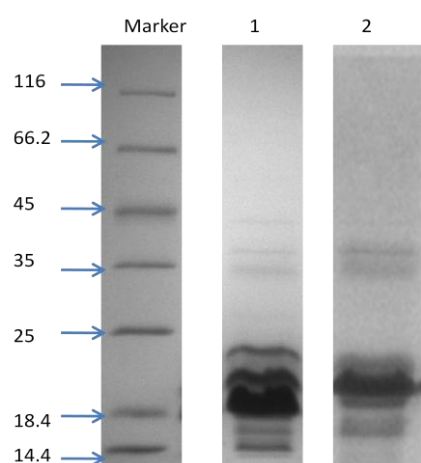


Figure 3.15 SDS-PAGE Results of Ion Exchange purified AGG2 Pools (Coomassie Stained) (1 – AGG2, 2 – AGG2*)

The pooled samples were dialysed against Hepes buffer (section 2.1.6.) and final concentration of AGG2 in the pools were in the range 3 to 5 mg/ml. Proteins were loaded on gels after 5-fold dilution to have better visualization of bands. Overloading created crown like smears on gels and prevented the visualization of any other band within the samples. Dialysed protein was directly transferred to the Size Exclusion Chromatography step.

3.4.3. Size Exclusion Chromatography

Proteins were eluted from the ion exchange column in app 400 mM NaCl. In order to transfer AGG2 pool into size exclusion chromatography (SEC) buffer, an o/n dialysis was performed and concentrations of collected samples were calculated. The HiLoad 16/60 Superdex 75pg size exclusion chromatography column (GE Lifesciences) yielded better separation when the total load was kept at around 10 mg AGG2 and the elution profiles of SEC are shown in the figure 3.16. As can be seen from these elution patterns, AGG2 peaks were obtained at 48 ml and 58 ml and AGG2* peak was observed at 59 ml. Corresponding molecular weights for the proteins are calculated from calibration curves using the equation detailed in 2.2.3.3. (Aydin, 2011).

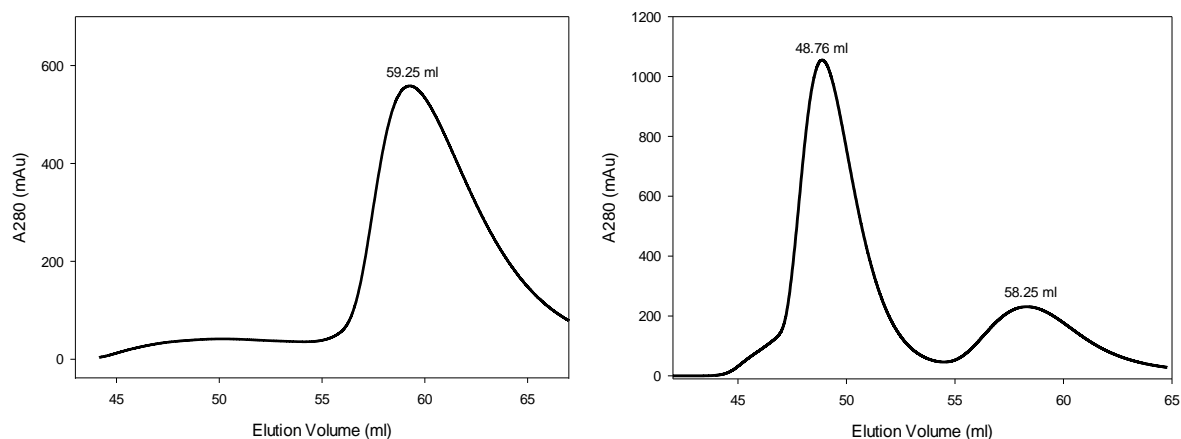


Figure 3.16 Elution profile of Size Exclusion Chromatography (Left: AGG2*, MW: 43 kDa) (Right: AGG2, left peak MW: 87 kDa, right peak MW: 46 kDa) Homogeneity in terms of contaminating proteins and polydispersity of oligomeric state were checked by analysing the samples by 12 % SDS-PAGE, by Western Blotting with RGS-6His antibody (Invitrogen) and by 8% Native – PAGE analysis as shown in figure 3.17.

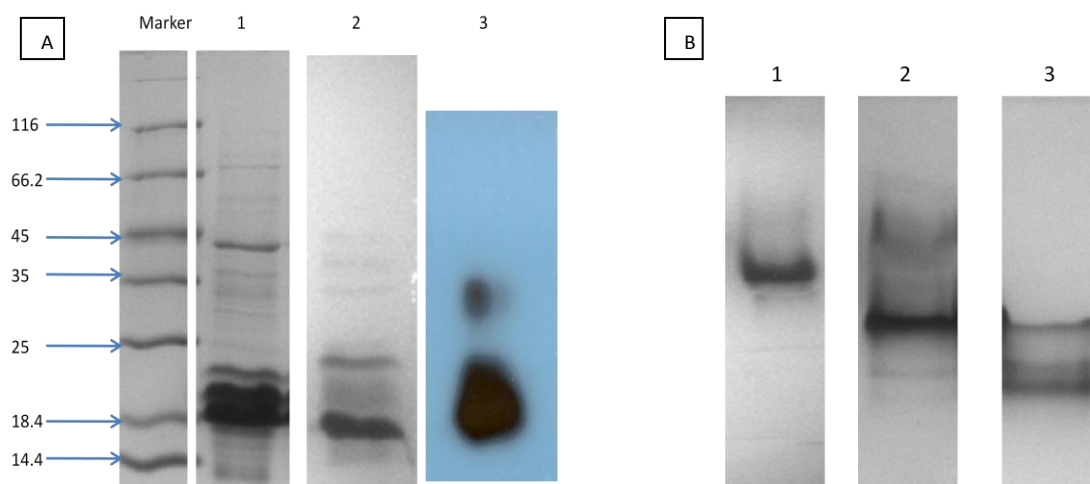


Figure 3.17 A: SDS-PAGE analysis results of Size Exclusion Chromatography peaks. 1- AGG2, 2 AGG2*, 3 Western blot of AGG2* B: Native Gel analysis for Size Exclusion Chromatography peaks; 1 AGG2*, 2 AGG2 left peak, 3 AGG2 right peak

After SEC AGG2 pool had a concentration around 1.2 mg/ml and that for AGG2* was around 2 mg/ml. The sample visualized in western blotting and the samples loaded on Native PAGE were adjusted to have a concentration of 1mg/ml (10 μ l were loaded on the wells). The buffer of AGG2* purification contained 1 mM DTT; whereas DTT was omitted from the buffer of AGG2. The elution volume of AGG2* is close to that of the second peak of the AGG2. This indicated that DTT influenced the oligomeric state of the protein and this effect was further investigated.

3.4.4. Comparative Analysis of AGG2 and AGG2*

Comparative studies were conducted to investigate biophysical characteristics of the purified proteins after size exclusion chromatography using Dynamic Light Scattering (DLS), Small Angle X-Ray Scattering (SAXS) and Circular Dichroism (CD).

A comparison of results, given in figure 3.18, shows that the secondary structure distribution of two proteins is highly similar. However, DLS results indicate a clear difference in the hydrodynamic radii for AGG2 and AGG2, consistent with the findings from SEC.

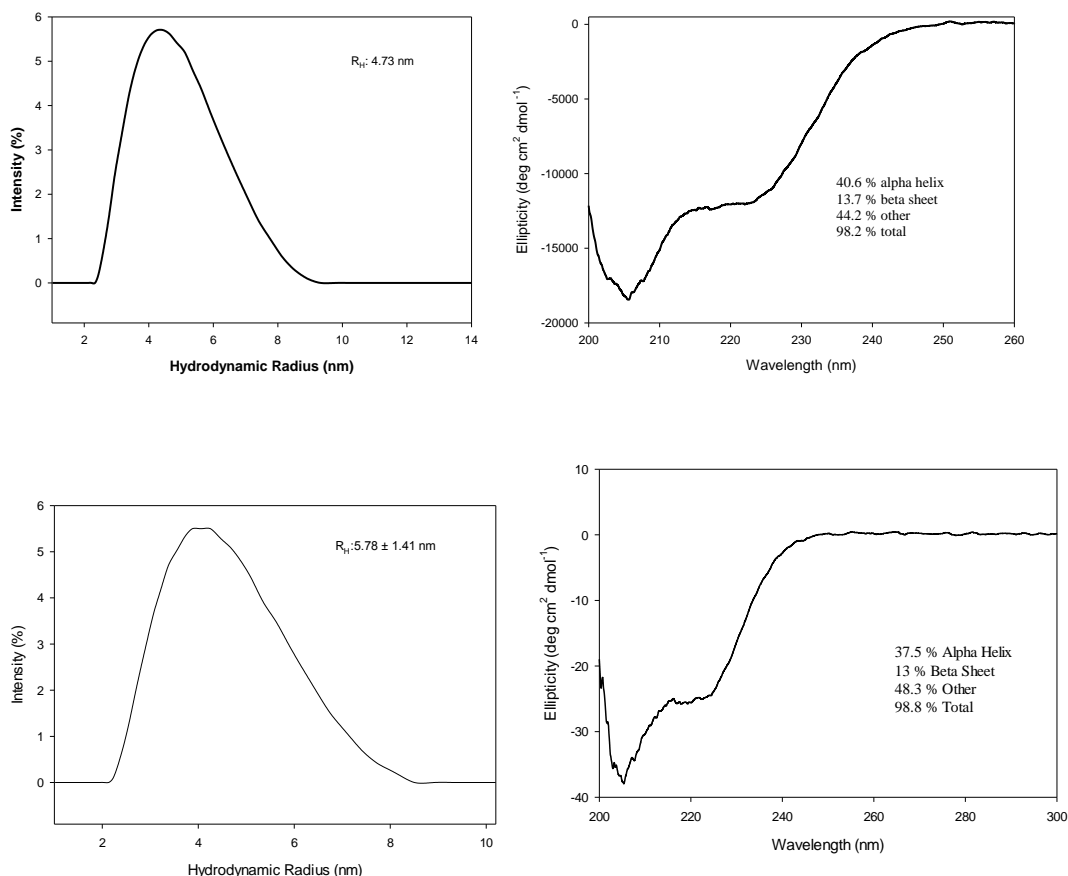


Figure 3.18 Results of DLS and CD measurements on AGG2* (top) and AGG2 (bottom)

Results of these measurements are summarized in table 3.1. This table does not include SAXS measurements for AGG2 samples because we did not get beamtime after we produced this recombinant protein. Furthermore, all results for AGG2 are obtained from the first peak of the size exclusion elution; the results of the second peak are quite close to the results of AGG2* and they are not shown. Results of CD measurements show that there is a small difference between AGG2 and AGG2* in the α -helical content. This may be significant since AGG2 structure consists of two α -helical domains. DLS results, on the other hand, show that there is a clear size difference between the two proteins.

SAXS (AGG2* only)	R_g (nm)	3,53	
	I₍₀₎	29,89	
	D_{MAX} (nm)	12,4	
	Mass (kDa)	34	
DLS	AGG2	R_H (nm)	5,78
		Std. Dev.	1,41
		Polydispersity	28%
	AGG2*	R_H (nm)	4,73
		Std. Dev.	1,35
		Polydispersity	28%
CD	AGG2	Alpha Helix (%)	37,5
		Beta Sheet (%)	13
		Other (%)	48,3
	AGG2*	Alpha Helix (%)	40,6
		Beta Sheet (%)	13,7
		Other (%)	44,2

Table 3.1 AGG2 Structural Characterization after Size Exclusion Chromatography

Having established that presence of DTT influences the oligomeric state of the protein in solution a systematic study of this effect was conducted.

3.5. DTT Effect on the Oligomeric State of the Protein

DTT effect is investigated with SAXS, CD, DLS and PAGE methods. The protein concentration is adjusted to be 1mg/ml for all the measurements and the concentration of the DTT is adjusted to be 0, 0.1, 0.3, 0.5, 1 or 5 mM in the protein solution. No other chemicals are added.

3.5.1. SAXS Measurements

The effect of DTT on the purified protein was first investigated by SAXS measurements at the X33 SAXS beamline of EMBL Outstation in DESY, Hamburg. AGG2* was purified at Sabanci University and samples were taken to the synchrotron for measurements. Figure 3.19

displays the scattering patterns taken at different DTT concentrations. The gradual change in $I(0)$ values, which are correlated with the scattering mass, indicates a change in the mass of protein as a function of DTT concentration. Similarly, as can be seen from figure 3.19 B, the radii of gyration get smaller as DTT concentration increases.

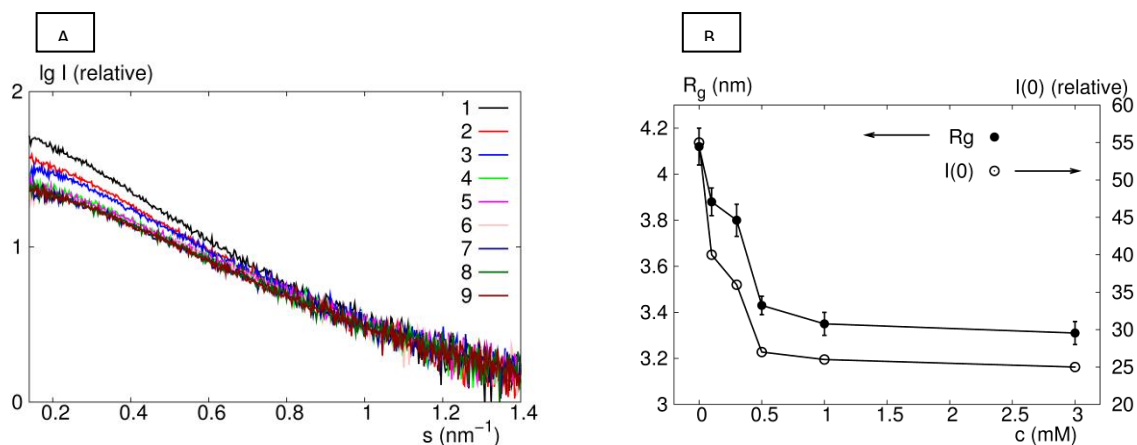


Figure 3.19 Dependence of the X-ray scattering from 1.2 mg/ml AGG2 on the DTT concentration in the buffers. (A) SAXS curves. 1: no DTT, 2: 0.1 mM, 3: 0.3 mM, 4: 0.5 mM, 5: 1 mM, 6: 3 mM, 7: 5 mM, 8: 10 mM, 9: 30 mM); (B) Dependence of the radius of gyration R_g and the forward scattering intensity $I(0)$ on the DTT concentration.

The change in oligomeric state of AGG2 has been also shown by comparative R_g and Molecular Mass (derived from $I(0)$) values of SAXS data. The transition is shown as in tetramer – dimer percentage shift in solution in table 3.2:

DTT c (mM)	R_g (nm)	MM (kDa)	volume fraction dimer	volume fraction tetramer
0	4.12 ± 0.08	64 ± 6	0*	100*
0.1	3.88 ± 0.06	47 ± 5	0.33 ± 0.03	0.67 ± 0.03
0.3	3.80 ± 0.07	42 ± 4	0.54 ± 0.04	0.46 ± 0.04
0.5	3.43 ± 0.04	31 ± 3	0.78 ± 0.03	0.22 ± 0.03
1	3.35 ± 0.05	30 ± 3	0.86 ± 0.03	0.14 ± 0.03
3	3.31 ± 0.05	29 ± 3	0.90 ± 0.03	0.10 ± 0.03
5	3.27 ± 0.05	28 ± 3	0.90 ± 0.03	0.10 ± 0.03
10	3.32 ± 0.05	29 ± 3	0.89 ± 0.03	0.11 ± 0.03
30	3.33 ± 0.05	29 ± 3	100*	0*

Table 3.2 Oligomeric state transition shown as tetramer – dimer percentages

The ratio of tetramer is observed to be 100% when there is no DTT in the solution, and the dimer is 100% in solution when DTT concentration is highly excess (30mM DTT).

SAXS curves were used to develop *ab initio* shape models for the various states of the protein in solution. Using modeling algorithms DAMMIN and GASBOR the likely shapes which would give rise to the observed scattering were calculated and the convergence of these models were established using the averaging algorithm DAMAVER. DAMMIN and GASBOR calculations gave converging models and those obtained with DAMAVER are shown in figure 3.20. In this figure, the structure shown in red is deduced from the β -subunit of transducin of mammalian cells (PDB: 1TBG), the green protein is the AGG2 with 1 mM DTT and the blue protein is AGG2 with no DTT in the buffer:

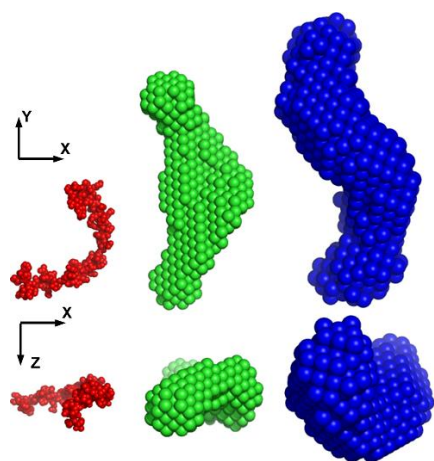


Figure 3.20. Averaged *ab initio* models of the no DTT containing (green) and 1 mM DTT containing (blue) AGG2 compared with the monomeric structure (red) extracted from the crystal structure of a G-protein beta gamma dimer (PDB code: 1TBG)

Model structures appear to be consistent with one another: the model structure shown in green corresponds to a protein which is twice as large as that shown in red and the structure shown in blue seems to contain two of the models shown in green attached from their ends. The model shown in red is simply a monomer. It is possible to conclude that the model shown in green is a dimer and the model in blue is a tetramer of the AGG2 protein. This finding is further investigated with DLS and CD methods.

3.5.2. CD Measurements

CD measurements provide information on the type and amount of secondary structure elements for biological macromolecules. Results can be quantified through comparison with known structures in databanks. CD profiles of AGG2 containing varying amounts of DTT are given in figure 3.21.

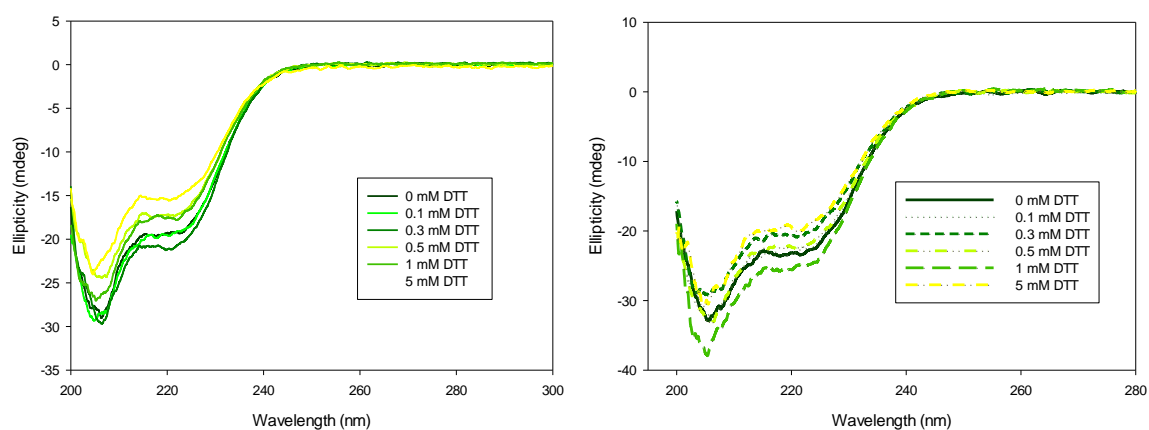


Figure 3.21 CD Spectra of DTT Concentration Series of AGG2 (left AGG2*, right AGG2)

Features of these spectra i.e. the minimum band at about 210(-) nm and the hump between 210(-) and 220(-) nm are typical features for α -helical structures and confirm that our recombinant AGG2 protein possesses the native fold. There is an upwards shift in the plots with increasing amount of DTT in the protein solution. The effect of this upward shift is related to the secondary structure of the protein, especially the alpha helix content which is further analyzed in table 3.2.

3.5.3. DLS Measurements

DLS measurements yield information about size and polydispersity of particles in a solution. In particular, size distribution as a function of scattered intensity is sensitive to the larger particles in solution. As can be seen from figure 3.22, change in the protein size as a function of DTT concentration is clear.

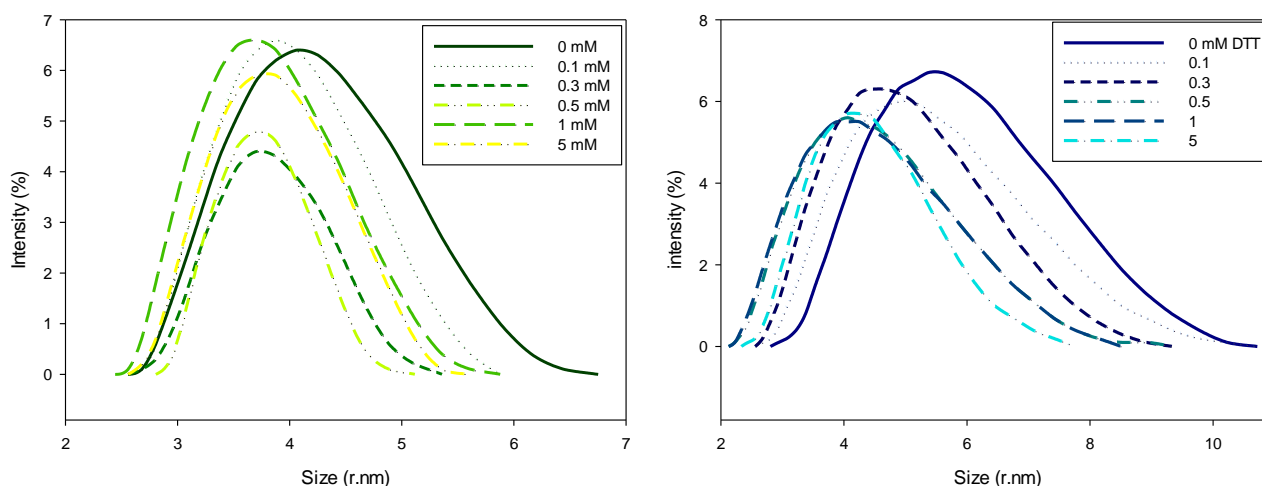


Figure 3.22 DLS measurements of change in size of AGG as a function of DTT concentration. Left AGG2*, Right AGG2

Hydrodynamic radii change as a function of DTT but R_H is not halved between 0 mM DTT and 5 mM DTT. This is partly due to the polydispersity in the solution and co-existence of multiple levels of oligomerization in solution. Another factor contributing to this observation is the assumption of scattering from spherical particles for calculation of R_H . The structure of AGG2 is known to be elongated (Clapham D. E., 1997).

3.5.4. PAGE Analysis of DTT Treated AGG2

The proteins were run on both SDS and Native Page. Protein oligomeric state is clearly visible in Native PAGE. SDS was run to see the protein when denatured and also to observe and prove the protein existence with Western blotting. All the samples were loaded 1mg/ml into the wells.

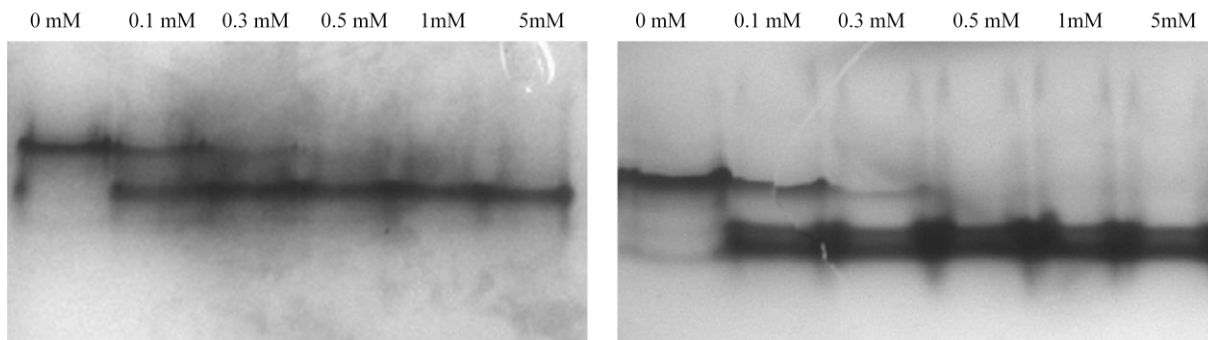


Figure 3.23 Coomassie Stained Native – PAGE for DTT Concentration Series of AGG2 (left: AGG2*, right: AGG2)

In the figure 3.23, the effect of DTT on AGG2 is clearly visible; with increasing amount of DTT, the protein goes through a transition of tetramer to dimer. The exact oligomeric state of the protein with these gel photos is not clear because sizes of proteins run on native gels can't be determined, but the size transition of AGG2 is visible, assuming migration of the protein on native gel is dependent on its size. The pixel calculation for AGG2* by the Discovery software shows that the percentage of the tetrameric form in 0.1 mM DTT is app. 30% and, in 0.3 mM DTT around 15% and for the higher DTT concentrations, the bigger protein fraction is almost gone at all. For AGG2, the tetramer is app 20 % in 0.1 mM DTT and 8 % for 0.3 mM DTT containing samples. The conversion of tetramer to dimer is faster for AGG2 samples than AGG2*.

The figure below belongs to a Western blotting film. The antibody used is RGS-6His antibody (Invitrogen) and the blotted protein is AGG2*. The transition here is also visible with SDS because in this particular gel, the protein samples were not denatured. When the samples were loaded to the gel after a denaturing process with DTT, β - Mercaptoethanol and heating, no oligomeric state difference between the DTT series samples were observed. The western blotting of AGG2 could not be retrieved, which will be discussed later.

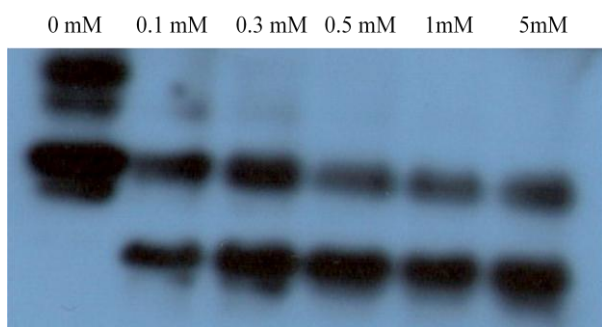


Figure 3.24 Western Blot Results of DTT Concentration Series of AGG2

A summary of all the results obtained from all the methods is listed in the table 3.2:

		0mM DTT	0.1 mM	0.3 mM	0.5 mM	1 mM	5 mM	
SAXS (AGG2*)	R _g (nm)	4,18	3,87	3,74	3,41	3,32	3,25	
	I ₍₀₎	55,09	39,84	35,76	27,37	26,27	24,37	
	D _{MAX} (nm)	14,6	13,6	13,1	11,9	10,9	10,9	
	Mass (kDa)	62	45	40	31	30	27	
DLS	AGG2*	R _H (nm)	5,26	5,85	4,84	4,53	4,11	Noisy
		Std. Dev.	0,947	0,874	1,15	0,834	0,546	Noisy
		Polydispersity(%)	18,0	14,9	23,8	18,4	13,3	Noisy
	AGG2	R _H (nm)	5,82	5,32	4,92	4,4	4,41	4,37
		Std. Dev.	1,45	1,4	1,26	1,2	1,23	0,954
		Polydispersity (%)	24,9	26,3	25,6	27,3	27,9	21,8
CD	AGG2*	Alpha Helix (%)	41,5	42,3	45	36,7	38	32,2
		Beta Sheet (%)	13,4	13,1	12,1	15,1	14,8	17,5
		Other (%)	43,6	43	41,1	46,9	46,2	51
	AGG2	Alpha Helix (%)	47,2	46,8	42,9	44,7	41,9	40,7
		Beta Sheet (%)	11,7	12,4	12,2	11,9	13,1	12,8
		Other (%)	39,8	38,6	41,9	41,6	45,7	45,2

Table 3.2 Effect of DTT on the oligomeric state of AGG2

SAXS measurements clearly state that the protein is shifting its oligomeric form from tetramer to dimer. This conclusion is based on the fact that the MM and the radii of gyration change accordingly. DLS measurements also show the state of change via values of the hydrodynamic radius. Both AGG2 and AGG2* show a decrease in hydrodynamic radius of the protein. The standard deviation also shows that proteins are not in a highly polydisperse oligomeric state. Hydrodynamic radius change for AGG2 is not a drastic as AGG2* and the standard deviation values are a bit higher. CD spectropolarimetry results show a less dramatic

change in the secondary structure of the protein. The alpha helical content of AGG2* shows a 10% variance and AGG2 shows an approximate 7% change. There is no major change in beta sheet content which is expected because these proteins do not contain any beta sheet structure.

3.6. Effect of Protein Concentration of AGG2

It is a known experimental fact that when the protein is highly concentrated, there is a tendency for aggregation. Thus, the effect of concentration on the oligomeric state of the protein was inspected for AGG2.

3.6.1. SAXS Measurements

The protein was concentrated with Protein Concentrators (Millipore) up to 5mg/ml and the measurements were done for varying concentrations with both no DTT and 1 mM DTT environment shown in figure 3.25.

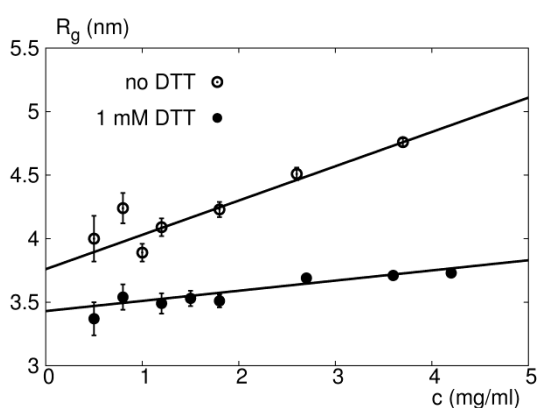


Figure 3.25 Dependence of radius of gyration (R_g) on the AGG2 concentration in different buffers with 1mM DTT (filled dot) and without DTT (empty dot).

The radius of gyration of the protein increases with increasing concentration of the protein. The change is even better visualized with no DTT containing environment. The effect can be caused by both the increasing concentration of the protein or the process of concentrating the protein (like concentration by centrifugation, etc). Either way, the effect is more readily observed when there is no DTT in solution.

Protein buffers contained no DTT for all the following biophysical experiments on the concentration series of AGG2 and AGG2*.

3.6.2. CD Measurements

For CD measurements, just like SAXS, the protein is concentrated and measurements were done by the diluted samples to have a concentration series. The concentrations of the samples are given in the legend of the figure 3.26 below:

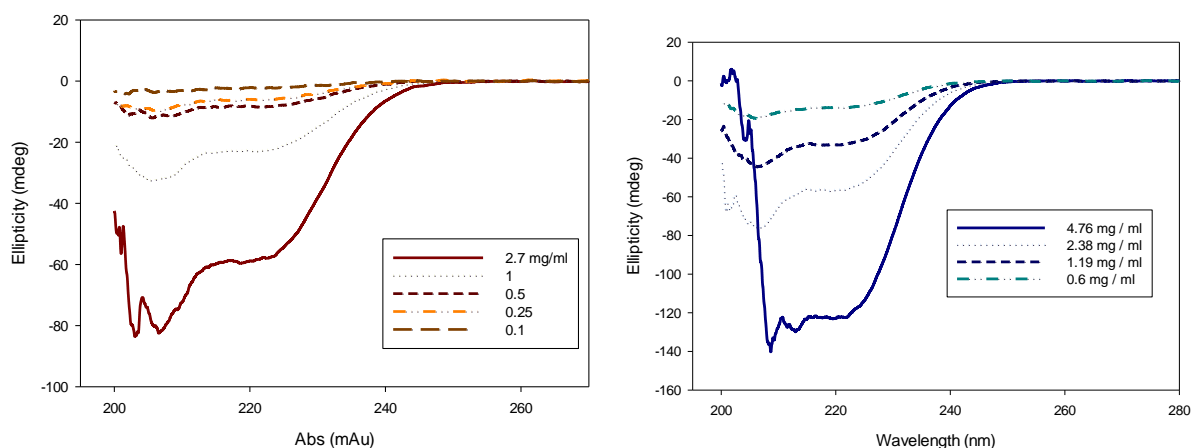


Figure 3.26 CD Spectra of DTT Concentration Series of AGG2 (left AGG2*, right AGG2)

The change in the spectra of the protein is directly caused by the concentration difference of the protein because when the spectra are normalized with respect to concentration no major difference between the curves is observed (data not shown). The shape of the plots and the percentages of the secondary structure of samples show a high correlation to the 0 mM DTT containing sample readings in DTT concentration series experiments.

3.6.3. DLS Measurements

The procedure is the same for the DLS measurements also. The intensity graphs of varying protein concentration samples are plotted together in figure 3.27.

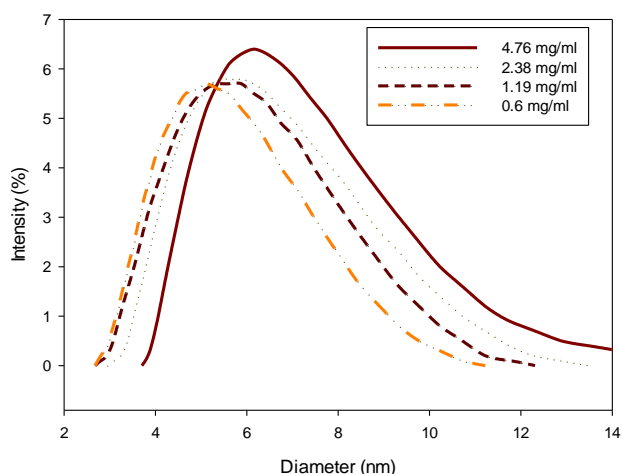


Figure 3.27 DLS Intensity Graph for Protein concentration series of AGG2

DLS measurements show that at 4.76 mg/ml, R_H is slightly larger than the other readings, this is likely to be due to the aggregation occurring within the sample. AGG2* readings show no difference (data not shown). Hydrodynamic radius of the samples show a very high correlation to the 0 mM DTT readings on DTT concentration series experiments detailed in above sections, which is approximately 5.2 nm.

3.6.4. Native – PAGE Results

Concentrated samples were loaded to 8% native gels directly to see the effect of the concentration of the protein. The figure 3.28 below shows that there is no difference among the samples except for the thickness of the bands which is basically caused by the concentration difference of the loaded samples.

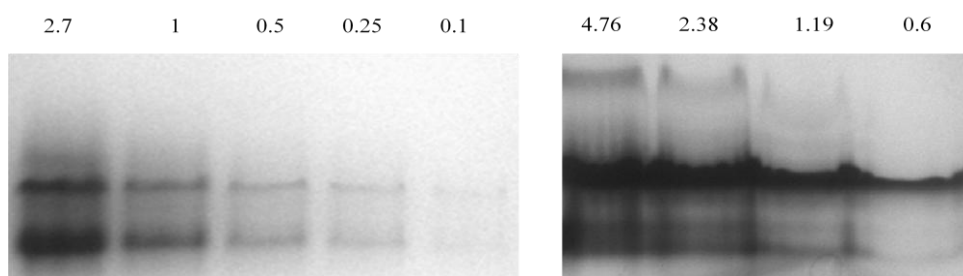


Figure 3.28 Coomassie stained Native –PAGE Results of Protein Concentration Series (left: AGG2*, right: AGG2)

The thicknesses of the bands are correlated with the concentrations of the loaded samples. The pixel calculation by the Discovery software verifies the fact. Additionally, two bands are observed just very similar to the results obtained in DTT series experiments. The percentages of the bands are also correlated.

3.7. Homology Modelling of AGG2

Homology modeling was pursued to obtain the structure AGG2 based on information on the structure of the mammalian g-subunit and also to investigate if the results of the *ab initio* models based on SAXS measurements were consistent with the known structure. Alignment of amino acid sequence of AGG2 with the γ subunit of transducin (1TBG) is the first step for homology modeling:

```

1tbg      -----APVIN--IEDLFEKDKLRMEVDQLKKEVT-----LPRML-VSKCCEFRDYVEERSGEDP-----LVKGIIP-EDKNPFK-
agg2      MRGSHHHHHHGSEAGSSNSSGQLSGRVVDTRGKHRIQAELEKRLLEQEARFLEEELEQLEKMDNASASCREFLDSVD--SKPDPLLPETTGFVNATWDQWFEFGPKKAKRCGCSILGTPGRPAAZLN-
          *... *... *... *... *... *... *... *... *... *... *... *... *... *... *... *... *... *... *... *... *... *...

```

Figure 3.29 Alignment of AGG2 amino acid sequence with that of gamma subunit of transducin (PDB: 1TBG)

The alpha helical region of transducin gamma subunit and AGG2 are aligned successfully. The overall protein conformation and secondary structure localization is very close to transducin subunit.

The alignment was loaded to Modeller program (Eswar, 2006) and a structure that has a long loop in the N-terminus and in C-terminus was obtained. The long loop in N-terminus is a result of the tag region of the protein introduced in the construct for purification reasons and the C-terminus loop is caused by the non-aligned region of AGG2 with transducin counterpart. The protein sequence was also uploaded to I-TASSER server to get a second *ab initio* model, but this model tried to compact the structure into a more condense state by adding additional alpha helices and beta sheets:

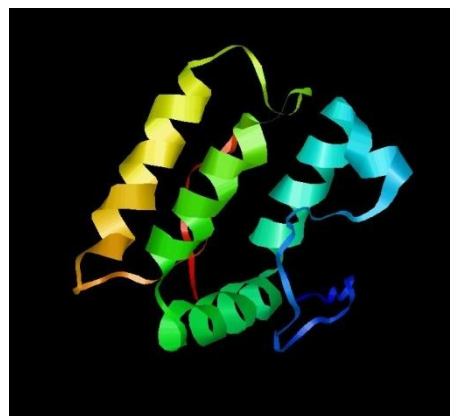
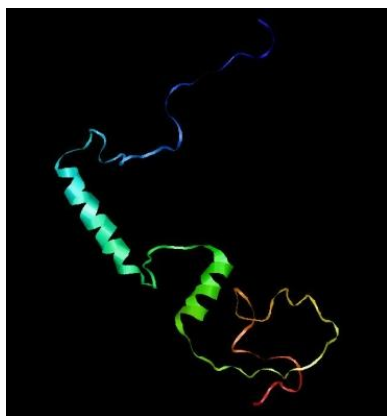


Figure 3.30 Homology Modelling of AGG2 by MODELLER program (left) and *Ab Initio* modeling of AGG2 of by the I-TASSER Server (right)

The biophysical characterization had shown that the protein is in dimer form. This was also applied to the model calculations and the protein was docked to itself by the Grammx and I-Tasser servers. Both docking processes were done as a self-alignment:

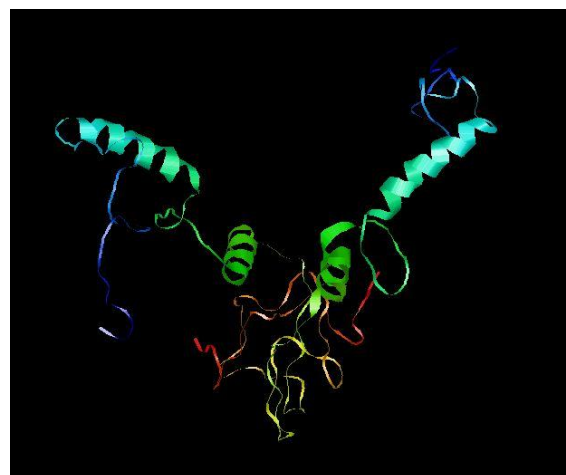


Figure 3.31 Protein Docking Server Results for the dimerization of AGG2 (Left: with Grammx server, Right: with I-Tasser server)

The docking obtained by the servers and the *ab initio* modeling by SAXS (with 1 mM DTT) were overlapped to see if any similarity occurs. The Grammx server result fit quite well with the SAXS results:

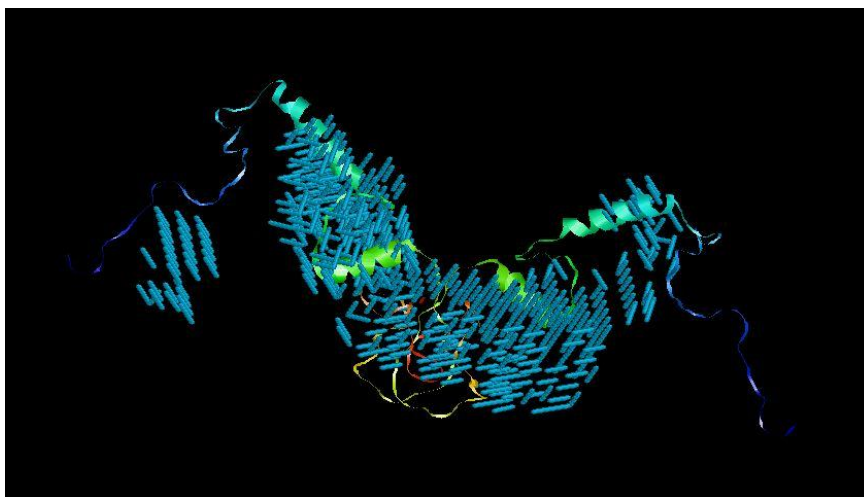


Figure 3.32 Overlap of GramMX docking result with *ab initio* modeling of SAXS measurement (1mM DTT)

A complete overlap is not observed most probably because of the loop regions in N and C termini, but the level of similarity is satisfactory. Verification of the structure similarity was done with CRY SOL software which fits the experimental curve to the theoretical scattering plot of the docking model of AGG2. The overlap between the curves can be seen in figure 3.33.

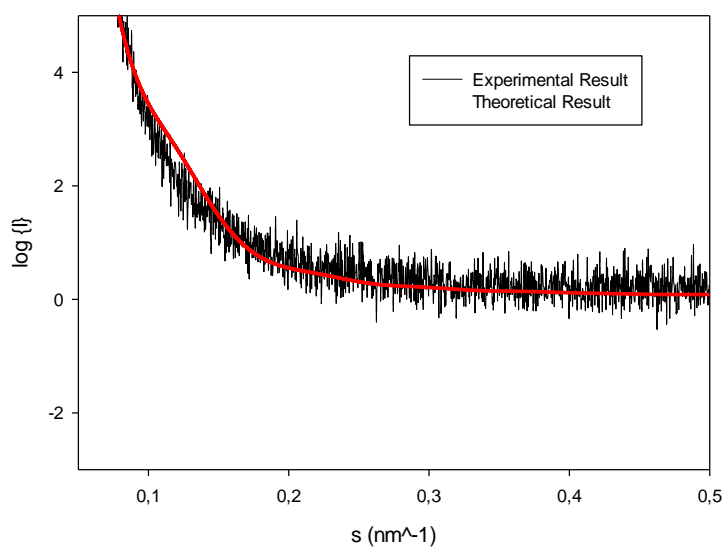


Figure 3.33 Overlapping the result obtained from the CRY SOL software and the data obtained from SAXS Measurement.

3.8. Crystallization of AGG2

Sample from the purified AGG2 protein was sent to EMBL Hamburg crystallization facility to screen a wide range of conditions for crystallization. The robotic system prepared the samples with various crystallization kits and with conditions that contained 0.3 M Na₂SO₂ + 20% PEG 3350, as can be seen in figure 3.34, some crystals formed. Whether they are salt crystals or actual crystals of AGG2 are going to be tested.

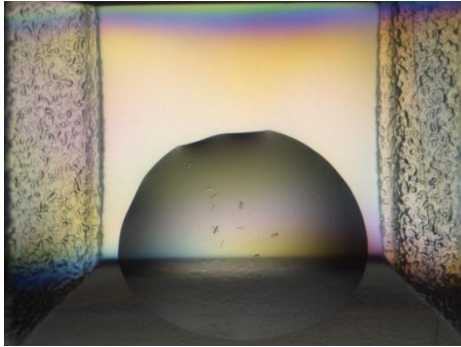


Figure 3.34 Picture taken by the robotic system at EMBL Hamburg PETRA crystallization facility, showing the crystals from an AGG2 solution.

4. DISCUSSION

4.1. AGG2 Cloning, expression and purification

In our lab *AGG2* gene, purchased from TAIR, had already been cloned to the pQE80-L (Kaplan, 2009) and expressed for purification of the synthesized protein. Preliminary biophysical characterization studies had been conducted on this protein. However, sequencing had shown that the gene contained coding for additional 11 amino acids attached to the N-terminus. Although this did not hinder expression and purification and the protein was observable with the western blotting, the influence of additional amino acids on the three dimensional structure of the protein was unknown. Moreover pQE80-L plasmid did not contain a cleavage site for removal of the His tag from the recombinant protein. It was, therefore, decided to investigate utilization of new systems for heterologous expression of the *AGG2* gene and biophysical characterization of the recombinant protein. It is also interesting to note that although the first report of the *A. thaliana* α -subunit appeared in 2001 (Mason et al., 2001), there has been no detailed biochemical or biophysical characterization studies on this protein. This lack of information led us to suspect instability of the protein under heterologous synthesis conditions. We explored more than one expression system for *AGG2* in case instability problem occurred when *AGG2* is expressed on its own without the beta subunit which is its native partner.

The two new plasmids we utilized were pMCSG-7 and pETM-41. The former contained a 6 histidine (6His)-tag and a cleavage site for Tobacco Etch Virus (TEV) protease enzyme (Kapust RB., 2002) allowing the removal of the tag after purification to yield the native protein. Cloning of the gene using pETM-41 plasmid, which contains Maltose Binding Protein (MBP) as a tag as well as the 6His tag, allows the recombinant protein to be purified using amylose resin for affinity chromatography.

The three constructs: pMCSG-7, pQE80-L and pETM-41 were all used in studies of *AGG2* gene expression in *E. coli* TOP10 cells and growth curves and gene expressions were obtained under identical conditions. Cultures were initially grown in LB medium, but 50%

better protein yield was obtained from 2 L cultures in TB. In TB, biomass was 2 times higher compared to LB. Protein yield was around 9 mg from LB grown and about 27 mg from TB cultures. It appears that TB affected not only biomass but also the level of expression in TOP10 cells.

As explained in chapter 3 purification of AGG2 was pursued using the pMCSG-7 (AGG2) and pQE80-L (AGG2*) constructs, which yielded very similar elution patterns from Ni-affinity column. At the first step of purification the inefficiency of the pETM-41 construct was observed Expression of the fusion protein MBP-AGG2 appeared to be very low. The only peak in the chromatogram, which is observed in all constructs, contained E. coli Ef-Tu protein which is involved in translation. Recombinant AGG2 synthesis was so low that it could not be detected even by western blotting after collecting the elution fractions of affinity chromatogram (data not shown). One band in the SDS-PAGE analysis may have corresponded to but even this was questionable. Since DNA sequencing showed the presence of AGG2 in the construct, reasons for not being able to detect the recombinant protein may lie either at the level of expression or at the level of synthesis and stability of the recombinant protein. It appears that the problem lies at the latter phase and possible reasons for problems with this construct may be the presence of MBP, which may hinder folding and rapid proteolysis may occur due to improper folding. There may also be targeting of the recombinant protein into inclusion bodies. This possibility was not checked since expression with the other constructs was satisfactory. It is also interesting that even the MBP on its own is not observed on the gel or with the western blotting. Here the protein was labeled with anti-his antibodies and the his-tag is located upstream of MBP and should not be affected by the condition of AGG2. As a conclusion, AGG2 could not be detected from the pETM-41 construct and although we made some attempts to see if we could improve expression eventually we decided that focusing on the other two constructs will be more efficient use of time.

SDS-PAGE analysis results of the protein from pMCSG-7 and pQE80-L constructs are very similar and show that proteins are homogeneous. The protein expression level is very satisfactory: the samples loaded to the gel are diluted 5 times (Figure 3.13). As can be seen from figure 3.13, affinity chromatography still left behind some contaminating factors and attempts were made to further purify proteins by ion exchange and size exclusion chromatography. The buffer of samples from affinity chromatography was exchanged with

Tris buffer pH 8.0 facilitate negative charging for anion exchange chromatography.. The reason behind is the fact that the AGG2 construct contained 6His tag which is highly positive which can bind to negatively charged resin. A comparison of the elution profiles shows that AGG2* from the pQE80-L construct is eluted at a lower NaCl concentration compared to AGG2. The existence of additional arginine, glycine and serine residues upstream of 6His tag may be involved in this behavior resulting in weaker binding of the protein to the negatively charged resin. It is seen, however, from SDS – PAGE results of the eluates that the two proteins are not different.

SEC was used to assess molecular mass of purified proteins independently from SDS-PAGE analyses, to monitor polydispersity in protein solutions and to analyze co-existing oligomeric forms. Protein concentrations of the samples were always measured before loading to the Superdex 16/60 column (GE Lifesciences). When overloaded with high concentration of proteins, the column loses its ability to clearly resolve proteins that differ in size. The system was run at 1ml/min speed to enhance the column's ability to separate proteins.

DTT was omitted from AGG2 protein solutions and from the buffers used for running the column. Under this condition the elution profile displayed two peaks (figure 3.16 right). The elution profile of AGG2*, on the other hand, contained only one peak (figure 3.16 left). The second peak of AGG2 is eluted in the same elution volume range as AGG2*, indicating that the proteins have similar masses, but in this chromatogram an additional bigger protein was also observed. The only difference between the two purifications is DTT in the buffer. DTT is known for its strong reducing capability of cysteine residues, breaking disulfide bonds. DTT is used to inhibit aggregation of proteins, because when exposed to outer surface, cysteine residues tend to form disulfide bridges establishing aggregates, and DTT reduces this phenomenon (Cleland W.W., 1964). SDS-PAGE analyses reveal AGG2* as a single band indicating a direct effect of DTT on the oligomeric state of the protein. Analyses showed that, the first peak in the AGG2 elution profile corresponds to a mass of 87 kDa and the second peak to 46 kDa. The molecular masses calculated from the elution volumes are not exactly two-fold, but a crude approximation can be made to confirm that the first protein is two times larger than the second one. The situation observed in SEC is also validated by Native-PAGE. In figure 3.17b, the comparison of AGG2 first and second peaks show a difference in the electrophoretic behavior size of the protein.

We came across another unusual observation with AGG2: no visible bands were observed in the western blots. This phenomenon occurred regardless of the step of purification: nickel affinity, ion exchange and size exclusion. RGS-6His antibody (Invitrogen) is used for AGG2* blotting and as seen in figure 3.17, the band is thick and visible. For AGG2 blots the 6His antibody (Roche) is used and no bands can be visualized. In control experiments, the same antibody was used for labeling the β subunit of G protein, AGB1, which was obtained from a pMCSG-7+AGB1 construct and the result was positive. It was thus clear that there was no problem with the antibody. Additionally, when AGG2* obtained from pQE80-L construct is blotted with 6His antibody, the bands are visible (data not shown). It appears that this anomaly may be due to interaction of His amino acids with the residues of AGG2 and not being available for antibody binding. However, it is still puzzling that 6 His residues are available to interact with the affinity column but not with the antibody. On the other hand, it is observed that no other difference occurs between AGG2 & AGG2*, so the problem should not arise from the different tag regions ligated to the proteins.

4.1.1. Biophysical characterization of the gamma subunit and its oligomeric forms

Results from SAXS measurements with AGG2* in 1mM DTT containing buffer yielded a molecular mass that is 3 times that of the monomer, indicating a mixture of tetramers and dimers in solution.

DLS results, obtained for the first peak of AGG2 and AGG2* indicated that the former appears as a much larger protein than the latter. For both measurements, the hydrodynamic radii of the proteins are larger than expected; a mass of app. 80 kDa is obtained for AGG2*, which is unexpected comparing to the other results obtained by other characterization methods. The reason behind this is the assumption of spherical shape, used by the software, for all proteins. This software determines the largest dimension of the particle in solution, and even if the particle is rod-shaped, it calculates a molecular mass assuming that the particle is spherical thus adding mass to a volume which does not belong to the particle. This yields a mass value which is much larger what is expected.

Differences in the features of CD spectra for the two proteins are not drastic, but still obvious. Presence of DTT results in 2.5 % increase in alpha helical content and 4% decrease in unstructured regions. The software tries to fit the data into a structure that contains all

structural elements. CD Deconvolution softwares compare spectra of proteins with known structures with that of experimental data. For AGG2, inevitably, the software inserts a certain ratio of beta-sheet to the overall percentage. The spectropolarimetry measurements are deviated by the unstructured regions of the proteins, so this may be the reason for the software to add a certain ratio of beta-sheet structure to the overall percentage.

4.2. DTT Effect on the Oligomeric State of AGG2

Differences in biophysical characteristics of samples with and without DTT led to investigation of effects of varying concentrations of DTT on the protein structure. Proteins were purified either with 1 mM (AGG2*) or 0 mM DTT (AGG2). When effects of DTT were investigated in detail, a range of buffers also containing 0.1, 0.3, and 0.5 mM DTT were prepared and proteins were incubated in these conditions.

Increasing DTT in the solution decreases the radius of gyration and the mass of the protein calculated from the extrapolated $I(0)$ values. A dramatic change is observed by comparison of results of 0 mM with 0.1 mM DTT and 0.3 mM with 0.5 mM DTT (figure 3.19). The initial addition of DTT initiates breakdown of the oligomeric state of AGG2 proteins, and the second high level of change, between 0.3 – 0.5 mM DTT, shows a saturation point of the protein with DTT. The change level is lower between 0.5 – 1 and approximately no change is observed between 1 – 3 mM DTT. The saturation point among the concentration values of DTT seems to be 1mM DTT.

Ab initio shape models of the protein based on SAXS data show good agreement with the structure of gamma subunit of transducin obtained from crystal structure analyses. Both *ab initio* models from SAXS yield structures that are bigger than the results from crystal structure; this is expected since SAXS models define an outer envelope of the protein and fills inside with decoy residues. On the other hand, the crystal results define precise amino acid residues and exact 3-D structure of a protein is formed. Thus, the thickness and low resolution of SAXS measurement modelings are in the scope of the technique.

Studies of structural changes and oligomeric state of AGG2 as a function of increasing DTT concentration using CD indicates that the decrease in the alpha helical content and increase in unstructured regions may be a sign of the protein becoming more disordered as the oligomeric state changes from tetrameric to dimeric form. It appears that the tetrameric form is more condensed. In the oligomeric state, the monomers are expected to interact either from

the N-terminus or C-terminus. In AGG2 both ends have unstructured loops, so the interaction of dimers can hide the loops to have a more stable state. New alpha helical content may not occur, but the hiding of unstructured region may hinder detection of the unstructured regions and the oligomers may be more compact.

Measurements with blanks showed that the differences observed in CD spectra were not due to the presence of DTT in the buffers, but differences exist in the secondary structure content structures of AGG2 and AGG2*. The alpha helical content of the AGG2 is higher than that of AGG2* and the opposite trend is observed for the unstructured regions. The higher percentage of unstructured region for AGG2* is likely to be due to the additional 11 amino acids in the C-terminus of the protein (G T P G R P A A K L N) added to the protein from the pQE80-L plasmid. 11 amino acids constitute around 11% of AGG2*, which is equal to the percentage variance between AGG2 and AGG2*.

Changes in protein structure with increasing DTT concentration were also detected in the DLS measurements. Here too increasing concentrations of DTT resulted in reduction in the size of the protein which is measured in terms of hydrodynamic radii. AGG2 is an elongated protein, so the decrease in size detected by DLS measurements is another sign that the protein is forming the tetramer by interaction of N or C termini. If the protein would interact from the middle regions, then the radius would not be affected in a drastic way. If the radius is decreasing, this should simply mean that dimers are detaching from the N or C termini when the tetramer decomposes. Changes in radii of protein molecules monitored by SAXS and DLS are consistent with each other; both measurements show 23 % radius change from 0 mM DTT to 5 mM DTT containing solutions.

Differences between the DLS measurements carried out with AGG2 and AGG2* are observable just like CD results. Although the number of residues is less, AGG2 seems to be larger than AGG2* for all the DTT concentration measurements. The reason behind this size difference opposite to what is expected, is not very clear, but based on CD results, one explanation may be that the additional 11 amino acids residues in the C-terminus of AGG2* makes the protein more compact and ordered. The additional residues, like the 6 His tag, introduce excess positive charge. The positive charges of two termini may force the protein into a more compact structure. So the size of AGG2* can be smaller than AGG2. One other

aspect may be the high polydispersity level of AGG2 DLS readings. The results may in fact be very similar after all.

Native-PAGE analysis allows direct monitoring of the oligomeric state change of AGG2 and AGG2* albeit due to lack of a reliable method for MM determination from native-PAGE, exact oligomeric state cannot be determined from the gels. This method also shows that the changes are more drastic in the transitions 0 – 0.1 mM and 0.3 – 0.5 mM DTT. The results correlate with those from SAXS measurements discussed above. There seems to be no variance between AGG2 and AGG2* bands in gels. The shift is clearly observed between the two proteins.

The bands observed in the western blotting are similar to the results obtained in Native-PAGE analyses. Although the western blot samples were not denatured for loading, the change observed is not as clear as in Native PAGE because of the SDS in the gel matrix and in the running buffer. No bands were observed for AGG2, as discussed above. Since oligomerization may be a consequence of protein concentration this factor was investigated for both AGG2 and AGG2*.

The protein concentration effect is more obvious in SAXS measurements when there is no DTT in the environment. This is likely to be due to the tendency of proteins to be in a higher oligomeric/aggregated state at high concentration. Radius of gyration change for 1 mM DTT containing sample is not large because the oligomeric state of the protein is determined to be a dimer and change in protein size should not be observed as drastic as 0 mM DTT containing samples.

CD plots of protein concentration series show large differences. Positions of the peaks are identical but the heights are different, and the height is directly proportional to the concentration of the protein measured. When the measurements are plotted in units of molar ellipticity spectra are normalized with respect to concentration and spectra become identical showing that the secondary structure content is independent of protein concentration. There is only a slight change in most concentrated protein sample, which is expected because the proteins tend to get aggregated when highly concentrated and this may deviate the actual measurement results..

DLS intensity graphs of the concentration series point to the same conclusions as the CD results. Only the highest concentration protein solution gives a somewhat larger

hydrodynamic radius which can be caused by protein aggregation. The Native-PAGE results of the concentration series also show no major differences among the samples. Taken together results show that the concentration has very little effect on the oligomeric state of the protein.

4.3. Structural Modelling of AGG2

Two approaches were used to obtain theoretical models for the structure of native AGG2. In one approach homology modeling based on transducin structure was pursued. Transducin (1TBG) crystal structure has been known for a long time (Sondek J., 1996). So, AGG2 protein was aligned to gamma subunit of transducin and the alignment score was good enough to continue to modeling except for 2 loops, one in the middle and one near the C-terminus of the protein. The plant homologs of γ subunits are longer than mammalian homologs, so the difference in length should not be a problem for the alignment. Modeller program was used for homology modeling of AGG2 and a structure with only two alpha helices and one loop in N terminus and one other in the C terminus was obtained.

In the alternative approach, AGG2 sequence was uploaded to I-TASSER server to obtain an *ab initio* model. The model obtained showed four alpha helices and one small beta sheet. The structure is highly compact which is unusual for the intrinsic nature of the protein. I-TASSER server seems to condense the primary structure of a protein into a very compact one. Thus, the I-TASSER model was not further studied.

All experiments done for AGG2 characterization showed that the protein is in dimeric form and it has not been possible to obtain the monomeric form. To understand this situation the protein was self-docked and the structure of the dimer was explored. Although several structures were obtained only one appeared to be in agreement with the *ab initio* model obtained from SAXS measurements. The agreement of the docked structure with experimental data was validated by calculating the scattering pattern from the model.

The G-protein Gamma subunits are always found as dimers in both plant and mammalian cells (Clapham D. E., 1997). The $\beta\gamma$ dimer is formed in Golgi Apparatus and then placed in the plasma membrane (Kato C., 2004). These facts point out that the gamma subunit is never observed as a monomer in the cell membrane. Thus, the protein is not observed as a monomer after purification from E.coli as well. No trace of the monomer can be retrieved in any stage of the study. Even highly denaturing conditions like 20 min boiling at 100 °C, addition of 100 mM DTT + 10 μ M Betamercaptoethanol could not change the dimeric nature

of the protein into monomeric. The absence of any trace of monomer structure after all these denaturing conditions shows that the dimer is highly stable. This stability is in agreement with studies reported in literature because $\beta\gamma$ dimer is found to be localized and replaced from the plasma membrane as a dimer (Mason MG., 2001). Gamma subunits are not stable as a monomer in any condition in a cell so the presence of the protein ligated to another protein is essential for the stability of the protein. This can be the main reason for the high stability of the AGG2 as a dimer through all the processes.

AGG2 contains a CAAX (x: any amino acid) box for isoprenyl modification for localization on the plasma membrane (Cook L., 2001). When overexpressed heterologously in E coli, the protein cannot undergo post-translational modification and hence does not acquire an isoprenyl group. Furthermore it cannot interact with any other proteins to stabilize the structure because simply there is no G-protein homolog in prokaryotes (McCudden C.R., 2005). Thus, in recombinant AGG2 the CAAX box does not interact with isoprenyl for membrane localization, leaving the Cys residue available for interactions. The obvious candidate may be a similar residue within another AGG2 protein and a disulfide bridge may be formed. A disulphide bridge prediction server, DiANNA, predicts that the Cys67 and Cys106 have a high probability to form a disulphide bridge but the Cys 108 appears to have low probability for disulfide formation. Cys108 is located in the CAAX box. Dimer structure obtained from homology modeling shows that the C termini loops of the two monomers form an intertwined ball like structure. The CAAX box is located in this structure and it is highly likely that Cys108 residues are involved in forming a disulfide bridge which stabilizes this structure. This disulfide bridge may be located deep in the intertwined region and may not be reachable by reducing agents. This prediction is also supported by finding no traces of monomer AGG2 in PAGE, SEC, DLS or SAXS analysis. It is also proposed two dimers may interact from their Cys67 residues to form a tetramer as observed when there is no reducing agent in the solution. This prediction is based on the tetramer-dimer conversion by reducing agents or by denaturation. The interaction of Cys67 does not occur in an end-to-end fashion, because DLS and SAXS results do not show a twofold change in radius of AGG2 when DTT is added.

5. CONCLUSION and Future Works

In this study, *AGG2* gene was inserted in to two different plasmids, pMCSG-7 and pETM-41, successfully for expression, purification and biophysical characterization of the recombinant protein. Protein from a previous construct of *AGG2* with pQE80-L plasmid was also used in characterization studies. High yields, in excess of 9 mg protein/2 L *E. coli* TOP10 culture were obtained. Proteins obtained from pMCSG-7 and pQE80-L were named *AGG2** & *AGG2* respectively. *AGG2* and *AGG2** proteins showed no variance when purified with the same conditions.

It was observed by SEC that presence of DTT in buffers of proteins affected their elution profiles. Investigations demonstrated that the change in protein size was directly related to the oligomeric state: *AGG2* purified in tetrameric form is converted to dimeric state with the addition of DTT. Dynamic Light Scattering (DLS) and Circular Dichroism (CD) measurements supported the findings of SEC.

Dependence of the oligomeric state of *AGG2* on DTT concentration, investigated in detail by SAXS and DLS, showed that the purified protein is in tetrameric form between 0 to 0.1 mM DTT; goes through a transition between 0.3 to 1 mM DTT where dimers and tetramers co-exist in solution and finally dimeric form is obtained above 1 mM DTT. It has not been possible to obtain *AGG2* in monomeric form by further increasing the DTT concentration. Oligomeric state of the protein was observed to be independent of the protein concentration.

Our results indicate that the dimeric form of *AGG2* is highly stable in solution. This may be a consequence of the general tendency of the γ - and β -subunits to form a complex *in vivo*.

The molecular shape models obtained from the SAXS data showed a high level of similarity to the crystal structure of mammalian G-protein, transducin, γ -subunit. The 3-D structure of the protein was further investigated with homology modeling. Alignment of *AGG2* with gamma subunit of transducin was satisfactory for homology modeling. The model of the monomer was self-docked to obtain the dimeric structure. The structure of the dimer

was validated by overlapping the *ab initio* SAXS model with the self-docked dimer and also by comparing the SAXS results with the theoretical scattering curve from the modeled dimer.

The dimer model of AGG2 shows that C-termini loops of monomers are intertwined. Within that region, the CAAX box domain of AGG2, an isoprenylation site, is located. It is proposed that the Cys108 of the two CAAX boxes of monomers may form a disulfide bridge. This prediction may constitute the core of the dimer stability in solution.

Future Works

Purified AGG2 samples are sent to the user facility at PETRA Synchrotron in Hamburg, Germany for crystallization trials. First trials did yield some crystals; however, it is unclear if these are protein or salt crystals. If these crystals originated from protein, electron density maps obtained from X-Ray measurements can be used to model the exact 3-D structure of the protein. This result would also show the validity of models from *ab initio* calculations and from homology modeling.

Tag polypeptide originated from the pMCSG-7 plasmid can be cleaved with Tobacco Etch Virus (TEV) protease. The characterization of the protein without the 6His tag should be analyzed and the results should be compared with the proteins characterized in this study.

The western blotting of AGG2 expressed with pMCSG-7 vector could not be obtained. The validation with western blotting is invaluable, so the reason behind not seeing any bands in western blotting film should be investigated in detail.

The starting point of this study was to form the heterotrimeric *A. thaliana* G-Protein complex. The other two subunits, α and β monomers, were purified separately, but neither the heterotrimer nor the beta-gamma dimer could be obtained *in vitro*. Purification processes of these proteins and the dimer-trimer forming conditions need to be optimized for further trials.

REFERENCES

- Arshavsky V. Y., P. E. (2002). G proteins and phototransduction. *Annu. Rev. Physiol.*, 64, 153 - 187.
- Arzensek D., K. D. (2010). *Dynamic light scattering and application to proteins in solutions*. London: University of Ljubljana.
- Avediano MI. (1995). Phospholipid solubilization during detergent extraction of rhodopsin from photoreceptor disk membranes. *Arch. Biochem. Biophys.*, 324, 331 - 343.
- Aydin, M. (2011). *BIOCHEMICAL AND BIOPHYSICAL CHARACTERIZATION OF MUTANT T. durum METALLOTHIONEIN*. Sabanci University, Istanbul.
- Berstein G., R. E. M. (1992). Phospholipase C-beta 1 is a GTPase activating protein for Gq/11, its physiologic regulator. *Cell*, 70, 411 - 418.
- Blundell TL., H. M. (2000). Protein-protein interactions in receptor activation and intracellular signaling. *Biol. Chem.*, 381, 955 - 959.
- Bohm A., S. P. B. (1997). *Curr. Opin. Biotechnol.*, 8, 480 - 487.
- Brahms, S., & Brahms, J. (1980). Determination of protein secondary structure in solution by vacuum ultraviolet circular dichroism. *J Mol Biol*, 138(2), 149-178.
- Catterall W.A. (2000). Structure and regulation of voltage-gated Ca²⁺ channels. *Annu. Rev. Cell Dev Bio*, 16, 521 - 555.
- Chang C., W. C. (1978). *Analytical Biochemistry*, 91, 13 - 31.
- Chen J.G., S. D. (2003). A seven-transmembrane RGS protein that modulates plant cell proliferation. *Science*, 301, 1728 - 1731.
- Chen JG., P. S., Huang J., Alonso JM., Ecker JR. (2004). GCR1 can act independently of heterotrimeric G-protein in response to brassinosteroids and gibberellins in Arabidopsis seed germination. *Plant Physiol.*, 135, 907 - 915.
- Clapham D. E., N. E. J. (1997). G protein beta gamma subunits. *Annu. Rev. Pharmacol. Toxicol*, 37, 167 - 203.
- Cleland W.W. (1964). Dithiothreitol, A New Protective Reagent for SH Groups. *Biochemistry*, 3, 480 - 482.
- Cook L., H. J. (2001). Identification of a region in G protein subunits conserved across species but hypervariable among subunit isoforms. *Protein Science*, 10, 2548 - 2555.
- Dmitri, I. S., & Michel, H. J. K. (2003). Small-angle scattering studies of biological macromolecules in solution. *Reports on Progress in Physics*, 66(10), 1735.
- Doupnik C.A., K. P. (1997). RGS proteins reconstitute the rapid gating kinetics of gbetagamma- activated inwardly rectifying K⁺ channels. *Proc Natl Acad Sci USA*, 94, 10461 - 10466.
- Druey K.M., K. J. H. (1996). Inhibition of G-protein-mediated MAP kinase activation by a new mammalian gene family. *Nature*, 379, 742 - 746.
- Eswar, N. S., A. (2006). Comparative Protein Structure Modeling With MODELLER. *Current Protocols in Bioinformatics*, 5(6), 1-30.
- Fletcher J. E., G. J. C. (1998). The G protein beta5 subunit interacts selectively with the Gq alpha subunit. *Journal of Biological Chemistry*, 273, 636 - 644.
- Fujisawa Y., K. H., Iwasaki Y. (2001). Structure and function of heterotrimeric G proteins in plants. *Plant Cell Physiol*, 42, 789 - 794.

- Gelli A., B. E. (1997). Activation of plant plasma membrane Ca^{2+} -permeable channels by race-specific fungal elicitors. *Plant Physiol.*, 113, 269 - 279.
- Guinier, A. (1955). *Small-angle scattering of X-rays*: New York, Wiley.
- Himmel H.M., R. U. (2000). Evidence for Edg-3 receptor-mediated activation of IK.ACh by sphingosine-1-phosphate in human atrial cardiomyocytes *Mol Pharmacol*, 58, 449 - 454.
- Instruments, M. (2009). Protein interactions investigated with dynamic light scattering: Malvern Instruments.
- Jacob T., G. S. (1999). Abscisic acid signal transduction in guard cells is mediated by phospholipase D activity. *Proc Natl Acad Sci USA*, 96, 12192 - 12197.
- Jastrzebska B., P. K. (2011). Role of membrane integrity on G protein-coupled receptors: Rhodopsin stability and function. *Progress in Lipid Research*, 50, 267 - 277.
- Kaplan, B. (2009). *Structural Investigation of G-Protein Signaling in Plants*. Sabanci University, Istanbul.
- Kapust RB., W. D. (2002). The P1' specificity of tobacco etch virus protease. *Biochim. Biophys. Acta*, 294, 949 - 955.
- Kato C., I. Y. (2004). Characterization of heterotrimeric G protein complexes in rice plasma membrane *Plant J.*, 38, 320 - 331.
- Kinnamon S. (2012). Taste receptor signalling - from tongues to lungs. *Acta Physiol*, 204, 158 - 168.
- Koch, M. H. J., & Bordas, J. (1983). X-ray diffraction and scattering on disordered systems using synchrotron radiation. [doi: 10.1016/0167-5087(83)91169-9]. *Nuclear Instruments and Methods in Physics Research*, 208(1-3), 461-469.
- Koch, M. H. J., Vachette, P., & Svergun, D. I. (2003). Small-angle scattering: a view on the properties, structures and structural changes of biological macromolecules in solution. *Quarterly Reviews of Biophysics*, 36(02), 147-227.
- Konarev, P. V., Volkov, V. V., Sokolova, A. V., Koch, M. H. J., & Svergun, D. I. (2003). PRIMUS: a Windows PC-based system for small-angle scattering data analysis. *Journal of Applied Crystallography*, 36(5), 1277-1282.
- Laemmli, U. K. (1970). Cleavage of Structural Proteins during the Assembly of the Head of Bacteriophage T4. [10.1038/227680a0]. *Nature*, 227(5259), 680-685.
- Lapik YR., K. L. (2003). The Arabidopsis cupin domain protein AtPirin1 interacts with the G protein α subunit GPA1 and regulates seed germination and early seedling development. *Plant Cell*, 15, 1578 - 1590.
- Lomakin A., B. G. (2005). Quasielastic Light Scattering for Protein Assembly Studies. *Methods in Molecular Biology*, 299, 153-165.
- Ma H. (2001). Plant G Proteins: the different faces of GPA1. *Curr. Biol.*, 21, 869 - 871.
- Ma H., M. E. (1990). Molecular cloning and characterization of GPA1, a G protein α subunit gene from Arabidopsis thaliana. *Proc Natl Acad Sci USA*, 87, 3821-3825.
- Mansfield T.A. (1998). Stomata and plant water relations: does air pollution create problem? *Environ. Pollut.*, 101, 1 - 11.
- Mark M.D., H. S. (2000). Completing the heterodimer: isolation and characterization of an Arabidopsis thaliana G protein γ -subunit cDNA. *Proc Natl Acad Sci USA*, 97, 14784 - 14788.
- Martin, S. R., & Schilstra, M. J. (2008). Circular dichroism and its application to the study of biomolecules. *Methods Cell Biol*, 84, 263-293.
- Mason MG., B. J. (2000). Completing the heterotrimer: isolation and characterization of an Arabidopsis thaliana G protein β -subunit cDNA. *Proc Natl Acad Sci USA*, 97, 14784 - 14788.

- Mason MG., B. J. (2001). Isolation of a novel G-protein γ -subunit from *Arabidopsis thaliana* and its interaction with G β . *Biochim. Biophys. Acta*(1520), 147 - 153.
- McCudden C.R., W. F. S. (2005). G-protein signaling: back to the future. *Cell. Mol. Life Sci.* , 62, 551 - 577.
- Morris AJ., M. C. (1999). Physiological regulation of G protein-linked signalling. *Physiol Rev.*, 79, 1373 - 1430.
- Neer E. J., S. C. J., Nambudripad R. and Smith T. F. (1994). The ancient regulatory-protein family of WD-repeat proteins. *Nature*, 371, 297 - 300.
- Ng C.K., H. A. M. (2001). Drought-induced guard cell signal transduction involves sphingosine-1-phosphate. *Nature*, 410, 596 - 599.
- Oldham, W. M. E. H. H. (2006). Structural basis of function in heterotrimeric G proteins. *Q Rev Biophys*, 39, 117-166.
- Perfus-Barbeoch L., J. A., Assmann SM. (2004). Plant heterotrimeric G protein function: insights from *Arabidopsis* and rice mutants. *Curr. Opin. Plant Biol.*, 7, 719 - 731.
- Petoukhov, M. V., Konarev, P. V., Kikhney, A. G., & Svergun, D. I. (2007). ATSAS 2.1 - towards automated and web-supported small-angle scattering data analysis. *Journal of Applied Crystallography*, 40(s1), s223-s228.
- Pierce KL., P. R., Lefkowitz RJ. (2002). Seven-transmembrane receptors. *Nat Rev Mol Cell Biol*, 3, 639 - 650.
- Porod, G. (1982). *Small Angle X-ray Scattering*: Academic Press, New York.
- Putnam, C. D., Hammel, M., Hura, G. L., & Tainer, J. A. (2007). X-ray solution scattering (SAXS) combined with crystallography and computation: defining accurate macromolecular structures, conformations and assemblies in solution. *Q Rev Biophys*, 40(3), 191-285.
- Ray K., K. C., Bonner L. M. and Robishaw J. D. (1995). Isolation of cDNA clones encoding eight different human G protein gamma subunits, including three novel forms designated the gamma 4, gamma 10, and gamma 11 subunits. *J. Biol. Chem.* , 270, 21765 - 21771.
- Rhee G. (2001). Regulation of phosphoinositide-specific phospholipase C. *Annu. Rev. Biochem.*, 70, 281 - 312.
- Roessle, M. W., Klaering, R., Ristau, U., Robrahn, B., Jahn, D., Gehrman, T., et al. (2007). Upgrade of the small-angle X-ray scattering beamline X33 at the European Molecular Biology Laboratory, Hamburg. *Journal of Applied Crystallography*, 40(s1), s190-s194.
- Ronnett G., M. C. (2002). G Proteins and Olfactory Signal Transduction. *Annu. Rev. Physiol.*(64), 189 - 222.
- Round, A. R., Franke, D., Moritz, S., Huchler, R., Fritsche, M., Malthan, D., et al. (2008). Automated sample-changing robot for solution scattering experiments at the EMBL Hamburg SAXS station X33. *Journal of Applied Crystallography*, 41(5), 913-917.
- Sambrook, J. a. R. (2000). *Molecular Cloning: A Laboratory Manual* (3rd ed.): Cold Spring Harbor Laboratory.
- Siderovski D.P., T. M. (1996). A new family of regulators of G-protein-coupled receptors? *Curr. Biol.*, 6, 211 - 212.
- Simon M. I., S. M. P. a. G. N. (1991). Diversity of G proteins in signal transduction. *Science*, 252, 802-808.
- Simon M.I., S. M. P. (1991). *Science*, 252, 802-808.
- Sondek J., S. P. (1996). Crystal structure of a G-protein beta gamma dimer at 2.1Å resolution. *Nature*, 25, 369 - 374.

- Stols L, G. M., Dieckman L, Raffin R, Collart FR, Donnelly MI. (2002). A new vector for high-throughput, ligation-independent cloning encoding a tobacco etch virus protease cleavage site. *Protein Expr Purif*, 25(1), 8-15.
- Stuhrmann, H. (1970a). Ein neues Verfahren zur Bestimmung der Oberflaechenform und der inneren Struktur von geloesten globularen Proteinen aus Roentgenkleinwinkelmessungen. *Zeitschrift fur Physikalische Chemie*(72), 177-198.
- Stuhrmann, H. (1970b). Interpretation of small-angle scattering functions of dilute solutions and gases. A representation of the structures related to a one-particle scattering function. *Acta Crystallographica Section A*, 26(3), 297-306.
- Sunahara R. K., T. R. (2002). Isoforms of mammalian adenylyl cyclase: multiplicities of signaling. *Mol. Interv.*, 2, 168 - 184.
- Svergun, D. (1992). Determination of the regularization parameter in indirect-transform methods using perceptual criteria. *Journal of Applied Crystallography*, 25(4), 495-503.
- Svergun D.I., B. C. K. M. H. J. (1995). CRY SOL – a Program to Evaluate X-ray Solution Scattering of Biological Macromolecules from Atomic Coordinates. *Journal of Applied Crystallography*, 28, 768-773.
- Svergun, D. I. (1999). Restoring low resolution structure of biological macromolecules from solution scattering using simulated annealing. *Biophys J*, 76(6), 2879-2886.
- Svergun, D. I., & Koch, M. H. J. (2003). Small-angle scattering studies of biological macromolecules in solution. *Reports on Progress in Physics*, 66(10), 1735.
- Svergun, D. I., Petoukhov, M. V., & Koch, M. H. (2001). Determination of domain structure of proteins from X-ray solution scattering. *Biophys J*, 80(6), 2946-2953.
- Swarbreck, D. (2000). Sequence and analysis of chromosome 3 of the plant *Arabidopsis thaliana*. *Nature*, 408(6814), 820-822.
- Temple B., J. M. (2007). The Plant Heterotrimeric G-Protein Complex. *Annu. Rev. Plant Biol.*, 58, 249 - 266.
- Tesmer J.J., S. S. R. (1997). Structure of RGS4 bound to AIF4-activated G(α 1): stabilization of the transition state for GTP hydrolysis. *Cell*, 89, 251 - 261.
- Thung L., B. J. (2012). G1 + G2 + G3 = G—————: The search for heterotrimeric G-protein subunits in *Arabidopsis* is over. *Journal of Plant Physiology*, 169, 542 - 545.
- Tovchigrecho A., V., IA. (2006). GRAMM-X public web server for protein-protein docking. *Nucleic Acids Res.*, 34, 310-314.
- Trusov Y., B. J. R. (2007a). Heterotrimeric G Protein g Subunits Provide Functional Selectivity in Gbg Dimer Signaling in *Arabidopsis*. *Plant Cell*, 19, 1235 - 1250.
- Trusov Y., B. J. R. (2007b). Heterotrimeric G protein g subunits provide functional selectivity in Gbg dimer signaling in *Arabidopsis*. *Plant Cell*, 19, 1235 - 1250.
- Trusov Y., B. J. R. (2008). Gg1 1 Gg2 Gb: Heterotrimeric G Protein Gg-Deficient Mutants Do Not Recapitulate All Phenotypes of Gb-Deficient Mutants. *Plant Physiol.*, 147, 636 - 649.
- Ullah H., J. A. M. (2003). The b-subunit of the *Arabidopsis* G protein negatively regulates auxin-induced cell division and affects multiple developmental processes. *Plant Cell*, 15, 393 - 409.
- Volkov, V. V., & Svergun, D. I. (2003). Uniqueness of ab initio shape determination in small-angle scattering. *Journal of Applied Crystallography*, 36(3 Part 1), 860-864.
- Wang X-Q., A. S. M. (2001). G protein regulation of ion channels and abscisic acid signalling. *Science*, 292, 20070 - 22072.

- Weiss CA., G. C., Mukai K., Hu Y., Ma H. (1994). Isolation of cDNAs encoding guanine nucleotide-binding protein b-subunit homologues from maize (ZGB1) and Arabidopsis (AGB1). *Proc Natl Acad Sci USA*, 91, 9554 - 9558.
- Wen J. H. (2010). Dynamic light scattering: Principles, measurements, and applications. from www.che.ccu.edu.tw/~rheology/DLS/outline3.htm
- Whitmore L., W. B. A. (2007). Protein Secondary Structure Analyses from Circular Dichroism Spectroscopy: Methods and Reference Databases. *Wiley Interscience*, 10.
- Whitmore L., W. B. A. (2011). *DichroWeb: On-line analysis for protein Circular Dichroism spectra*
- Yao B. (2004). *Dynamic Light Scattering Technology and Application to Protein Crystallization*: Proteion Corporation.

APPENDIX A

CHEMICALS

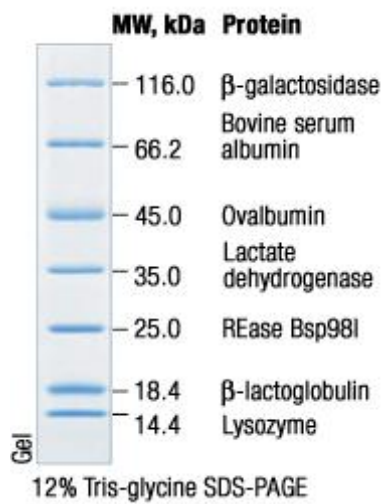
Acetic acid (glacial)	Riedel-de Haen, Germany	27225
30 % Acrylamide-0.8 % Bisacrylamide	Sigma, Germany	A3699
<i>BamHI</i>	Fermentas, Germany	ER0051
Bromophenol blue	Applichem, Germany	A3640
Coomassie Brilliant Blue R-250	Fluka, Switzerland	27816
EDTA- Free Complete Protease Inhibitor	Roche	11873580001
Cocktail Tablets		
dNTP mix	Fermentas, Germany	R0241
1,4-Dithiothreitol	Fluka, Switzerland	43815
<i>EcoRI</i>	Fermentas, Germany	ER0271
Ethanol	Riedel-de Haen, Germany	32221
Ethylenediaminetetraaceticacid	Riedel-de Haen, Germany	27248
Glycerol (87 %)	Riedel-de Haen, Germany	15523
Glycine	Amresco, USA	0167
HEPES	Fluka, Switzerland	54461
Hydrochloric acid (37 %)	Merck, Germany	100314
Imidazole	Sigma, USA	I5513
IPTG	Fermentas, Germany	R0392
KH ₂ PO ₄	Amresco, USA	0781
K ₂ HPO ₄	Amresco, USA	0782
Lysozyme	Sigma, USA	L7651

MassRuler DNA Ladder Mix	Fermentas, Germany	SM0403
2-Mercaptoethanol	Aldrich, Germany	M370-1
Methanol	Riedel-de Haen, Germany	24229
Na ₂ HPO ₄	Duchefa, Germany	S0522
NaH ₂ PO ₄	Duchefa, Germany	S0521
<i>NcoI</i>	Fermentas, Germany	ER0571
Non-Fat Bovine Milk Powder	Sigma, USA	C3400
PageRuler protein ladder	Fermentas, Germany	SM0661
Phenylmethylsulphonylfluoride	Amresco, USA	0754
2-Propanol	Merck, Germany	100996
Protein Molecular Weight Marker	Fermentas, Germany	SM0431
PVDF Membrane	Sigma, USA	P2938
Qiaprep Miniprep Kit	Qiagen, USA	19064
Qiaquick PCR Purification Kit	Qiagen, USA	28104
Qiaquick Gel Extraction Kit	Qiagen, USA	28704
Sodium Chloride	Riedel-de Haen, Germany	13423
Sodium dodecyl sulphate	Sigma, Germany	L-4390
<i>SspI</i>	Fermentas, Germany	ER0771
T4 DNA Ligase	Fermentas, Germany	EL0011
T4 DNA Polymerase	Fermentas, Germany	EP0061
<i>Taq</i> polymerase	Fermentas, Germany	EP0401
Tris	Fluka, Switzerland	93349
Triton X-100	Applichem, Germany	A1388
Tryptone	Sigma, Germany	61044
Tween-20	Sigma, USA	P1379
Yeast Extract	Sigma, Germany	Y1625

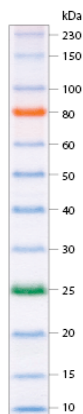
APPENDIX B

MOLECULAR WEIGHT MARKERS

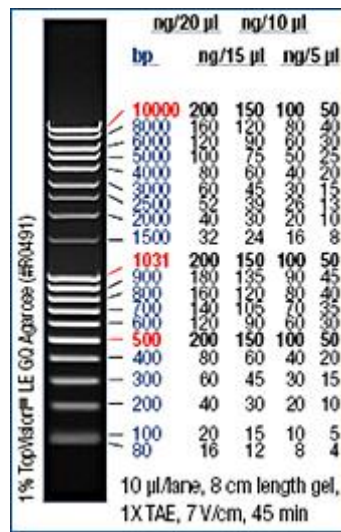
Fermentas Unstained Protein Molecular Weight Marker



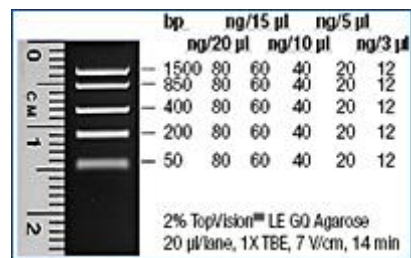
BioLabs ColorPlus Prestained Protein Ladder, Broad Range



Fermentas MassRuler DNA Ladder Mix

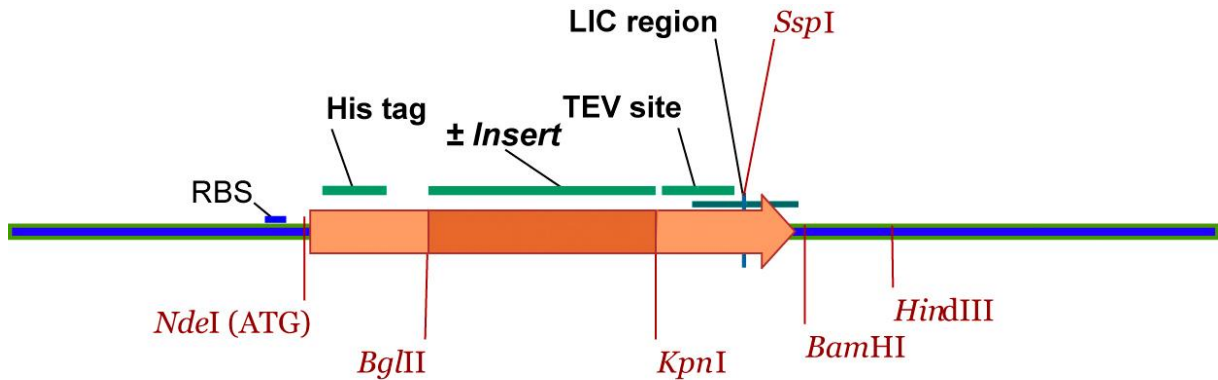
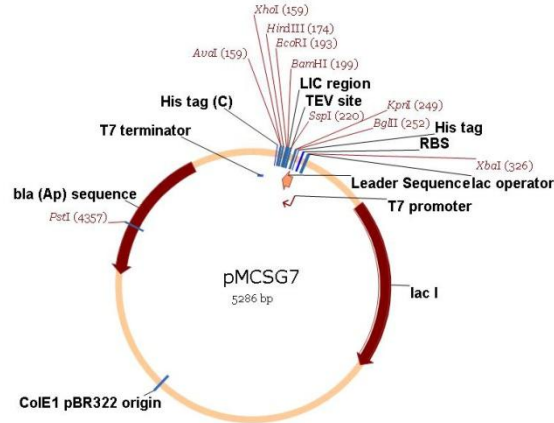


Fermentas FastRuler Low Range DNA Ladder



APPENDIX C

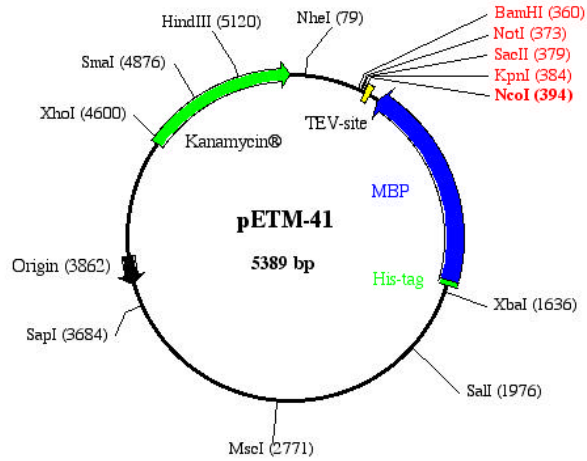
pMCSG-7 vector map and LIC site with available restriction enzyme sites



pMCSG-7 + AGG2 Construct Sequencing Result

AGG2 seq	ATGGAAGCGG	GTAGCTCCAA	TTGGTGGGGT	CAGGTATCCG	GGGGGGTTCGT	TGATACAAGA	GGCAAAACACA	70
pMCSG-7 Cons Seq	NNNNNNNNNN	NNNNTTNNNN	-----GGGGN	CNGGTATCCN	NGNGGGTTCGT	TGATACAAGA	GGCAAAACACA	65
AGG2 seq	GGATTTAAGC	TGAACTTAAA	AGGTTTGAAC	AAGAAGCTTG	ATTCTTAGAG	GAAGAAGTGG	AGCAGTTTGA	140
pMCSG-7 Cons Seq	GGATTTAAGC	TGAACTTAAA	AGGTTTGAAC	AAGAAGCTTG	ATTCTTAGAG	GAAGAAGTGG	AGCAGTTTGA	135
AGG2 seq	GAAGATGGAC	AATGCATCAG	CATCCTGAAA	AGAGTTCTTA	GACAGTGTTG	ACAGAAAAAC	CGATCCTCTT	210
pMCSG-7 Cons Seq	GAAGATGGAC	AATGCATCAG	CATCCTGAAA	AGAGTTCTTA	GACAGTGTTG	ACAGAAAAAC	CGATCCTCTT	205
AGG2 seq	CTTCCCGAAA	CAACAGGTCC	GGTGAATGCG	ACATGGGATC	AATGGTTTGA	AGGCCCTAAA	GAAGAAAAAC	280
pMCSG-7 Cons Seq	CTTCCCGAAA	CAACAGGTCC	GGTGAATGCG	ACATGGGATC	AATGGTTTGA	AGGCCCTAAA	GAAGAAAAAC	275
AGG2 seq	GATGTGGCTG	TCCATTCTT	-----	-----	-----	-----	-----	300
pMCSG-7 Cons Seq	GATGTGGCTG	TCCATTCTT	GGTACCCTGG	GTTGACCTG	AGCAAGCTT	AATTAGCTGA	GTTTGGACTC	345

pETM-41 vector map and multiple cloning site



T7 promoter --> XbaI
 GAAATTAATACGACTCACTATAGGGAGACCACAACGGTTTCCTCTAGAAAATAATTTGTGTTA
 CTTTAATTATGCTGAGTGATATCCCTCTGGTGTGCCAAAGGAGATCTTTATTAACAACAAAT

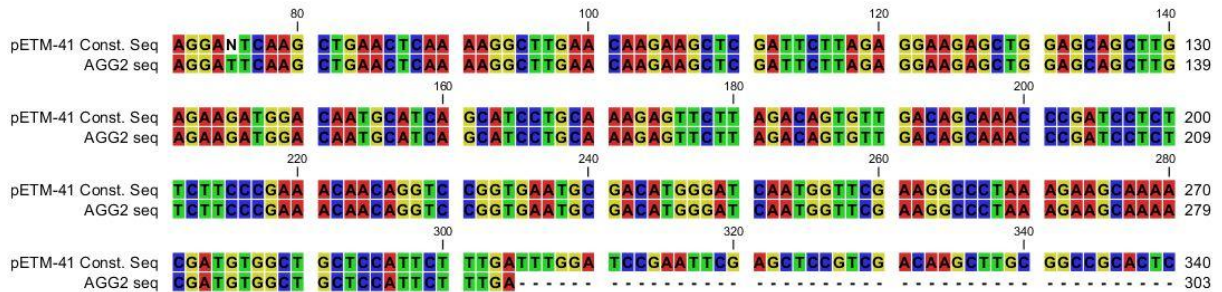
rbs His-tag
 ACTTTAAGAAGGAGATATACCATGAAACATCACCATCACCATCACCCCATGAAAATCGAAGAA
 TGAAATCTTCCTCTATATGGTACTTTGTAGTGGTAGTGGTAGTAGGGTACTTTTAGCTTCTT
 METLysHisHisHisHisHisHisHisProMETLysIleGluGlu

GGTAAACTGGTA...1056bp...CTGAAAGACGCGCAGACTAATTCGAGCTCGAACACAAC
 CCATTTGACCAT...MBP...GACTTTCTGCGCGTCTGATTAAGCTCGAGCTTGTGTGTG
 GlyLysLeuVal...352aa...LeuLysAspAlaGlnThrAsnSerSerSerAsnAsnAsn

TEV-site NcoI
 AACAAATAACAATAACAACAACCCCATGAGCGAGAATCTTTATTTTCAG GCGGCCATGGACTAA
 TTATTGTTATTGTTGTTGTTGGGGTACTCGCTCTTAGAAAATAAAGTC CCGCGGTACCTGATT
 AsnAsnAsnAsnAsnAsnAsnProMETSerGluAsnLeuTyrPheGln|GlyAlaMETAla***

SacII KpnI NotI BamHI
 TGAGGTACCGCGCCGCGAGCTCGGATCCGGCTGCTAACAAAGCCCGAAAGGAAGCTGAGTTG
 ACTCCATGGCGCCGCGCTCGAGCCTAGGCCGACGATTGTTTCGGGCTTTCCTTCGACTCAAC

pETM-41 + AGG2 Construct Sequencing Result



APPENDIX D

BUFFERS AND SOLUTIONS

Tris Acetate EDTA Buffer (TAE) (50X): 121.1 g Tris Base, 28.55 ml Glacial Acetic acid, 7.3 g EDTA, completed to 500 ml.

Native-PAGE:

8% Separating Gel:

	for 2 gels	for 1 gel	[final]
dH ₂ O	6 ml	3 ml	
3 M Tris, pH 8.9	1.25 ml	625 µl	3.75 mM
30 % Acryl-0.8 % Bisacryl	2.67 ml	1.335 ml	8 %
10 % APS	75 µl	37.5 µl	0.075 %
TEMED	5 µl	2.5 µl	0.05 %

3 % Stacking Gel:

	for 2 gels	for 1 gel	[final]
dH ₂ O	4.2 ml	2.1 ml	
1 M Tris, pH 6.8	250 µl	125 µl	50 mM
30 % Acryl-0.8 % Bisacryl	510 µl	255 µl	3 %
10 % APS	37.5 µl	18.75 µl	0.075 %
TEMED	2.5 µl	1.25 µl	0.05 %

2X Native Sample Buffer: 200 mM Tris-HCl pH 7.5, 20 % (v/v) Glycerol, 0.05 % (w/v) Bromophenol Blue in ddH₂O.

Native-PAGE Running Buffer: 25 mM Tris, 192 mM Glycine in ddH₂O

SDS-PAGE:

12 % Separating Gel:

	for 2 gels	for 1 gel	[final]
dH ₂ O	4.62 ml	2.31 ml	
3 M Tris, pH 8.9	1.25 ml	625µl	3.75 mM
30 % Acryl-0.8 % Bisacryl	4 ml	2 ml	12 %
20 % SDS	50 µl	25 µl	0.1 %
10 % APS	75 µl	37.5µl	0.075 %
TEMED	5 µl	2.5 µl	0.05 %

5 % Stacking Gel:

	for 2 gels	for 1 gel	[final]
dH ₂ O	3.850 ml	1.925 ml	
3 M Tris, pH 8.9	250 µl	125 µl	50 mM
30 % Acryl-0.8 % Bisacryl	850 µl	425µl	5 %
20 % SDS	10 µl	5 µl	0.1 %
10 % APS	37.5 µl	18.75 µl	0.075 %
TEMED	2.5 µl	1.25µl	0.05 %

2X SDS Sample Buffer: 4 % (w/v) SDS, 20 % (v/v) Glycerol, 0.004 % (w/v) Bromophenol blue, 10 % (v/v) 2-mercaptoethanol, 0.125 M Tris-HCl, pH 6.8 in ddH₂O.

SDS-PAGE Running Buffer: 25 mM Tris, 192 mM Glycine, 0.1 % (w/v) SDS in ddH₂O.

Coomassie Staining Solution: 0.1 % (w/v) Coomassie Brilliant Blue R-250, 40 % (v/v) Methanol, 10 % (v/v) Glacial Acetic acid in ddH₂O.

Destaining Solution: 4 % (v/v) Methanol, 7.5 % (v/v) Glacial Acetic acid, completed to 1 L.

10X Transfer Buffer: 1,92 M Glycine, 250 mM Tris Base in 1 L. 200 ml Methanol is added to the solution containing 1X Transfer Buffer

10X TBS Solution: 500 mM Tris Base, 45% NaCl, pH: 8.4. 500 μ l Tween-20 is added to 1X TBS buffer

APPENDIX E

EQUIPMENTS

AKTA Prime:	GE-Healthcare, SWEDEN
Autoclave:	Hirayama, Hiclave HV-110, JAPAN
	Certoclav, Table Top Autoclave CV-EL-12L, AUSTRIA
Centrifuge:	Eppendorf, 5415C, GERMANY
	Eppendorf, 5415D, GERMANY
	Eppendorf, 5415R, GERMANY
	Hitachi, Sorvall RC5C Plus, USA
	Hitachi, Sorvall Discovery 100 SE, USA
Dynamic Light Scattering:	Malvern, Zetasizer Nano-ZS, UK
Deepfreeze:	-80 °C, Kendro Lab. Prod., Heraeus Hfu486, GERMANY
	-20 °C, Bosch, TURKEY
Distilled water:	Millipore, Elix-S, FRANCE
	Millipore, MilliQ Academic, FRANCE
Electrophoresis:	Biogen Inc., USA
	Biorad Inc., USA
Ice Machine:	Scotsman Inc., AF20, USA
Incubator:	Memmert, Modell 300, GERMANY

	Memmert, Modell 600, GERMANY
Laminar Flow:	Kendro Lab. Prod., Heraeus, HeraSafe HS12, GERMANY
Magnetic Stirrer:	VELP Scientifica, ARE Heating Magnetic Stirrer, ITALY
	VELP Scientifica, Microstirrer, ITALY
Microliter Pipette:	Gilson, Pipetman, FRANCE
Microwave Oven:	Bosch, TURKEY
pH Meter:	WTW, pH540 GLP MultiCal, GERMANY
Power Supply:	Biorad, PowerPac 300, USA
	Wealtec, Elite 300, USA
Refrigerator:	+4 °C, Bosch, TURKEY
Semi-Dry Western	
Transfer Machine	Novex, USA
Shaker:	Forma Scientific, Orbital Shaker 4520, USA
	GFL, Shaker 3011, USA
	New Brunswick Sci., Innova 4330, USA
Sonicator:	BioBlock Scientific, Vibracell 7504, FRANCE
Spectrophotometer:	Nanodrop, ND-1000, USA
Speed Vacuum:	Savant, Speed Vac Plus Sc100A, USA
	Savant, Refrigerated Vapor Trap RVT 400, USA
Thermocycler:	Eppendorf, Mastercycler Gradient